Alma Mater Studiorum - Università di Bologna

DOTTORATO DI RICERCA IN

NANOSCIENZE PER LA MEDICINA E PER L'AMBIENTE

Ciclo 36

Settore concorsuale: 03/C1 - CHIMICA ORGANICA

Settore Scientifico Disciplinare: CHIM/06 – CHIMICA ORGANICA

GRAPHENE BASED MATERIALS FOR WATER PURIFICATION: CHARACTERIZATION AND APPLICATION

Presentata da: Sara Khaliha

Coordinatore Dottorato

Matteo Calvaresi

Supervisore

Manuela Melucci

Co-supervisore

Marco Bandini

Esame finale anno 2024

Abstract

This PhD thesis addresses the critical issue of water purification, an evolving field with increasing importance year by year, as highlighted by the recent revision of EU Drinking water directive (EU2020/2184). Current water treatment methods are insufficient for efficiently removing Emerging contaminants (ECs) and new materials and technologies are required. Among these strategies, graphene-based materials, particularly Graphene Oxide (GO), have emerged as promising candidates for water purification. Key properties of GO are remarkable surface area, multi-site interaction with organic molecules and tailorable surface chemistry.

The research objective was to assess GO effectiveness in different configurations (i.e., nanosheets, composites) as a sorbent of various ECs, such as pharmaceutical and personal care products (PPCPs), heavy metals, and Per- and Poly-Fluorinated Substances (PFAS).

To investigate the adsorption mechanism of GO, a standardized protocol based on adsorption, kinetic and efficiency tests was employed to compare different type of GO, with various amount of defects, holes and oxygenated group on the graphene sheet surface. The role of defect was modelled by MD simulations, highlighting a mechanism driven by shape complementarity. Defect-rich graphene oxide (dGO) exhibited superior adsorption capacity toward Ofloxacin, an antibiotic, compared less defected form (650 mg/g vs 204 mg/g, respectively)

Despite the remarkable adsorption capacity, the use of GO nanosheets as sorbent are limited by tedious recovery process after treatments. A standard protocol (referred to as GO+MF) was proposed to fully exploit the adsorption capacity of GO as nanosheets, which is then separated from treated water trough dead-end microfiltration on hollow fiber modules. The optimized procedure was applied to rGO on PFAS, with an adsorption capacity of 138 µg/g in only 30 min.

Taking a step further in applicability of GO in water purification, Polysulfone-GO hollow fiber membranes (PSU-GO HFs) were developed, combining simultaneous adsorption and ultrafiltration capabilities. Morphology, surface properties, and porosity of PSU-GO HFs were investigated in relation to different GO:PSU ratios (1–5% w/w). PSU-GO HF 3,5% was selected as case study and tested on PFAS and heavy metals, exhibiting higher adsorption capacity compared

to Granular Activated Carbon (GAC). Furtherly, the release of GO from the composite was investigated through a state-of-the-art technique (0.1 ppb) and no detectable GO was found in treated water, confirming their safety and effectiveness in water purification.

In addition, the selectivity of standard GO was tuned by chemical modification of nanosheets using amino acids (GO-AA), including L-glutamic acid, L-methionine, and Lysine. GO-AA, with a loading in the range 5-15%, exhibited significantly improved adsorption capacities for select contaminants, including bisphenol A (BPA), benzophenone-4 (BP4), and carbamazepine (CBZ), when compared to standard GO, indicating the active role of amino acids in enhancing performance.

Index

List of Acronyms & abbreviations

SDGs	*Sustainable development Goals*
DWD	*Drinking water directive*
PFAS	*Per- and Poly-Fluorinated substances*
ECs	*Emerging contaminants*
EPA	*Environmental protection agency*
PPCPs	*Pharmaceutical and Personal Care products*
EDCS	*Endocrine-Disrupting Chemicals*
DCF	*Diclofenac*
CIPRO	*Ciprofloxacin*
OFLOX	*Ofloxacin*
CBZ	*Carbamazepine*
BP3	*Benzoophenone-3*
BP4	*Benzophenone-4*
CAF	*Caffeine*
RhB	*Rhodamine-B*
BPA	*Bisphenol-A*
WWTPS	*Wastewater treatment plants*
AOPs	*Advanced oxidation processes*
MF	*Micro-filtration*
NF	*Nano-filtration*
UF	*Ultrafiltration*
RO	*Reverse osmosis*
PAC	*Powder Activated carbon*
GAC	*Granular activated carbon*
POU	*Point of use*
GRM	*Graphene related materials*
CNT	*Carbon nanotubes*
GO	*Graphene oxide*
rGO	*Reduced Graphene oxide*
dGO	*Defective Graphene oxide*
HF	*Hollow fiber*

PSU	*Polysulfone*
PES	*Poly ether sulfone*
hGO	*Hummer graphene oxide*
bGO	*Brodie graphene oxide*
BET	*Brunauer–Emmett–Teller*
XPS	*X-ray photoelectron spectroscopy*
SEM	Scanning electron spectroscopy
TEM	Transmission electron microscopy
SERS	Surface-enhanced raman spectroscopy
UPLC-MS/MS	Ultrahigh Performance liquid chromatography coupled with Mass Spectroscopy
FTIR	*Fourier-transform infrared spectroscopy*
TGA	*Thermogravimetric analysis*
HPLC	*High-performance liquid chromatography*
MD	*Molecular dynamic*
AFM	*Atomic force microscopy*

1 Introduction

1.1 A water issue

During the last decade water pollution has become a critical global issue, posing significant threats to human health and ecosystems. Growing population and expanding urban areas increase water demand, straining existing resources.[1] Moreover, climate change further impacts on water scarcity by altering precipitation, causing droughts and reduced water availability in an increasing number of areas around the world. In fact, water pollution is strictly connected with water scarcity, primarily caused by factors such as population growth, climate change, inefficient water use, and inadequate infrastructures. Contamination may come from various sources, including urbanization, industrial discharges, and improper waste disposal.[2]

The urgency to face the water pollution problem is also highlighted by the Sustainable Development Goals (SDGs), 17 global targets established by the United Nations in 2015 as part of the 2030 Agenda for Sustainable Development.[3] These goals aim to address social, economic and environmental challenges to achieve a more sustainable and equitable world by the year 2030. Among the 17 SDGs, the number 6 is focused on various water-related challenges, including water scarcity, water pollution, inadequate sanitation facilities, and lack of access to safe drinking water. In particular, it aims to improve clean water and sanitation access by 2030, particularly for marginalized groups. It stresses water quality enhancement, pollution reduction, and water-use efficiency. Integrated water resource management is called for, with a focus on protecting water-related ecosystems to preserve quality and availability. The goal also promotes international collaboration in water and sanitation programs.

SDG 6 is crucial for achieving sustainable development, because as water and sanitation are essential for human well-being, public health, economic development, and environmental sustainability, and ultimately, human well-being. Access to clean water and sanitation has impacts on various aspects of life, including poverty reduction, gender equality, education, and ecosystem preservation. Unfortunately, COVID-19 has hindered progress, and 28 developing nations are not expected to achieve SDGs 1, 2, 4, 6, and 7 by 2030.[4]

European Union guidelines about water align with the policies promoted by the United Nations, as highlighted by the recently adopted Drinking Water Directive 2020/2184.[5] This guideline emphasizes the need for enhanced water quality standards and improved treatment methods, setting quality standards for drinking water in the European Union. The directive, updated in 2022, introduces specific parameters and maximum allowable concentrations for various substances and microorganisms in drinking water, including chemicals, bacteria, and parasites. It introduces the concept of risk assessments and management plans, to identify and address potential risks to drinking water quality. It also emphasizes the importance of providing consumers information about the quality of their drinking water and potential risks related to water use.

The DWD 2020/2184 introduces new limits for a list of substances and compounds of concern related to water for human consumption. This list includes potential water pollutants that should be carefully monitored by the EU member states to determine the risk they pose. The ultimate goal is to achieve a good chemical and ecological status of European aquatic ecosystems and protect citizen's health.[2] Members states must monitor these substances at least once per year for up to four years. This list includes certain metals (Lead and Chromium) and industrial chemical (i.e. pharmaceuticals or UV filters) and Per- and Poly-fluoroalkylsubstances (PFAS).

The mentioned examples are commonly known as "emerging contaminants" (ECs). This term refers primarily to contaminants for which there is currently no regulation, requiring monitoring or public reporting of their presence in our water supply or wastewaters. Included within this category are various substances such as drugs (antibiotics, painkillers, etc.), diagnosis products, steroids and hormones, antiseptics, personal care products (sun creams, fragrances, etc.), petrol additives, heavy metals and metalloids, surfactants endocrine disruptors and more.[6] Currently, most of the ECs are not routinely monitored by water utilities due to the absence of regulatory requirements.

ECs can easily enter the environment thanks to their resistance to depuration technologies conventionally employed in urban wastewater treatment facilities (i.e. activated sludge,[7] filtration,[8] and disinfection[9, 10]) and so they are as well regarded as the potential sources of ECs in the environment.[6]

Great interest has been devoted to these compounds, as reflected in a high number of publications on this subject.[11-15] Nevertheless, their effects on both the environment and human health remain largely unknown and under evaluation.[6]

Academics, scientists and also industries need to work urgently to find solutions for environmentally friendly and economically viable water purification, to meet the needs of their communities without compromising the natural environment. To achieve this, taking action in key areas is essential, which includes preventing further pollution from various sources (i.e. inadequate waste management) and establishing effective water treatment systems.

1.2 Emerging contaminants

According to the US Environmental Protection Agency (EPA), an emerging contaminant is a chemical or material which poses a perceived, potential, or real threat to the human health or the environment. The risk may be evident because of a recently discovered, or a new pathway that has developed, and for which there is a lack of published health standards.[16, 17] It has been estimated that the worldwide production of ECs has increased from 1 million to 500 million tons each year.[18]

Many classes of molecules and products are considered ECs,[18-21] including:

- *Pharmaceutical and Personal Care products (PPCPs)*: drugs, medications, cosmetics, UV-filters, cleaning products and fragrances.
- *Per- and Polyfluoroalkyl substances (PFAS)*: synthetic chemicals widely employed in various industrial and consumer applications, including uses as adhesive and water repellents.
- *Endocrine-Disrupting Chemicals (EDCs)*: substances that can interfere with the hormonal system of humans and wildlife. They include chemicals used in plastics, pesticides, and certain industrial processes.[22]

These contaminants are becoming ubiquitous in the environment (Fig. 1.1). For example, more than 80 ECs have been found in drinking waters in Milan urban area, the most inhabited and industrialized city of Italy. These ECs included pharmaceuticals, illicit drugs, PFAS, anthropogenic markers and plasticizers. In each water source tested, ECs were typically detected in trace amounts (ng/L), indicating a negligible risk to human health. The ubiquity of these contaminants in drinking water emphasizes the urgent need for in-depth research concerning their

occurrence, behaviour, fate and potential risks. This research is critical for the development of regulatory guideline values and the potential incorporation of the most hazardous ECs into future legislation.

While the toxicity of certain ECs has already been confirmed, [18] a majority of these substances are still undergoing evaluation, with new regulations aligning with these assessments. Many on these ECs have been included in the European watch list, together with heavy metals, which have been extensively investigated.[23]

Contrarily to the ECs, heavy metals present a well-documented toxicity and cancerogenic properties at specific exposure levels. However, they are daily released into water from various natural and anthropogenic sources, raising a serious health concern.[24, 25]

In the following chapters, it will be provided an overview of the contaminants of environmental concern I focused most on during my PhD, which include organic pollutants, heavy metals and PFAS.

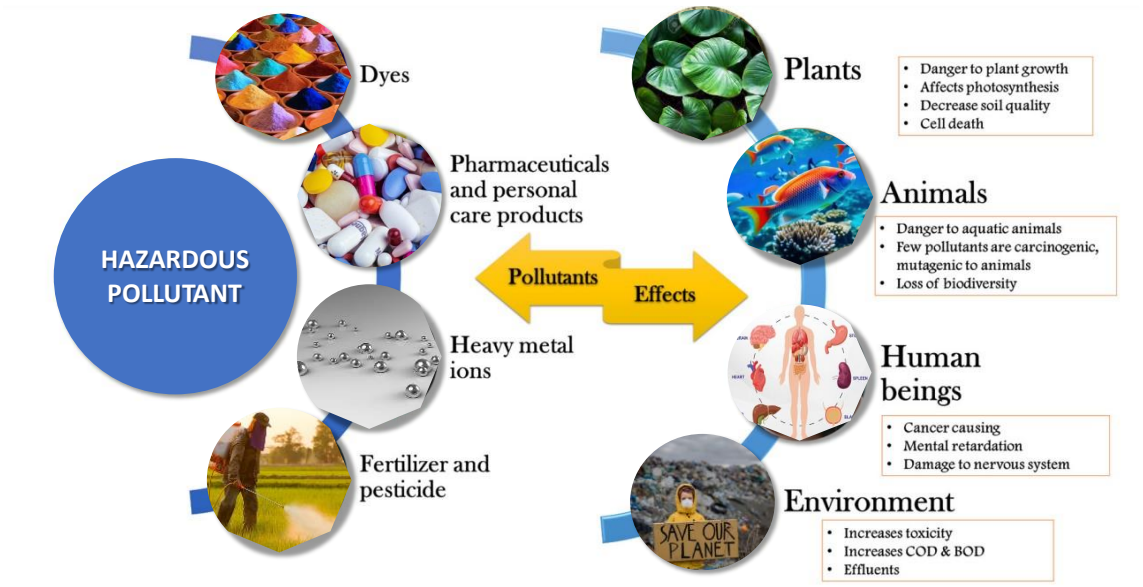

Fig. 1.1 *Broad classification and effects of hazardous pollutants.*

1.2.1 Heavy metals

Although heavy metals are not considered as ECs, they are listed as potential environmental hazards due to their well-established adverse effects on both health and the environment.

Heavy metals and metalloids are a group of elements characterized by their high density (> 4g/cm^3) and atomic weight. Heavy metals commonly occurring as

contaminants within domestic water supplies include copper (Cu), cadmium (Cd), zinc (Zn), lead (Pb), mercury (Hg), arsenic (As), chromium (Cr), iron (Fe), nickel (Ni) and manganese (Mn).

Although heavy metals are naturally found on earth, most environmental contamination results from anthropogenic activities, such as mining and smelting operations, industrial production and use, domestic and agricultural use of compounds containing such metals.[26] These toxic elements persist in the environment as highly stable and non-degradable contaminants, leading to their bioaccumulation.[24, 27] It has been reported that approximately 40% of the lakes and rivers of the planet are polluted by heavy metals.[28]

Various regions worldwide exhibit alarmingly high concentrations of metals in their drinking water.[24, 29, 30] In India, arsenic levels reached 107 g/L, while in Nigeria, water near lead-zinc mining communities contained excessive levels of multiple heavy metals. Latin America had 4.5 million people exposed to arsenic levels exceeding 50 g/L, sometimes reaching 2000 g/L. China reported river waters with concentrations of Cd, Cu, and Zn exceeding acceptable limits. In Venezuela, mercury contamination in the Coyuni river basin was linked to gold mining processes. Turkey's Antalya region recorded concentrations of Sr and Al surpassing water quality standards. These findings raise significant health concerns, especially in developing nations that may face economic limitations in addressing this issue.[24, 29, 30]

When released into the environment, even at very low concentrations, heavy metals have the potential to cause harm to various multiple organs, including the lungs, liver, prostate, stomach, and skin. The toxicity has been discussed since 1980, when the first attempt to limit their harmful effects was done (Table 1.1).[31] Their toxicity arises from the ability to bind protein site in blood, displacing the original essential metals and bioaccumulating on bodies, leading to harmful effect.[31] They are associated with the development of neurodegenerative disorders like Alzheimer's and Parkinson's diseases.[24, 29, 30] Moreover, heavy metals can lead to the occurrence of genetic abnormalities, physiological and morphological issues, hindered developmental progress, carcinogenic effects, and increased mortality rates.[32]

Table 1.1 *Comparison of current EPA, EU, and newly approved EU drinking water guidelines for selected parameters*

Contaminant	Maximum concentration limit (µg/L)			Effect
	EPA	WHO	UE DW directive	
Cu	1300	2000	2000	Liver damage, Wilson disease, insomnia
Cd	5	3	5	Kidney damage, renal disorder, human carcinogen
Zn	5000	3000	3000	Gastrointestinal distress, depression, lethargy, neurological signs and increased thirst
Pb	15	10	10	Demage to fetal brain, disease of kidneys, nervous system
Hg	2	6	1	Rheumatoid arthritis, disease of kidneys, nervous system
As	10	10	10	Skin damage, vascular disease, visceral cancers
Cr	100	50	25	Lung and stomach cancer, increased risk lymphomas
Fe	300	3000	200	Haemochromatosis
Ni	100	70	20	Dermatitis, nausea, chronic asthma, human carcinogen
Mn	50	400	50	Staining and discoloration

1.2.2 Pharmaceutical and Personal care products

The increasing population and evolving lifestyles have resulted in a growing utilization and demand for Pharmaceutical and Personal Care products (PPCPs).[33] However, this intensive use of new compounds is not always aligned with the adoption of updated regulations and treatment technologies. As a results, these substances can be easily detected in water sources worldwide.[18]

Among the frequently reported pharmaceuticals in both drinking and wastewater are Diclofenac, Ofloxacin and Ciprofloxacin (antibiotics) and Carbamazepine.[34] Caffeine, Bisphenol A and Benzophenone are not pharmaceutical, but they can be frequently monitored in PPCs products, as active molecule, additives or UV filters. Rhodamine B, as well, is frequently detected in PPCPs products, used as organic dye (Fig.1.2).

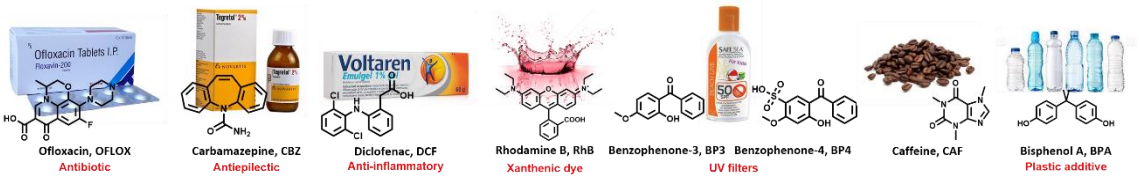

Fig. 1.2 Chemical structure of PPCPs herein described.

-

- **Diclofenac**

Diclofenac (DCF) is a non-steroidal anti-inflammatory drug widely used in the treatment of inflammatory disorders and is among the pharmaceutical listed in the Commission Implementing Decision (EU) from March 2015.[35] Its extensive use has led to frequent occurrences of DCF in surface, ground, and even drinking water,[36] with a maximum concentration of 836 µg/L in some cases.[37] Long-term exposure to has demonstrated to have negative impact on ecosystem health[35, 38, 39] and caused severe visceral gout or renal failure to humans even if the low concentration.[39-41]

- **Ciprofloxacin and Ofloxacin**

Ciprofloxacin (CIPRO) and Ofloxacin (OFLOX) are quinolone antibiotics which employed for the treatment of various types of bacterial infections.[42, 43] They gained greater concern due to their widespread utilization, and their occurrence in aquatic environments is associated with the potential for inducing antimicrobial resistance.[44, 45]

CIPRO has been widely detected in the environment over the past decade,[43, 46] exhibiting the highest recorded concentrations, with a maximum concentration of 2500-6500 mg/L, in India. This concentration are notably higher with the one observed in United States and Europe, where ciprofloxacin is typically found at much lower ng/L levels in surface and groundwater.[44, 47] OFLOX, on the other hand, is usually found in lower concentrations and less frequently, but it is among the main antibiotic compounds present in effluents from treatment plants and surface waters.[44]

- **Carbamazepine**

Carbamazepine (CBZ) is a drug used in the treatment of epilepsy, neuropathic pain and certain psychiatric disorders with a global usage amount of 1,014 tons per year. [48-50] In the human body, CBZ is extensively metabolized, with only a small fraction (<2%) being eliminated unchanged.[48] Despite this, CBZ is continuously released into the environment, due to low removal rates in wastewater treatment processes (<45%).[51] It exhibits resistance to degradation in the environment and can persist in both freshwater and marine environments, with concentrations ranging from ng/L to a few µg/L. It has been widely detected in Milan drinking water, up to 0.18 ng/L.[15, 48, 52, 53]

CBZ exposure can have harmful effects on aquatic and terrestrial organisms, such as reproduction toxicity, developmental delay and carcinogenicity.[54-57] Consequently, CBZ is considered a pollutant of environmental and human health concern[57] and has even been proposed as a potential marker of human activity in water bodies. [55]

- **Benzophenones**

Sunscreen products have gained widespread popularity to minimize sun exposure and protect from UV radiation, with Benzophenones (BPs) being a commonly utilized class of organic UV filters. Two well-known members of this group are Benzophenone-3 (BP3) and Benzophenone-4 (BP4), which are frequently incorporated as active.[58, 59] Although UV-filters can protect the skin from UV radiation, the BP-type UV-filters exhibit potential endocrine disrupting activity and genotoxicity, being included in the group 2B of AIRC classification (Possibly carcinogenic to human).[60]

These UV-filters are commonly detected in various aquatic environments, including wastewater, swimming pools, rivers, lakes, with concentrations reaching up 13.3 µg/L for BP4 and up to 700 ng /L for BP3 in specific cases.[60]

Although these substances are widespread and can reach high concentrations in specific environments, there is a lack of research on their ecological impact, and they are not currently included in any environmental regulations or discharge standards.[60]

- **Caffeine**

In addition to the mentioned pharmaceutical compounds, central nervous system stimulants are also frequently detected in environmental compartments at relevant concentrations.[61] One notable example is caffeine (CAF), which is contained in many medications, drugs, cosmetics and beverages. In small doses, caffeine stimulates the nervous system, while larger doses can lead to nerve cell depletion, and extremely high doses may even be fatal.[62] Although caffeine is effectively removed during wastewater treatment, its growing consumption is leading to an influx into aquatic ecosystems at higher amounts than what is effectively degraded.[61] As a result, caffeine is frequently detected in drinking surface waters with maximum concentration found of 57 µg/L.[62, 63]

- **Rhodamine B**

Another class of contaminants strictly connected with the increasing PPCP use are synthetic organic dyes, extensively utilized in various sectors, such as textiles, tanneries, cosmetics, food manufacturing, and pharmaceuticals for both human and animal use.[64] Due to the quick industrialization and rapid population growth, the textile sector produces about 7 x 10^5 tons/year of synthetic dyes, with 10% of toxic dyestuffs released into the environment, since no regulation prevent the discharge in water stream. [1, 65, 66]

In the textile industry, Rhodamine B (RhB) is a common water-soluble organic dye, used as fabric colouring. Even at very low concentrations (1.0 mg/L), it imparts vivid colour to water, but the limit concentration to protect against hazardous effects is 140 µg/L.[67, 68] RhB presence in aquatic ecosystems is expected due to its use in various industries, but it has been associated with environmental problems and potential health hazards for both humans and animals.[67] In fact, RhB is harmful if ingested and may cause soreness of the skin, eyes and respiratory tract, and may also affect photosynthesis and respiration rates.[66, 69]

- **Bisphenol A**

Bisphenol-A (BPA) is a representative type of EDC commonly used as plasticizers. Despite not being intentionally added as ingredient, BPA might be contained in certain PPCs (i.e. toothpaste, soaps, cosmetics, and medical products) due to migration from plastic containers or component degradation.[70-73] The presence of BPA in PCPs is concerning because it has the potential to affect human health, from prenatal development through adulthood, and can exhibit genotoxic, neurotoxic, cytotoxic, reproductive, and endocrine-disrupting effects.[72] Recent Global research has revealed the widespread presence of BPA in groundwater,[72, 74-76] categorizing it as a ubiquitous pollutant, frequently found in various water sources, including industrial and domestic wastewater and water used for irrigation.[77, 78] Given that groundwater is a vital source of freshwater for approximately one-third of the world's population, this issue is of critical significance. [72, 79]

1.2.3 Per- and polyfluoroalkyl substances

Per- and polyfluoroalkyl substances (PFAS) are a class of synthetic chemicals known as "forever chemicals" due to their persistence in the environment. These substances have been widely used in various industrial and commercial products

since the 1940s, including adhesives, fire-fighting foams, cosmetics, paper products, and water repellents.[80-82]

PFAS consist of a carbon backbone with fluorinated carbon atoms (CF_n, where n represents the number of fluorinated carbon atoms) and a polar head group, either sulfonic or carboxylic acid (Fig.1.3). Due to their unique chemical structure, PFAS possess surfactant-like properties and exhibit high thermal and chemical stability, primarily because of the strong C-F bonds they contain, making them excellent choices for applications as water and oil repellents.[83, 84]

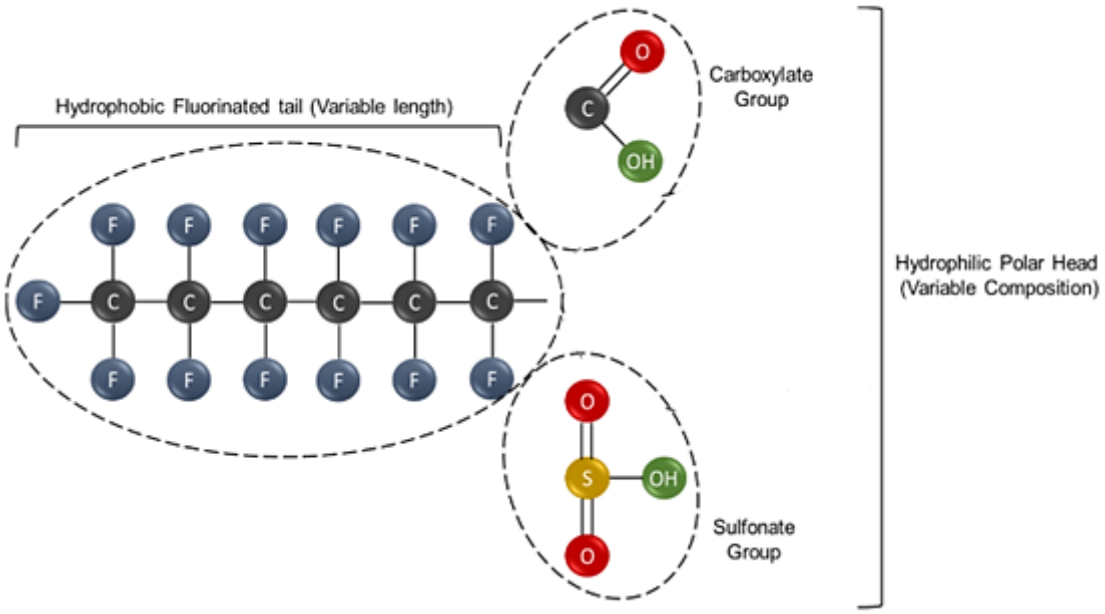

Fig. 1.3 *Overview of the general structure of perfluorinated PFAS substances. These are represented by the hydrophobic tail, composed by a variable number of carbon atoms at different degree of fluorination, and the hydrophilic head, which contains polar groups. The specific combination of these chemical determinants, namely the carbon chain length, the type of functional groups and the number of fluoride atoms, generates an enormous number of different PFAS molecules with ample downstream applicability. Adapted with permission* [85]

PFAS have been detected ubiquitous in almost all aquatic matrices, including surface water, rainwater, drinking water, and groundwater. [86-92] Notably, short-chain PFAS, like PFBA, are mobile and can infiltrate the unsaturated soil zone, potentially traveling over substantial distances through groundwater.[93, 94] These chemicals are also commonly found in various consumer products, such as cosmetics,[95] food packaging,[96] agricultural food items[97] as well as toilette paper.[14]

The ubiquity of these contaminants is particularly concerning in the Veneto region of Italy, where groundwater has found to be contaminated with PFAS from manufacturing plant activity since 1960. Residents have been exposed to elevated

PFAS concentrations in their drinking water for over 50 years (up to 1.4 µg/L of PFOA, 0,6 ug/L of PFBA), resulting in an average tested concentration of 44.4 µg/L of PFOA in citizens' blood.[98] More recently, PFAS have been ubiquitously found in drinking water of Milan, even though at non-risky concentrations (i.e. 0.07 ng/L). Worldwide, higher concentration has been found,[99] with groundwater concentrations up to 3.7 µg/L for perfluoroalkyl carboxylic acids and 25 µg/L perfluoroalkyl sulfonic acids.[99]

The toxicity of PFAS is under continuous evaluation and they are categorized under group 2B in the AIRC classification, suggesting potential carcinogenicity in humans.[17] Furthermore, studies have linked PFAS exposure to various acute and chronic human diseases, including thyroid disorders, immune toxicity, cardiovascular disease, activation of nuclear receptors, tissue-level changes, and potential impacts on embryonic development and motor functions. [22, 94, 100]

Despite the documented toxicity, there are not restriction on their use in consumer product or for industrial applications. The risk depends on factors like exposure source, source concentration and frequency of exposure and production method. A high number of aspects must be considered and a clear guideline are not easy to redact due to the lack of reliable and reproducible data.

Several countries have published administrative guidelines for level of PFAS in water (Table 1.2).

Table 1.2. Concentration limits for PFOA and PFOS[82]

Country	PFOA (ng/L)	PFOS (ng/L)	Year
Australia	560	70	2017
Canada	200	600	2018
Denmark	100	100	2015
Germany	300	300	2006
Italy	500	30	2017
Netherlands	390	200	2020
Sweden	90	90	2014
United Kingdom	10	10	2021

The European commission has declared PFAS as emerging contaminants, and PFOS as priority hazardous substances. The revised European drinking water directive2020/2184, sets maximum combined concentration for all PFAS

compounds at 0.5 µg/L of water. Alternatively, member states can monitor the total of 20 PFAS compounds, with a maximum limit of 0.1 µg/L.

1.3 Current technologies in water treatments

Conventional wastewater treatment plants (WWTPs) employ established technologies to eliminate various contaminants from wastewater streams, including nutrients, dissolved organics, colloidal and suspended particulates, and pathogens. However, these systems are not primarily designed to target ECs. [101] Nevertheless, WWTPs exhibit some effective removal capabilities, primarily influenced by the physico-chemical properties of ECs and by the specific treatment conditions. [89, 102-105]

WWTPs generally employ primary, secondary, and occasionally tertiary treatment steps to eliminate insoluble contaminants and soluble pollutants, combining physical, chemical, and biological processes, along with sewage removal activities.[106, 107] During the primary treatment step, suspended solids (e.g., oils, fats, grease, sand, grit, and settable solids) are reduced, contributing to ECs removal with an efficiency in the range of 20–50%, while a slightly better removal (30–70%) is achieved in the secondary treatment step,[106] designed to remove organic matter and/or nutrients using biodegradation. Tertiary treatment mechanisms, especially filtration, oxidation processes (e.g., ozonation, UV treatment, chlorination, photocatalysis), and adsorption are the most efficient in ECs removal.[108, 109]

However, various limitations may occur, such as the formation of oxidation byproducts with ozonation, reduced effectiveness of bacterial inactivation with adsorption on activated carbon, and the challenges related to concentrate disposal and high energy demand with membrane filtration.[9] Consequently, WWTPs often fail to achieve satisfactory removal efficiency, allowing a portion of these pollutants to enter the environment, which raises concerns about public health.[110]

To further reduce the release of ECs and address these disadvantages, it is imperative to enhance and upgrade WWTPs by implementing advanced treatment technologies. [108, 111] Among the available options, advanced oxidation, filtration, and adsorption are economically viable and have been implemented for WWTP upgrade,[9] demonstrating effective EC removal. [106, 112]

1.3.1 Advanced oxidation method

Advanced oxidative processes (AOPs) have gained increasing attention as alternative treatment method in the degradation of toxic organic compounds present in wastewater. This processes, if used under mild conditions, present environmental compatibility, high efficiency, versatility, low energy cost and ease of automation. [113]

AOPs have the capability to completely mineralize persistent organic pollutants into CO_2, water, and inorganic ions or convert them into less toxic and easily degradable forms. These processes use electric current to generate free radicals in situ ($HO•$, $O_2•-$, $HO_2•$) without the need of additional chemical reagents or large amounts of catalyst. AOPs can be employed either before or after conventional treatment, depending on the characteristics of the effluent.[113, 114]

Among AOPs, ozonation is one of the most promising techniques for reducing ECs in WWTPs.[108] Ozonation introduce ozone (O_3) into the water producing highly reactive oxygen species, that target the organic compounds and microorganism present in water preferentially attacking ECs electron-rich or with deprotonated amine groups at low pH. Remarkably, removal up to 90%, has been reported for a wide range of contaminants, including diclofenac and carbamazepine. [108]

Although single ozonation is commonly employed in WWTPs, its application is constrained by certain limitations. These include selective reactions between ECs and ozone, slow and incomplete oxidation, reduced ozone solubility and stability in water, and the potential formation of toxic oxidation by-products when ozone doses are insufficient. Moreover, the methods require high energy consumption, expensiveness due to the short lifetime of ozone, and interference from $HO•$ in wastewater need to be considered for further enhancements in ECs removal.

1.3.2 Filtration

Among physical treatment systems, membrane-based water treatment has proven highly effective in removing many persistent ECs by retaining active biomass. This method exploits filtration of water stream to isolate the contaminants, allowing water to flow through the membrane while molecules are retained and concentrated at the membrane surface.

The efficiency of membrane-based treatment depends on the membrane's characteristics, including porosity, surface charge, and hydrophobicity.[101] Based on these characteristics, filtration can be classified as microfiltration (MF, pore size = 0.1–1 μm), ultrafiltration (UF, pore size = 0.01–0.1 μm), nanofiltration (NF, pore size = 0.001–0.01 μm), and reverse osmosis (RO, pore size = 0.1-1 nm). In reverse osmosis, the filtration process is driven by an osmotic pressure gradient, while in standard membrane filtration, hydrostatic pressure allows water to flow through the membrane (Fig. 1.4). [108] Also physio-chemical properties of ECs (size, concentration, functional group, charge, polarity) and operating conditions (pH, temperature and redox condition) influence the efficiency of treatment.

Non-polar ECs are mainly removed via adsorption onto membrane surface or onto the biofilm layer. In contrast, the adsorption of polar ECs is negligible, and biodegradation becomes the principal mechanism. Removal of ECs via size exclusion can be achieved significantly only with NF and RO membranes. [115]

Membranes have proven to be sustainable and highly effective strategies for removing ECs, and nanocomposite mixed matrix membranes represent a promising frontier in materials innovation to further enhance water treatments. [101] However, higher energy is required during the process (1 kW/m^3 for UF),[116] and the deposition of organic and inorganic matter can lead to membrane fouling. Moreover, ECs are not removed from the environment but are concentrated in the rejected effluent, which requires further treatment before disposal.

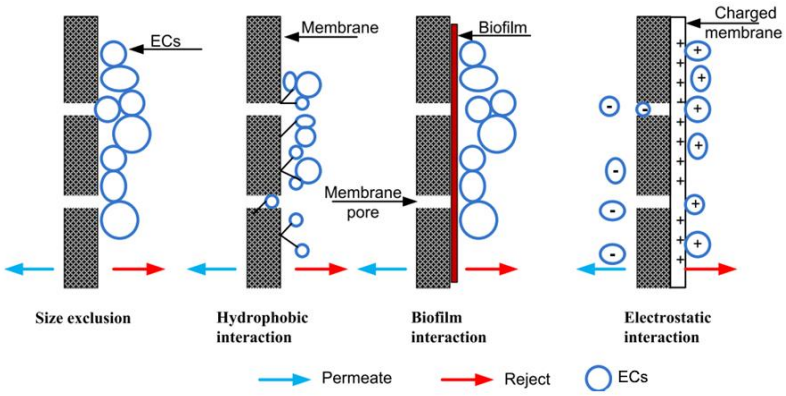

Fig.1.4. Possible mechanism of ECs removal in membrane processes.

1.3.3 Adsorption

Adsorption is a surface phenomenon based on a phase changing mechanism in which the contaminant (*adsorbate*) is removed from water through an adsorption on a solid phase (*sorbent*). This technique has been extensively explored for the

removal of ECs [13] and it is one of the most efficient and reliable, due to its simplicity of use, flexibility and low cost. Additionally, it offers the possibility to recover and reuse the sorbent. [106]

The adsorption efficiency depends on various factors, including the properties of ECs (molecular size, polarity, functional group, K_{OW}, Kd, pKa), environmental conditions (pH, temperature, wastewater type) and on the properties of the sorbent (particle size, surface area, pore diameter, mineral content).

A great plethora of sorbents is currently used to remove ECs from water sources, including activated carbons, zeolites, metal organic framework, bio chars, carbon nanotubes and graphene.[106] Among them all, activated carbon is the most extensively sorbent used, and it is considered as the benchmark,[106] mainly due to his high porosity, large specific surface area and the high degree of surface interactions. The adsorption efficiency is clearly related to the characteristic of the sorbent such as particle size, which distinguishes powder activated carbon (PAC, ~44 µm) and granular activated carbon (GAC 0,6-4 mm). On the other hand, AC can be classified by the pore size, as macroporous (≥50 nm), mesoporous (2–50 nm), and microporous (2−0.8 nm). Moreover, the source of the raw material for AC may led to different carbon structure of the final sorbent, determining a different adsorption capacity.[13]

AC treatments appear as an attractive method for upgrading WWTPs, also due to the easy integration methods. PAC can be added directly in the activated sludge tank or as a post treatment system, like a tertiary filter, but it is difficult to pack in fixed bed and has higher cost if compared to the granular one. Similarly, GAC, which is hard and resistant to abrasion, can be filled into existing sand filters or as a replacement for the upper layer of a tertiary step. [117] However, the operational condition of WWTPs must be considered. For example, the presence of more organic content in the wastewater interferes in ECs removal efficiency by competing for adsorption active sites.

Generally, the advantages of adsorption compared to ozonation are the no-production of by-product and lower energy consumption (Table 1.3).[108]

However, the sustainability of AC production is a significant disadvantage since it requires a high amount of energy. GAC has a smaller CO_2 footprint if compared to PAC due to the possibility to be reused again due to their ability to

be reactivated and reused again. However, the regeneration and reuse require high energy to desorb the adsorbed compounds of higher molecular weight. Furthermore, the saturated sorbent must be properly disposed and treated, for example, using a hot stream that becomes a hazardous waste itself. [118]

Table 1.3. Advantages and limitation of adsorption, membrane filtration and AOP

Technique	Advantages	Limitations
Adsorption	• Simple technique • Wide variety of asorbents to treat various contaminants • Numerous commercial sorbent	• Causes secondary pollution • Regeneration is costly and not effective • Cost of sorbent effect the overall cost of treatment • pH-dependant • Pre-post-treatment required
Membrane filtration	• Small space required • Commercial membrane • Fast and efficient process with high quality effluent	• Investment, maintenance and operating cost are high • Energy required is high • Membrane clogging
Advanced oxidation processes	• In situ radical production • Efficient for recalcitrant pollutants	• Formation of by products • Energy intensive

1.3.4 Point of use (POU)

As discussed in the previous section, the limited effectiveness of current drinking water treatment plants in removing ECs from water sources is not a result of a limitation of WWTPs but rather the rapid emergence of contamination. Wastewater treatment plants are extensive and expensive infrastructure that often operate continuously to supply water to populations. Technological progress in these facilities is extremely slow, primarily because integrating research findings is both time-consuming and financially demanding. This slow progression is inadequate to address the emergence of new ECs that may potentially infiltrate water bodies.

An efficient way to take action is thought the use of Point of Use (POU) technologies, which have emerged as a solution to enable people to improve the quality of drinking water at home through simple, safe, and low-cost treatment methods.[119] This system has already been adopted by households lacking safe water (i.e. China and India),[120] providing an effective and sustainable solution to treat water at home. Their market is significantly increased in the recent years, due to their simplicity and customization capacities.[119, 120] These filtration systems can be directly installed in any water source requiring treatment, and depending on the contaminant, various sorbents can be used, including bio-sand,[121, 122] ceramic,[121] granular activated carbon.[123]

1.4 Nanomaterials

In recent decades, nanotechnology and nanoscience have rapidly advanced, leading to the exploration of advanced nanostructured materials. Thanks to their advantageous and unique properties, nanomaterials provide a sustainable and efficient solutions to contemporary water-related challenges.[124] [125]

Typically, nanomaterials dimensions are in a range between 1 and 100 nm and, thanks to their small size, they result in a reduce number of atoms. This results in a greater surface area-to-volume ratio, leading to unique properties distinct from bulk materials, while their macro-structured properties remain unchanged. Nanomaterials offer versatile solutions for various applications and can be synthesized through top-down or bottom-up approaches using a range of methods, including chemical, physical, mechanical, and biological processes.[125] [126]

Notable examples of these materials include titanium dioxide, zeolite, MXenes, metal-organic frameworks (MOF) and graphene-based materials. Ceramic nanomaterials and 2D crystalline materials, like borophene, germanene, and 2D silica, are also making significant contributions in various applications.[126].

Nanotechnology has emerged significantly, finding many applications across various scientific and technological branches including catalysis, functional coatings, nanoelectronics, sensors [127] and excel in adsorption. [118, 128]

Nanomaterials have proven effective in purifying air and water, enhancing processes like filtration, adsorption, and oxidation.[129] Their high surface area, along with their porosity, provides numerous active sites for interacting with different chemical species, making them excellent sorbents. Driven by the useful application, a great number of porous materials have been developed and among all, carbon-based sorbents (i.e. activated carbon, carbon nanotubes, fullerenes and graphene), are notable for their high adsorption capacity and remarkable thermal stability. [129]

1.4.1 Graphene related materials

Graphene-related materials (GRM) have experienced significant growth in past years, risen great attention in various scientific and technological fields due to their exceptional electronic, thermal, optical, mechanical and morphological properties.

[130] These materials have found utility in numerous sectors, spanning energy storage, catalysis, medicine, sports, environmental remediation, drug delivery, biosensors, strain sensors, antibacterial materials, optics, and optoelectronics. [130]

Structurally, graphene is a 2D material consisting of a single layer of sp^2-hybridized carbon atoms arranged in a honeycomb lattice with the thickness of an atom. This honeycomb lattice serves as the basic building block for other allotropes, including 3-D graphite, 1-D carbon nanotubes (CNT), and 0-D fullerenes. Graphene has a theoretical specific surface area of 2630 m^2g^{-1}, high young's modules (~1.0 TPa) and exceptional thermal conductivity (~5000 $Wm^{-1}K^{-1}$). Additionally, it has optical transparency (~98%) and excellent electrical conductivity, making it a highly valuable option for applications such as transparent conductive electrodes.[131, 132] Moreover, to obtain specific characteristic, graphene materials can be functionalized with various atoms or molecules, such as amine, nucleic acids, proteins and metals. [132]

The synthesis of GRM, as mentioned earlier, primarily employs two approaches: top-down and bottom-up. The top-down approach involves reducing larger carbon structures to create graphene (i.e. exfoliation of a layer of graphene from a graphitic materials), while the bottom-up approach entails building graphene from molecular precursors. The bottom-up approach is simple, but yields materials with relatively higher defect density compared to the top-down method. In contrast, top-down methods involve separating stacked sheets by disrupting the van der Waals forces binding them together, causing sheet damage during exfoliation and re-agglomeration of separated sheets.[132]

Graphene oxide (GO) is obtained by oxidizing graphite, transforming it into a single-atomic layered material with epoxy groups, hydroxyl groups, and carboxyl group on the basal plan of graphite layers. [128] One of the earliest attempts to synthetized GO was made by Brodie in 1859, using $KClO_3$ and fuming HNO_3 to oxidize graphite, resulting in GO with C/O ratio of 2.2 and good solubility in water. Variation such as Staudenmaier's and Hofmann's methods have been proposed. The most commonly used technique is the Hummer method, which employs $KMnO_4$, $H2SO_4$, and $NaNO_3$, resulting in GO with a C/O ratio around 2.25 (Fig.1.5).[130, 133, 134]

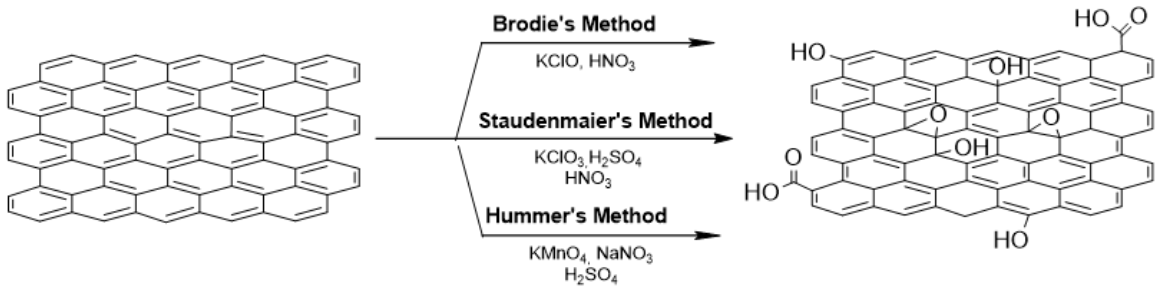

***Fig. 1.5**. Graphene oxide synthesis methods*

All the mentioned methods introduce polar oxygenated groups to the surface of GO, providing advantages such as functionalization and hydrophilicity, enabling dispersibility in solvents, particularly in water. In contrast, graphene has poor water solubility, limiting its applicability in certain areas. [135]

However, these oxygen groups can lead to disadvantages such as electrical insulation in GO. Nevertheless, the conductivity of GO can be partially restored by chemically reducing it with agents, like hydrazine or ascorbic acid. The obtained material, reduced graphene oxide (rGO), recovers a conjugated structure and shares properties with pristine graphene, differing for the presence of some residual functional oxygenated group on the surface. By regulating the quantity of retained functional groups, the electrical performance and solubility of rGO can be easily controlled (Fig. 1.6). [135]

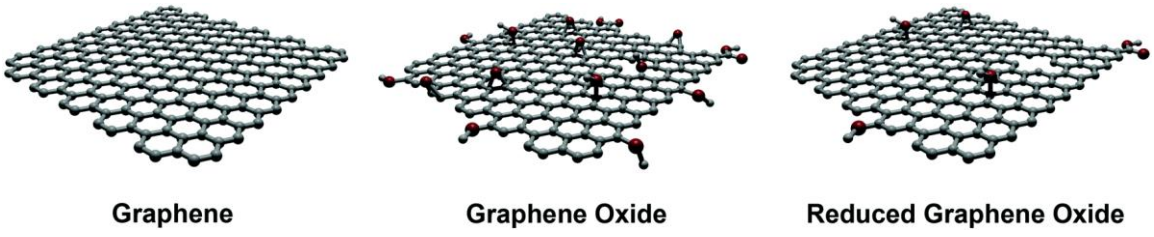

***Fig. 1.6**. Molecular structure of graphene, GO and rGO (adapted with permission, [136] published by RSC)*

1.4.2 Graphene in water treatments

GRM have gained significant attention in environmental applications, particularly in water and wastewater treatments. These materials are characterized by their highly hydrophobic surfaces, open-layer structures, and strong adsorption affinity for a wide range of contaminants (i.e. organic contaminants organic dyes, metallic ions, PFAS). The use of graphene for the adsorption of various classes of organic contaminants (i.e., polycyclic aromatic hydrocarbons (PAHs), halogenated aliphatic, pharmaceuticals and personal care products (PPCPs), plasticizers,

pesticide, dyestuff, and polychlorinated biphenyls (PCBs)) has been reported in the literature. [132]

Among GRM, GO exhibits distinctive adsorption characteristics due to its surface oxygenated groups, which reduce hydrophobicity and enhance its reactivity, making it a suitable candidate for adsorption applications. These oxygen functionalities, particularly carboxylic acids, epoxy groups, and hydroxyl groups, introduce a negative charge to the GO surface, facilitating electrostatic interactions with cationic organic dyes. GO also serves as a potential sorbent for metal ion complexation through both electrostatic and coordinate bonding approaches. [137]

Additionally, hydrogen bonding can occur through the oxygen groups, covalently bonded to GO, and H of contaminant, bonded to a highly electro-negative atom. Aromaticity in GO enables π-π interactions with aromatic organic pollutants, resulting in noncovalent bonds with pollutants possessing aromatic rings. Moreover, the functional groups present on GO, including carboxylic acids, epoxy rings, and hydroxyl groups, provide reactive sites for further functionalization, allowing a broad range of modifications and enhancing its versatility (Fig.1.7).[138] For example, the epoxy ring on the surface of GO is available and can be easily opened by the nucleophilic attack.[139, 140]

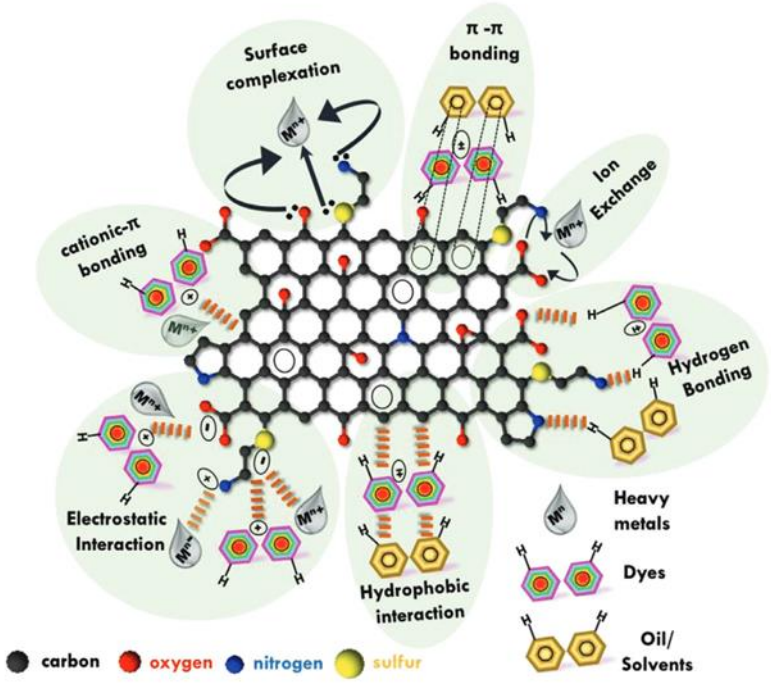

Fig. 1.7. *Overview of possible interaction mechanisms between contaminants and graphene oxide in water system. Adapted with permission, published by ACS.*[141]

To further enhance the potential of GO in water treatment, it is possible to integrate inorganic particles (i.e. TiO_2, ZnO), including metal and non-metal nanoparticles and their oxides, with graphene-based materials.[128]

However, one of the main challenges still under evaluation pertains to the fate, transformations, and toxicological impacts of GRM in the environment, which have already been explored in the literature.[138] Detailed ecotoxicological assessments are still necessary to identify the best graphene-based nanomaterials. Additionally, graphene presents limitations in separations and reuse after adsorption, which may lead to secondary contamination. These disadvantages constrain the application of graphene for the removal of contaminants.[142]

To address these issues, the synthesis of 3D graphene materials has been explored,[143] resulting in the creation of aerogels or hydrogels employed in water remediation. [144-146] Chitosan and alginate have been used due to their biocompatibility and non-toxicity to create graphene-polymer composites. This solution has emerged as a promising alternative for water purification, including the removal of metals (i.e. GO-Chitosan with a capacity of 202.5 mg/g for Cu(II)).[144, 147] These composites exhibit excellent tolerance to changes in pH, can be stored for later use, and are easier to handle than GO nanosheets.[142]

Finally, composite materials of GRM with synthetic polymers have been widely studied, driven by the versatile applications of polymers.[148-150] As membrane technology rapidly advances for various purposes, including water purification,[151] various polymer, such as PVDF,[152] PP,[153] PS,[154] PES[155] have been used as matrices and GO have been employed as material for membrane manufacture.[149] These membranes, whether in flat sheet or hollow fiber structures, enhance the capabilities of graphene in seawater desalination and wastewater treatment. They combine the microfiltration (MF) or ultrafiltration (UF) properties of membranes with the adsorption capacity of GO.[156]

1.5 References

1. B. S. Rathi, P. S. Kumar and D.-V. N. Vo, *Sci. Total Environ.*, 2021, **797**, 149134.
2. T. Backhaus, *Environmental Sciences Europe*, 2023, **35**, 22.
3. https://sdgs.un.org/goals,
4. R. Bhattacharya and D. Bose, 2023, **42**, e14018.
5. https://eur-lex.europa.eu/legal-content/EN/TXT/?uri=CELEX%3A32020L2184 , 2020
6. G. Teijon, L. Candela, K. Tamoh, A. Molina-Díaz and A. R. Fernández-Alba, *Sci. Total Environ.*, 2010, **408**, 3584-3595.
7. L. Rizzo, A. Fiorentino, M. Grassi, D. Attanasio and M. Guida, *J. Environ. Chem. Eng*, 2015, **3**, 122-128.
8. P. Krzeminski, M. C. Tomei, P. Karaolia, A. Langenhoff, C. M. R. Almeida, E. Felis, F. Gritten, H. R. Andersen, T. Fernandes, C. M. Manaia, L. Rizzo and D. Fatta-Kassinos, *Sci. Total Environ.*, 2019, **648**, 1052-1081.
9. L. Rizzo, S. Malato, D. Antakyali, V. G. Beretsou, M. B. Đolić, W. Gernjak, E. Heath, I. Ivancev-Tumbas, P. Karaolia, A. R. Lado Ribeiro, G. Mascolo, C. S. McArdell, H. Schaar, A. M. T. Silva and D. Fatta-Kassinos, *Sci. Total Environ.*, 2019, **655**, 986-1008.
10. M. Puri, K. Gandhi and M. S. Kumar, *J. Environ. Manage.*, 2023, **332**, 117344.
11. R. Kumar, M. Qureshi, D. K. Vishwakarma, N. Al-Ansari, A. Kuriqi, A. Elbeltagi and A. Saraswat, *Case Stud. Chem. Environ. Eng.*, 2022, **6**, 100219.
12. B. Petrie, R. Barden and B. Kasprzyk-Hordern, *Water Res.*, 2015, **72**, 3-27.
13. O. M. Rodriguez-Narvaez, J. M. Peralta-Hernandez, A. Goonetilleke and E. R. Bandala, *Chem. Eng. J.*, 2017, **323**, 361-380.
14. J. T. Thompson, B. Chen, J. A. Bowden and T. G. Townsend, *Environmental Science & Technology Letters*, 2023, **10**, 234-239.
15. F. Riva, S. Castiglioni, E. Fattore, A. Manenti, E. Davoli and E. Zuccato, *Int. J. Hyg. Environ. Health*, 2018, **221**, 451-457.
16. N. Morin-Crini, E. Lichtfouse, G. Liu, V. Balaram, A. R. L. Ribeiro, Z. Lu, F. Stock, E. Carmona, M. R. Teixeira, L. A. Picos-Corrales, J. C. Moreno-Piraján, L. Giraldo, C. Li, A. Pandey, D. Hocquet, G. Torri and G. Crini, *Environ. Chem. Lett.*, 2022, **20**, 2311-2338.
17. https://nepis.epa.gov/Exe/ZyPURL.cgi?Dockey=P100LTG6.txt
18. S. Khan, M. Naushad, M. Govarthanan, J. Iqbal and S. M. Alfadul, *Environ. Res.*, 2022, **207**, 112609.
19. Y. Luo, W. Guo, H. H. Ngo, L. D. Nghiem, F. I. Hai, J. Zhang, S. Liang and X. C. Wang, *Sci. Total Environ.*, 2014, **473-474**, 619-641.
20. S. Khan, Z. Dan, Y. Mengling, Y. Yang, H. Haiyan and J. Hao, *Fullerenes, Nanotubes and Carbon Nanostructures*, 2018, **26**, 158-167.
21. C. J. Houtman, *Journal of Integrative Environmental Sciences*, 2010, **7**, 271-295.
22. N. Caporale, M. Leemans, L. Birgersson, P.-L. Germain, C. Cheroni, G. Borbély, E. Engdahl, C. Lindh, R. B. Bressan, F. Cavallo, N. E. Chorev, G. A. D'Agostino, S. M. Pollard, M. T. Rigoli, E. Tenderini, A. L. Tobon, S. Trattaro, F. Troglio, M. Zanella, Å. Bergman, P. Damdimopoulou, M. Jönsson, W. Kiess, E. Kitraki, H. Kiviranta, E. Nånberg, M. Öberg, P. Rantakokko, C. Rudén, O. Söder, C.-G. Bornehag, B. Demeneix, J.-B. Fini, C. Gennings, J. Rüegg, J. Sturve and G. Testa, 2022, **375**, eabe8244.

23. M. Du, M. Zheng, A. Liu, L. Wang, X. Pan, J. Liu and X. Ran, *Sci. Total Environ.*, 2022, **832**, 155118.
24. C. Zamora-Ledezma, D. Negrete-Bolagay, F. Figueroa, E. Zamora-Ledezma, M. Ni, F. Alexis and V. H. Guerrero, *Environmental Technology & Innovation*, 2021, **22**, 101504.
25. G. Gupta, J. Khan and N. K. Singh, *Materials Today: Proceedings*, 2021, **43**, 2958-2964.
26. P. B. Tchounwou, C. G. Yedjou, A. K. Patlolla and D. J. Sutton, in *Molecular, Clinical and Environmental Toxicology: Volume 3: Environmental Toxicology*, ed. A. Luch, Springer Basel, Basel, 2012, DOI: 10.1007/978-3-7643-8340-4_6, pp. 133-164.
27. A. Kumar, M. Cabral-Pinto, A. Kumar, M. Kumar and P. A. Dinis, 2020, **10**, 7078.
28. Q. Zhou, N. Yang, Y. Li, B. Ren, X. Ding, H. Bian and X. Yao, *Global Ecology and Conservation*, 2020, **22**, e00925.
29. M. M. S. Cabral-Pinto, M. Inácio, O. Neves, A. A. Almeida, E. Pinto, B. Oliveiros and E. A. Ferreira da Silva, *Exposure and Health*, 2020, **12**, 629-640.
30. M. M. S. Cabral Pinto, P. Marinho-Reis, A. Almeida, E. Pinto, O. Neves, M. Inácio, B. Gerardo, S. Freitas, M. R. Simões, P. A. Dinis, L. Diniz, E. Ferreira da Silva and P. I. Moreira, 2019, **16**, 4560.
31. A. García-Miranda Ferrari, P. Carrington, S. J. Rowley-Neale and C. E. Banks, *Environ. Sci. Water Res. Technol.*, 2020, **6**, 2676-2690.
32. S. Rajendran, T. A. K. Priya, K. S. Khoo, T. K. A. Hoang, H.-S. Ng, H. S. H. Munawaroh, C. Karaman, Y. Orooji and P. L. Show, *Chemosphere*, 2022, **287**, 132369.
33. A. Nikolaou, S. Meric and D. Fatta, *Anal. Bioanal. Chem.*, 2007, **387**, 1225-1234.
34. S. A. Snyder, *OzSE*, 2008, **30**, 65-69.
35. M. S. Shamsudin, S. F. Azha and S. Ismail, *J. Environ. Chem. Eng*, 2022, **10**, 107541.
36. H. Xu, S. Zhu, M. Xia and F. Wang, *J. Hazard. Mater.*, 2021, **402**, 123815.
37. M. Ashfaq, K. Nawaz Khan, M. Saif Ur Rehman, G. Mustafa, M. Faizan Nazar, Q. Sun, J. Iqbal, S. I. Mulla and C.-P. Yu, *Ecotoxicol. Environ. Saf.*, 2017, **136**, 31-39.
38. L. Lonappan, S. K. Brar, R. K. Das, M. Verma and R. Y. Surampalli, *Environ. Int.*, 2016, **96**, 127-138.
39. V. K. Parida, D. Saidulu, A. Majumder, A. Srivastava, B. Gupta and A. K. Gupta, *J. Environ. Chem. Eng*, 2021, **9**, 105966.
40. M. Patel, R. Kumar, K. Kishor, T. Mlsna, C. U. Pittman, Jr. and D. Mohan, *Chem. Rev.*, 2019, **119**, 3510-3673.
41. T. Xiong, X. Yuan, H. Wang, Z. Wu, L. Jiang, L. Leng, K. Xi, X. Cao and G. Zeng, *Chem. Eng. J.*, 2019, **366**, 83-91.
42. M. S. de Ilurdoz, J. J. Sadhwani and J. V. Reboso, *J. Water Process Eng.*, 2022, **45**, 102474.
43. M. G. Oliveira, M. P. Spaolonzi, E. D. V. Duarte, H. P. S. Costa, M. G. C. da Silva and M. G. A. Vieira, *Environ. Res.*, 2023, **233**, 116503.
44. P. Kovalakova, L. Cizmas, T. J. McDonald, B. Marsalek, M. Feng and V. K. Sharma, *Chemosphere*, 2020, **251**, 126351.
45. T. Mathai, T. Pal, N. Prakash and S. Mukherji, *Biosens. Bioelectron.*, 2023, **237**, 115478.
46. R. Hernández-Tenorio, E. González-Juárez, J. L. Guzmán-Mar, L. Hinojosa-Reyes and A. Hernández-Ramírez, *Journal of Hazardous Materials Advances*, 2022, **8**, 100172.

47. M. Kumar, B. Ram, R. Honda, C. Poopipattana, V. D. Canh, T. Chaminda and H. Furumai, *Sci. Total Environ.*, 2019, **693**, 133640.
48. Â. Almeida, A. M. V. M. Soares, V. I. Esteves and R. Freitas, *Environ. Toxicol. Pharmacol.*, 2021, **86**, 103661.
49. Y. Zhang, S.-U. Geißen and C. Gal, *Chemosphere*, 2008, **73**, 1151-1161.
50. A. F. Ambrósio, P. Soares-da-Silva, C. M. Carvalho and A. P. Carvalho, *Neurochem. Res.*, 2002, **27**, 121-130.
51. P. Verlicchi, M. Al Aukidy and E. Zambello, *Sci. Total Environ.*, 2012, **429**, 123-155.
52. S. Ebrahimzadeh, S. Castiglioni, F. Riva, E. Zuccato and A. Azzellino, 2021, **13**, 2539.
53. M. Biel-Maeso, R. M. Baena-Nogueras, C. Corada-Fernández and P. A. Lara-Martín, *Sci. Total Environ.*, 2018, **612**, 649-659.
54. M. A. Décima, S. Marzeddu, M. Barchiesi, C. Di Marcantonio, A. Chiavola and M. R. Boni, 2021, **13**, 11760.
55. F. I. Hai, S. Yang, M. B. Asif, V. Sencadas, S. Shawkat, M. Sanderson-Smith, J. Gorman, Z.-Q. Xu and K. Yamamoto, 2018, **10**, 107.
56. L. H. M. L. M. Santos, A. N. Araújo, A. Fachini, A. Pena, C. Delerue-Matos and M. C. B. S. M. Montenegro, *J. Hazard. Mater.*, 2010, **175**, 45-95.
57. S. Webb, T. Ternes, M. Gibert and K. Olejniczak, *Toxicol. Lett.*, 2003, **142**, 157-167.
58. S. Kim and K. Choi, *Environ. Int.*, 2014, **70**, 143-157.
59. P. Chaturvedi, P. Shukla, B. S. Giri, P. Chowdhary, R. Chandra, P. Gupta and A. Pandey, *Environ. Res.*, 2021, **194**, 110664.
60. M. Esperanza, M. Seoane, C. Rioboo, C. Herrero and Á. Cid, *Sci. Total Environ.*, 2019, **669**, 412-420.
61. L. R. Vieira, A. M. V. M. Soares and R. Freitas, *Chemosphere*, 2022, **286**, 131675.
62. I. Anastopoulos, I. Pashalidis, A. G. Orfanos, I. D. Manariotis, T. Tatarchuk, L. Sellaoui, A. Bonilla-Petriciolet, A. Mittal and A. Núñez-Delgado, *J. Environ. Manage.*, 2020, **261**, 110236.
63. T. Deblonde, C. Cossu-Leguille and P. Hartemann, *Int. J. Hyg. Environ. Health*, 2011, **214**, 442-448.
64. P. Sharma, H. Kaur, M. Sharma and V. Sahore, *Environ. Monit. Assess.*, 2011, **183**, 151-195.
65. S. Singh, N. Parveen and H. Gupta, *Environmental Technology & Innovation*, 2018, **12**, 189-195.
66. A. K. Al-Buriahi, A. A. Al-Gheethi, P. Senthil Kumar, R. M. S. Radin Mohamed, H. Yusof, A. F. Alshalif and N. A. Khalifa, *Chemosphere*, 2022, **287**, 132162.
67. T. L. Yusuf, B. O. Orimolade, D. Masekela, B. Mamba and N. Mabuba, *RSC Advances*, 2022, **12**, 26176-26191.
68. J. Sharma, S. Sharma, U. Bhatt and V. Soni, *Journal of Hazardous Materials Letters*, 2022, **3**, 100069.
69. M. Imran, D. E. Crowley, A. Khalid, S. Hussain, M. W. Mumtaz and M. Arshad, *Reviews in Environmental Science and Bio/Technology*, 2015, **14**, 73-92.
70. L. N. Vandenberg, R. Hauser, M. Marcus, N. Olea and W. V. Welshons, *Reprod. Toxicol.*, 2007, **24**, 139-177.
71. S. Lu, Y. Yu, L. Ren, X. Zhang, G. Liu and Y. Yu, *Sci. Total Environ.*, 2018, **621**, 1389-1396.
72. J. Dueñas-Moreno, A. Mora, P. Cervantes-Avilés and J. Mahlknecht, *Environ. Int.*, 2022, **170**, 107550.

73. M. Deng, X. Han, J. Ge, X. Liang, B. Du, J. Li and L. Zeng, *J. Hazard. Mater.*, 2021, **413**, 125322.
74. U. Kotowska, J. Kapelewska and R. Sawczuk, *Environ. Pollut.*, 2020, **267**, 115643.
75. S. Saha, N. Narayanan, N. Singh and S. Gupta, *International Journal of Environmental Science and Technology*, 2022, **19**, 11459-11474.
76. T. Salaudeen, O. Okoh, F. Agunbiade and A. Okoh, *Chemosphere*, 2018, **203**, 336-344.
77. Y. Qian, X. Jia, T. Ding, M. Yang, B. Yang and J. Li, *Sci. Total Environ.*, 2021, **758**, 143606.
78. L. E. Lesser, A. Mora, C. Moreau, J. Mahlknecht, A. Hernández-Antonio, A. I. Ramírez and H. Barrios-Piña, *Chemosphere*, 2018, **198**, 510-521.
79. P. Li, D. Karunanidhi, T. Subramani and K. Srinivasamoorthy, *Arch. Environ. Contam. Toxicol.*, 2021, **80**, 1-10.
80. L. G. T. Gaines, 2023, **66**, 353-378.
81. G. K. Longendyke, S. Katel and Y. Wang, *Environmental Science: Processes & Impacts*, 2022, **24**, 196-208.
82. S. Kurwadkar, J. Dane, S. R. Kanel, M. N. Nadagouda, R. W. Cawdrey, B. Ambade, G. C. Struckhoff and R. Wilkin, *Sci. Total Environ.*, 2022, **809**, 151003.
83. C. F. Kwiatkowski, D. Q. Andrews, L. S. Birnbaum, T. A. Bruton, J. C. DeWitt, D. R. U. Knappe, M. V. Maffini, M. F. Miller, K. E. Pelch, A. Reade, A. Soehl, X. Trier, M. Venier, C. C. Wagner, Z. Wang and A. Blum, *Environmental Science & Technology Letters*, 2020, **7**, 532-543.
84. V. Mulabagal, L. Liu, J. Qi, C. Wilson and J. S. Hayworth, *Talanta*, 2018, **190**, 95-102.
85. R. Kumar, T. K. Dada, A. Whelan, P. Cannon, M. Sheehan, L. Reeves and E. Antunes, *J. Hazard. Mater.*, 2023, **452**, 131212.
86. R. A. Dickman and D. S. Aga, *J. Hazard. Mater.*, 2022, **436**, 129120.
87. L. Gobelius, C. Persson, K. Wiberg and L. Ahrens, *J. Hazard. Mater.*, 2019, **362**, 230-237.
88. M. G. E. Guardian, E. G. Boongaling, V. R. R. Bernardo-Boongaling, J. Gamonchuang, T. Boontongto, R. Burakham, P. Arnnok and D. S. Aga, *Chemosphere*, 2020, **256**, 127115.
89. M. Sun, E. Arevalo, M. Strynar, A. Lindstrom, M. Richardson, B. Kearns, A. Pickett, C. Smith and D. R. U. Knappe, *Environmental Science & Technology Letters*, 2016, **3**, 415-419.
90. E. F. Houtz, C. P. Higgins, J. A. Field and D. L. Sedlak, *Environ. Sci. Technol.*, 2013, **47**, 8187-8195.
91. K. A. Barzen-Hanson, S. C. Roberts, S. Choyke, K. Oetjen, A. McAlees, N. Riddell, R. McCrindle, P. L. Ferguson, C. P. Higgins and J. A. Field, *Environ. Sci. Technol.*, 2017, **51**, 2047-2057.
92. B. Xu, S. Liu, J. L. Zhou, C. Zheng, J. Weifeng, B. Chen, T. Zhang and W. Qiu, *J. Hazard. Mater.*, 2021, **412**, 125159.
93. F. Li, J. Duan, S. Tian, H. Ji, Y. Zhu, Z. Wei and D. Zhao, *Chem. Eng. J.*, 2020, **380**, 122506.
94. H. Brunn, G. Arnold, W. Körner, G. Rippen, K. G. Steinhäuser and I. Valentin, *Environmental Sciences Europe*, 2023, **35**, 20.

95. S. E. Mousavi, J. M. Delgado-Saborit and L. Godderis, *J. Hazard. Mater.*, 2021, **405**, 124256.
96. I. Zabaleta, E. Bizkarguenaga, D. Bilbao, N. Etxebarria, A. Prieto and O. Zuloaga, *Talanta*, 2016, **152**, 353-363.
97. S. Genualdi, N. Jeong, L. deJager and T. Begley, *Food Additives & Contaminants: Part A*, 2017, **34**, 2181-2189.
98. G. Pitter, F. D. Re, C. Canova, G. Barbieri, M. Z. Jeddi, F. Daprà, F. Manea, R. Zolin, A. M. Bettega, G. Stopazzolo, S. Vittorii, L. Zambelli, M. Martuzzi, D. Mantoan and F. Russo, 2020, **128**, 027007.
99. G. R. Johnson, M. L. Brusseau, K. C. Carroll, G. R. Tick and C. M. Duncan, *Sci. Total Environ.*, 2022, **841**, 156602.
100. T. Ruan and G. Jiang, *TrAC, Trends Anal. Chem.*, 2017, **95**, 122-131.
101. M. K. Shahid, A. Kashif, A. Fuwad and Y. Choi, *Coord. Chem. Rev.*, 2021, **442**, 213993.
102. V. Boiteux, X. Dauchy, C. Bach, A. Colin, J. Hemard, V. Sagres, C. Rosin and J.-F. Munoz, *Sci. Total Environ.*, 2017, **583**, 393-400.
103. T. A. Ternes, M. Meisenheimer, D. McDowell, F. Sacher, H.-J. Brauch, B. Haist-Gulde, G. Preuss, U. Wilme and N. Zulei-Seibert, *Environ. Sci. Technol.*, 2002, **36**, 3855-3863.
104. M. Petrovic, A. Diaz, F. Ventura and D. Barceló, *Environ. Sci. Technol.*, 2003, **37**, 4442-4448.
105. P. Westerhoff, Y. Yoon, S. Snyder and E. Wert, *Environ. Sci. Technol.*, 2005, **39**, 6649-6663.
106. B. S. Rathi, P. S. Kumar and P.-L. Show, *J. Hazard. Mater.*, 2021, **409**, 124413.
107. N. H. Tran, M. Reinhard and K. Y.-H. Gin, *Water Res.*, 2018, **133**, 182-207.
108. P. R. Rout, T. C. Zhang, P. Bhunia and R. Y. Surampalli, *Sci. Total Environ.*, 2021, **753**, 141990.
109. M. de Oliveira, B. E. F. Frihling, J. Velasques, F. J. C. M. Filho, P. S. Cavalheri and L. Migliolo, *Sci. Total Environ.*, 2020, **705**, 135568.
110. D. P. Mohapatra and D. M. Kirpalani, 2019, **97**, 2621-2631.
111. P. Roccaro, *Current Opinion in Environmental Science & Health*, 2018, **2**, 46-54.
112. J. F. J. R. Pesqueira, M. F. R. Pereira and A. M. T. Silva, *Journal of Cleaner Production*, 2020, **261**, 121078.
113. D. da Silva Vilar, N. H. Torres, R. N. Bharagava, M. Bilal, H. M. N. Iqbal, G. R. Salazar-Banda, K. I. B. Eguiluz and L. F. R. Ferreira, in *Microbe Mediated Remediation of Environmental Contaminants*, eds. A. Kumar, V. K. Singh, P. Singh and V. K. Mishra, Woodhead Publishing, 2021, DOI: https://doi.org/10.1016/B978-0-12-821199-1.00001-8, pp. 1-14.
114. F. C. Moreira, R. A. R. Boaventura, E. Brillas and V. J. P. Vilar, *Applied Catalysis B: Environmental*, 2017, **202**, 217-261.
115. R. B. Schäfer, P. C. von der Ohe, R. Kühne, G. Schüürmann and M. Liess, *Environ. Sci. Technol.*, 2011, **45**, 6167-6174.
116. E. Arkhangelsky, I. Levitsky and V. Gitis, *Water Supply*, 2017, **17**, 1212-1218.
117. R. Soni, S. Bhardwaj and D. P. Shukla, in *Inorganic Pollutants in Water*, eds. P. Devi, P. Singh and S. K. Kansal, Elsevier, 2020, DOI: https://doi.org/10.1016/B978-0-12-818965-8.00014-7, pp. 273-295.

118. A. I. Shah, M. U. Din Dar, R. A. Bhat, J. P. Singh, K. Singh and S. A. Bhat, *Ecol. Eng.*, 2020, **152**, 105882.
119. B. L. S. Freitas, U. C. Terin, N. M. N. Fava, P. M. F. Maciel, L. A. T. Garcia, R. C. Medeiros, M. Oliveira, P. Fernandez-Ibañez, J. A. Byrne and L. P. Sabogal-Paz, *Water Res.*, 2022, **208**, 117870.
120. P. Westerhoff, P. Alvarez, Q. Li, J. Gardea-Torresdey and J. Zimmerman, *Environ. Sci.: Nano*, 2016, **3**, 1241-1253.
121. E. Menya, J. Jjagwe, H. M. Kalibbala, H. Storz and P. W. Olupot, *Chem. Eng. Res. Des.*, 2023, **192**, 412-440.
122. J. Magdalera, P. A. Sanchez, M. Sobremisana and R. Bautista, 2020, 19-5080.
123. L. Fewtrell, B. Majuru and P. R. Hunter, *Environ. Health*, 2017, **16**, 66.
124. H. Lu, J. Wang, M. Stoller, T. Wang, Y. Bao and H. Hao, *Advances in Materials Science and Engineering*, 2016, **2016**, 4964828.
125. K. K. Singh, A. Singh and S. Rai, *Materials Today: Proceedings*, 2022, **51**, 1157-1163.
126. T. A. Saleh, *Environmental Technology & Innovation*, 2020, **20**, 101067.
127. L. A. Kolahalam, I. V. Kasi Viswanath, B. S. Diwakar, B. Govindh, V. Reddy and Y. L. N. Murthy, *Materials Today: Proceedings*, 2019, **18**, 2182-2190.
128. N. Baig, Ihsanullah, M. Sajid and T. A. Saleh, *J. Environ. Manage.*, 2019, **244**, 370-382.
129. C. Santhosh, V. Velmurugan, G. Jacob, S. K. Jeong, A. N. Grace and A. Bhatnagar, *Chem. Eng. J.*, 2016, **306**, 1116-1137.
130. S. A. Mazari, E. Ali, R. Abro, F. S. A. Khan, I. Ahmed, M. Ahmed, S. Nizamuddin, T. H. Siddiqui, N. Hossain, N. M. Mubarak and A. Shah, *J. Environ. Chem. Eng*, 2021, **9**, 105028.
131. Y. Zhu, S. Murali, W. Cai, X. Li, J. W. Suk, J. R. Potts and R. S. Ruoff, 2010, **22**, 3906-3924.
132. G. Ersan, O. G. Apul, F. Perreault and T. Karanfil, *Water Res.*, 2017, **126**, 385-398.
133. A. Jiříčková, O. Jankovský, Z. Sofer and D. Sedmidubský, 2022, **15**, 920.
134. H. L. Poh, F. Šaněk, A. Ambrosi, G. Zhao, Z. Sofer and M. Pumera, *Nanoscale*, 2012, **4**, 3515-3522.
135. W.-P. Zhu, S.-P. Sun, J. Gao, F.-J. Fu and T.-S. Chung, *J. Membr. Sci.*, 2014, **456**, 117-127.
136. G. Reina, J. M. González-Domínguez, A. Criado, E. Vázquez, A. Bianco and M. Prato, *Chem. Soc. Rev.*, 2017, **46**, 4400-4416.
137. R. K. Thines, N. M. Mubarak, S. Nizamuddin, J. N. Sahu, E. C. Abdullah and P. Ganesan, *J. Taiwan Inst. Chem. Eng.*, 2017, **72**, 116-133.
138. P. L. Yap, S. Kabiri, Y. L. Auyoong, D. N. H. Tran and D. Losic, *ACS Omega*, 2019, **4**, 19787-19798.
139. S. Mantovani, S. Khaliha, L. Favaretto, C. Bettini, A. Bianchi, A. Kovtun, M. Zambianchi, M. Gazzano, B. Casentini, V. Palermo and M. Melucci, *Chem. Commun.*, 2021, **57**, 3765-3768.
140. S. Mantovani, S. Khaliha, T. D. Marforio, A. Kovtun, L. Favaretto, F. Tunioli, A. Bianchi, G. Petrone, A. Liscio, V. Palermo, M. Calvaresi, M. L. Navacchia and M. Melucci, *Chem. Commun.*, 2022, **58**, 9766-9769.
141. P. L. Yap, M. J. Nine, K. Hassan, T. T. Tung, D. N. H. Tran and D. Losic, 2021, **31**, 2007356.

142. M.-f. Li, Y.-g. Liu, G.-m. Zeng, N. Liu and S.-b. Liu, *Chemosphere*, 2019, **226**, 360-380.
143. Q. Zhang, Q. Hou, G. Huang and Q. Fan, *Environ. Sci. Pollut. Res.*, 2020, **27**, 190-209.
144. G. Z. Kyzas and K. A. Matis, *J. Mol. Liq.*, 2015, **203**, 159-168.
145. Xuetonng Yang and S. S. Ling Xia, 2017, **24**, 1730001.
146. X. Yi, F. Sun, Z. Han, F. Han, J. He, M. Ou, J. Gu and X. Xu, *Ecotoxicol. Environ. Saf.*, 2018, **158**, 309-318.
147. Y. Yang, W.-q. Wu, H.-h. Zhou, Z.-y. Huang, T.-t. Ye, R. Liu and Y.-f. Kuang, *Journal of Central South University*, 2014, **21**, 2826-2831.
148. D. An, L. Yang, T.-J. Wang and B. Liu, *Industrial & Engineering Chemistry Research*, 2016, **55**, 4803-4810.
149. R. K. Joshi, S. Alwarappan, M. Yoshimura, V. Sahajwalla and Y. Nishina, *Applied Materials Today*, 2015, **1**, 1-12.
150. R. M. Nauman Javed, A. Al-Othman, M. Tawalbeh and A. G. Olabi, *Renewable and Sustainable Energy Reviews*, 2022, **168**, 112836.
151. Y.-C. An, X.-X. Gao, W.-L. Jiang, J.-L. Han, Y. Ye, T.-M. Chen, R.-Y. Ren, J.-H. Zhang, B. Liang, Z.-L. Li, A.-J. Wang and N.-Q. Ren, *Environ. Res.*, 2023, **223**, 115409.
152. Y. Fan, X. Quan, H. Zhao, S. Chen, H. Yu, Y. Zhang and Q. Zhang, 2017, **134**.
153. F. M. Kafiah, Z. Khan, A. Ibrahim, R. Karnik, M. Atieh and T. Laoui, *Desalination*, 2016, **388**, 29-37.
154. S. Nasseri, S. Ebrahimi, M. Abtahi and R. Saeedi, *J. Environ. Manage.*, 2018, **205**, 174-182.
155. N. Gholami and H. Mahdavi, 2018, **37**, 3529-3541.
156. N. F. D. Junaidi, N. H. Othman, M. Z. Shahruddin, N. H. Alias, F. Marpani, W. J. Lau and A. F. Ismail, 2020, **95**, 1308-1320.

2 Aim of the thesis

This thesis explores the potential of graphene-based materials as innovative technologies for the removal of emerging contaminants (ECs) from drinking water, contributing to the advancement of sustainable water treatment technologies. To simulate real-case conditions, municipal tap water from Bologna was used as matrix and spiked with contaminants of environmental interest. In the following chapters will be investigated various aspect of graphene-based materials and their application as sorbent in water purification.

The first step to understand the possible application of graphene as sorbent involved investigating the interaction and adsorption mechanisms occurring between graphene and organic molecules. This study, extensively discussed in **Chapter 3,** involved various types of graphene materials with different surface chemistry (i.e. different number of defects on the nanosheet structure, which correlate with the amount of oxygenated group). A deep understanding of the role of oxygenated groups and sheets structure in the adsorption mechanism is crucial to enabling the tailoring of new materials with specific and maximized sorption properties. The role of defects on selectivity adsorption was evaluated trough dedicated experiments, supported by molecular dynamic simulations. Additionally, isotherm studies with selected contaminants were then performed, to deeply evaluate the maximum adsorption capacity of graphene materials, compared to standard and state-of-the-art sorbents.

After demonstrating the adsorption capacity of graphene, **Chapter 4** propose a procedure to use GO nanosheets as sorbent in real application. We demonstrated that microfiltration through commercial hollow fiber module (PES-HF) enables the complete retention of both nanosheets and pollutants.This procedure, called GO + MF, demonstrates the successful recovery, washing, and reuse of nanosheets and filtration module.

Chapter 5 proposes a further technology based on hollow fiber membranes, introducing coextruded PSU-GO hollow fibers (HFs) for Point of use (POU) drinking water purification. The preparation and characterization of these HFs is described, focusing on their filtration capabilities, adsorption-ultrafiltration properties. The study emphasizes the benefits of these HFs over traditional

Granular Activated Carbon (GAC) filters and ensures the absence of GO release into treated water.

Chapter 6 presents chemically modified nanosheets, demonstrating the possibility to tune adsorption selectivity of GO and widen its application. Amino acids (i.e. Lysine, Methionine and Glutamate) were chosen as building blocks to tune the surface chemistry due to their availability, small size, and large chemical variety. The obtained modified nanosheets (GO-Lys, GO-Met and GO-Glu) exhibit different selectivity and higher adsorption capacities for specific contaminants compared to standard GO, correlating the enhanced performance with the amino acid loading.

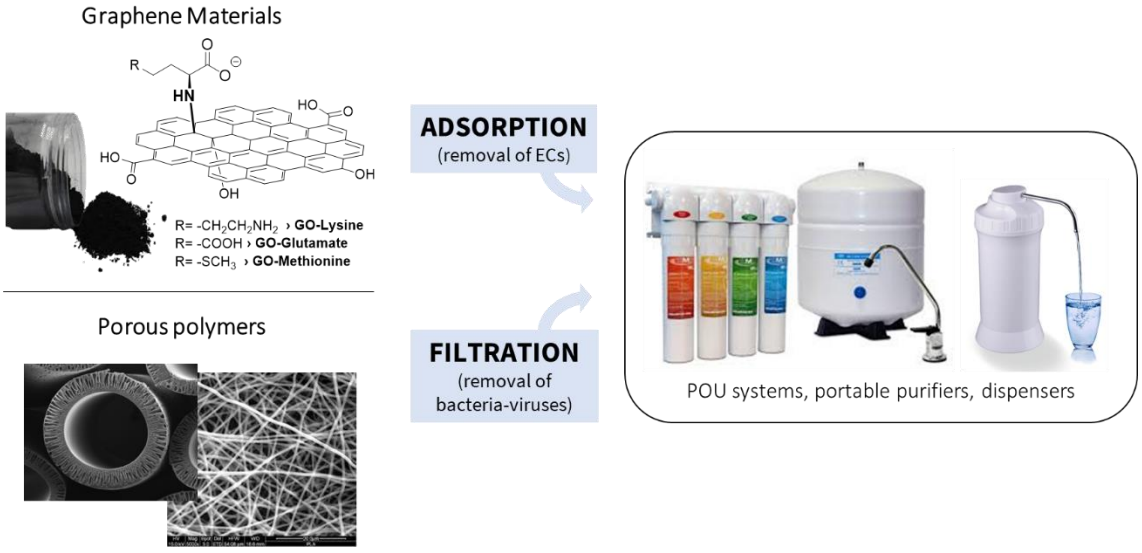

Fig.2.1 *Aim of the thesis: development of POU drinking water system exploiting adsorption properties of graphene materials and filtration capacity of porous membranes.*

3 Insight on Graphene oxide adsorption mechanism

Defective graphene nanosheets for drinking water purification: Adsorption mechanism, performance, and recovery

Adapted with permission from FlatChem, 29, (2021), 100283, Elsevier
DOI 10.1016/j.flatc.2021.100283

3.1 Introduction

The occurrence of the so called 'emerging contaminants' in worldwide surface, ground and even drinking water is currently one of the most urgent challenges to be faced to answer to the United Nations sustainable Goal 6 'Ensure access to water and sanitation for all'.[1-4] The European Commission has recently published the new Drinking Water Directive EU2020/2184,[5] which regulates the quality of EU waters and aims to the enhancement of public access to safe water. It also introduces the water safety plan approach. Such new and more stringent requirements ask to the water suppliers and operators to be ready to exploit new and efficient depuration strategies when required. In particular, new technologies are required for the removal of the so-called Emerging Contaminants (ECs [6], including Personal Care and Pharmaceutical Products (PCPPs), additives, dyes), compounds that are largely used at domestic and industrial level and that are strongly resistant to conventional depuration strategies.[7] In this scenario, due to their chemical versatility and high surface-area nanomaterials have shown high potential as active systems for adsorption, photocatalytic degradation and oxidation of ECs for water purification purposes.[8, 9] Nanometal oxides such as aluminum oxide (Al_2O_3), magnetite (Fe_3O_4), zinc oxide (ZnO), silicon dioxide (SiO_2), and titanium oxide (TiO_2), as well as carbon nanotubes, have been extensively studied.[10, 11] Adsorption or synergic adsorption-photodegradation of heavy metals, dyes and organic compounds with removal capacity up to hundreds mg per g of sorbent have been reported.[12-15]

Among nanomaterials, graphene derivatives are receiving increasing interest in this sector, mainly due to the large commercial availability, high surface area and promising results in both adsorption and filtration scenarios.[16-18]

We have recently demonstrated the possibility to exploit graphene oxide (GO) to integrate adsorption functionality in commercially available polysulfone hollow fiber filtration modules and to enhance the range of application of such filters in the adsorption of ECs from drinking water.[19]

For instance, high adsorption efficiency was demonstrated for core-shell polyethersulfone-GO (PES-GO) hollow fibers in the removal of OFLOX, a fluoroquinolone antibiotic (molecular structure in Fig. 8.1, Appendix).[20] We found for this material an adsorption performance more than three order of magnitude higher than that of powdered activated carbon (PAC) ,about 14 mg/g for GO and 20µg/g for PAC, respectively.[21]

The adsorption of this molecule seems to be mainly driven by an interplay of surface interaction with GO oxygenated groups, this possibly explaining the higher adsorption capacity with respect to activated carbon. However, a clear understanding on the role of oxygenated groups and sheets structure in the adsorption mechanism is still missing, this limiting the possibility to tailor new materials with specific and maximized sorption properties. Aiming to a deeper understanding of the adsorption mechanisms on graphene nanosheets, here we consider different types of GO having a different amount of carboxylic (O-C=O) and carbonyl groups (C=O groups), i.e. Hummers derived GO (hGO), Brodie derived GO (bGO) and reduced GO (rGO) with a decreasing number of ‘defects’ in the order rGO-hGO-bGO.

Hummers and Brodie preparation procedures consist of oxidation of graphite in harsh conditions, by using potassium permanganate and sodium nitrate in sulphuric acid for Hummers method and fuming nitric acid and sodium chlorate for Brodie method, respectively.

bGO and hGO are similar in oxidation degree and some general properties but also distinctly different in many other properties.[22] Indeed, bGO shows higher temperature of exfoliation,[23] very different swelling properties,[24, 25] superior mechanical strength of single flakes,[26] and multilayered membranes,[27] swelling transitions not found in hGO[28, 29] and sorption properties.[30] bGO also has fewer defects and more homogeneous distribution of functional groups over its surface.[30, 31] hGO shows a relatively high percentage of carbonyl and carboxyl groups with a significant number of holes in the flakes and a stronger disruption of the graphene structure.[27]

We compared the adsorption properties of these materials to that of a tailored highly defected graphene sample, namely defective GO (dGO), having and higher number of holes and vacancies in GO sheets associated to an increased number of carbonyl and carboxylic (C=O and O-C=O) groups, which is associated with the amount of holes.[32] Thanks to such peculiarity, dGO provides an ideal case study to establish the relationships between graphene sheets chemical functionalization and structure and adsorption performance.

We compared the selectivity of these materials toward a mixture of eight ECs (Fig. 8.1, Appendix) and studied more deeply the molecules-sorbent interaction mechanisms through molecular dynamic (MD) simulations to gain predictive and general rules to select the best graphene sorbents case-by-case. The selection includes drugs as Ofloxacin (OFLOX)[33], a fluoroquinolone antibiotic, Bisphenol A (BPA),[3] used in food and drink packaging, and Benzophenone-3 (BP3),[34] which use in organic UV filters has resulted in extensive release into the aquatic environment.[6]

We then estimated the adsorption performance in terms of number of sites of each specific pair substrate–molecule and nature of molecule-molecule and molecule-substrate interactions, through dedicated isotherms studies performed on a selection of ECs of environmental concern, two fluoroquinolone antibiotics and a textile dye, (Fig. 8.1, Appendix). Furthermore, we compared the maximum adsorption capacity of GO samples to that of the Granular Activated Carbon (GAC), the industrial adsorption standard technology, and demonstrated the superior sorption capability of dGO.[35] Finally, targeting a real exploitation for water treatment, we demonstrated that dGO sheets can be removed from treated water by ultrafiltration on commercial hollow fiber modules.[36]

3.2 Experimental

3.2.1 Materials

hGO was purchased by Abalonyx, bGO was synthesized according to Brodie method using one step oxidation,[30, 31] while dGO was prepared according to previously reported procedures.[32] Ofloxacin (OFLOX), diclofenac (DCF), benzophenone-4 (BP4), carbamazepine (CBZ), bisphenol A (BPA), benzophenone-3 (BP3), rhodamine B (RhB), methylene Blue (MB), ciprofloxacin

(CIPRO) and caffeine (CAF) were purchased by Sigma-Aldrich and used without any further purification (Fig. 8.1 Appendix).

3.2.2 Synthesis of rGO. and dGO

GO powder (4 g in one batch) was thermally exfoliated in air inside of large volume container (1-1.5 L) made of aluminum foil. The container was not sealed tightly to allow evolving gases to escape. The container was rapidly inserted into a furnace pre-heated to 240°C, annealed for 6 minutes with the furnace door closed and removed from the furnace to provide rapid cooling. Rapid heating results in the explosion of GO powder and formation of rGO powder.[37] This procedure for preparation of rGO provides maximal BET surface area according to our earlier studies.[38] Using higher exfoliation temperatures, vacuum or inert gas does not provide advantages for achieving higher surface area but using a relatively large volume of the container is essential.[38] Higher gas pressure (above ambient) has an adverse effect on exfoliation.[37] The rGO powder was used as a precursor for the oxidation using standard Hummer's procedure but with adjusted proportions between reagents.

For the synthesis of dGO, 1 g of sodium nitrate was added into 40 mL sulfuric acid while stirring. 1 g of rGO was then added and the whole container placed into an ice bath while stirring. Next, 1 g of potassium permanganate was slowly added to the mixture with frequent controls of the suspension temperature, keeping it below ~20°C as this is a very exothermic process. When all the potassium permanganate was added, the suspension was stirred for 2 h, counted after the first introduction of potassium permanganate. The container was then placed in an oil bath and heated at 30°C for 1 h. The container was then placed back into the ice bath and 40 mL of deionized water was very slowly added, as this too is a very exothermic process. Once the water was added to the suspension and the reaction seemed to stop, the container was placed back into the oil bath and maintained at 90°C for 15 minutes. The suspension was then taken out of the oil bath and placed at room temperature. 90mL of 6% hydrogen peroxide was then added and the mixture was left stirring overnight at room temperature. Finally, the mixture was rinsed by washing with 10% hydrochloric acid as following: the mixture was poured in centrifugation containers and mixed with the acid solution, well shaken and centrifuged (Allegra 64R Centrifuge, Beckman Coulter) at 10.000 rpm for 10 minutes. This washing process was repeated 6 times. Then, the

remaining material was repeatedly washed with deionized water until the pH of the solution was around 4 to 5. The mixture was shaken each time and centrifuged at 20.000 rpm for 30 minutes. The product was vacuum filtered using 1 μm PTFE membrane (Omnipore, ref JAWP04700) and freeze dried over a few days. The preparation of a batch using 9 g rGO resulted in 8.6 g dGO, which is a yield of 95.5%. TEM and SEM images of dGO flakes and aggregates are shown in Fig. 8.2, Appendix.

3.2.3 Characterization

Composition and relative abundance of carbon-oxygen groups were obtained from X-Ray Photoelectron spectroscopy (XPS). XPS spectra of rGO and bGO were recorded with an Axis Ultra DLD spectrometer (Kratos Analytical Limited, Great Britain) using Al Kα radiation (hv =1486.6 eV, 150 W). The pass energy of the analyzer was 160 eV for survey spectra and 40 eV for high resolution scans. A Kratos charge neutralizer system was used, and the binding energy scale was adjusted with respect to the C1s line of aliphatic carbon set at 285.0 eV. All spectra were processed with the Kratos software and analysed as described in reference[32] and are shown in Appendix (Fig. 8.3-8.6 Appendix). SEM/TEM full characterization of dGO, bGO and hGO (from the same synthesis batches) by XRD, FTIR, TGA and microscopy was presented in our earlier studies.[30, 32]

3.2.4 Selectivity-kinetic experiments

GO, rGO, dGO and bGO (milliQ dispersion at 1 mg/mL) were sonicated for 3 h, then 5 mL of the resulting dispersion was added to 100 mL of the mixture of ECs (Fig. 8.1 Appendix) (conc. 5 mg/L each in tap water). The solution was then left in darkness under gentle agitation for 24 h. During this time, 1 mL withdrawals were made after contact times of 15 min, 1 h, 4 h, 24 h and after centrifugation of the samples (10 min/10.000 rpm), then HPLC analyses were performed.

3.2.5 HPLC method analysis

HPLC analyses of the selected ECs in mixture were performed on a Dyonex Ultimate 3000 system equipped with a diode array detector. 0.5 mL samples were used as sources for the automated injection. The chromatographic separation was performed on a reverse phase Zorbax XDB-C8 column (4.6 x 150 mm, 5 μm) at flow rate of 1.0 mL/min, detection at λmax of each analyte, linear gradient TFA 0.05% aqueous solution/acetonitrile from 80:20 to 0:100. In every experiment, the removal of each analyte was determined by comparison with that of the initial

untreated solution. The results are expressed as the mean of three independent experiments ± SD.

3.2.6 Molecular Dynamics simulations

The Amber force field (ff14SB)[39] was used to parameterize OFLOX and RhB molecules; atomic charges were obtained by standard procedures, compatible with the used force field, using quantum-mechanical (QM) calculation at the HF/6-31G(d) level of theory, followed by a Restrained Electrostatic Potential (RESP) calculation.

The model-systems representing reduced rGO, dGO, hGO and bGO were modelled on a 40 Å x 40 Å graphene sheet created with VMD.[40] The epoxy, hydroxyl, carbonyl, and carboxylic acid groups were randomly positioned on rGO, dGO and hGO/bGO to reproduce the experimental XPS data (Fig. 8.3-8.6, Appendix).[32] Three different sized vacancies (~7, ~12 and ~16 Å of diameter) were generated on the dGO[32] and carbonyl and carboxylic acid groups were placed on the vacancy rim. The General Amber Force Field (GAFF)[41] was used to describe rGO, dGO and hGO/bGO and atomic charges were obtained by AM1 calculations. An accurate sampling of the interactions of OFLOX and RhB on rGO, dGO and hGO/bGO was carried out placing the two molecules on 16 different positions of the graphene sheet (Fig. 3.1). Each complex was inserted into a box of TIP3P[42] water molecules and counterions were added to neutralize the total charge.

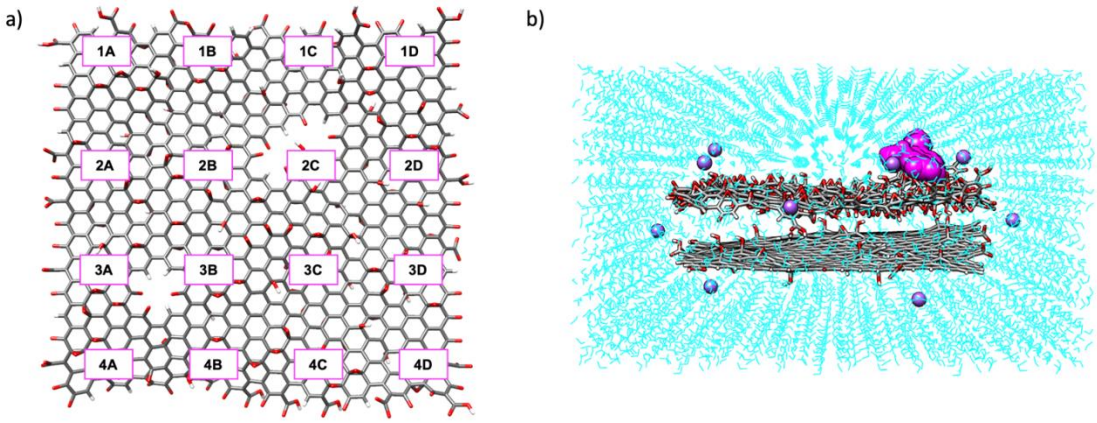

Fig. 3.1. *a)Sampling of the interactions of OFLOX and RhB with "graphene" using 16 diverse initial positions on the graphene sheet. b) Representative initial snapshot of the constructed system which was implemented in the MD simulations.*

Molecular Mechanics – Generalized Born Surface Area (MM-GBSA) method[43, 44] implemented in Amber 16.0 software package,[40] was applied to

compute the binding affinity of OFLOX and RhB (ligands) to rGO, dGO and hGO/bGO. For each calculation, 5000 frames were used, extracting the snapshots from the MD trajectories.

From the MD trajectories, a set of 100 frames was extracted. These snapshots were used to identify the cavities and calculate their volumes, using Surfnet,[45] a tool implemented in Chimera.[46]

Molecular electrostatic potential (MEP) maps of OFLOX and RhB were obtained from the RESP charges calculated during the parametrization step of the molecules, employing Gaussian16 software[47] and the cubegen utility.[47]

3.2.7 Isotherms experiments

The adsorption isotherm of the selected contaminants (RhB, OFLOX and CIPRO) on the different GO samples were performed at fixed concentration of contaminant by varying the amount of sorbent. In a total volume (5 mL, milliQ water) of hGO suspension sonicated 2 h at different concentration, RhB or OFLOX or CIPRO were added. The solutions were gently stirred in darkness for 24 h and then centrifuged at 10.000 rpm for 10 min. The solutions were analyzed by UV-vis spectroscopy. Isotherms were fitted by BET and Langmuir models and the equation, are reported in Appendix (Table 8.1). The saturation concentration Cs present in BET equation was optimized during the fit and, to be physically significant, it was constrained at the maximum value of solubility experimentally determined for each molecule: 3 mg/mL for OFLOX, 2 mg/mL for RhB and 1 mg/mL for CIPRO.[48]

3.3 Results and Discussion

3.3.1 Graphene materials

Extremely defect rich dGO (Fig. 3.2d) was prepared according to previously reported procedures.[32] Briefly, explosive thermal exfoliation of graphite oxide was used to prepare rGO with high abundance of holes and vacancy defects. Defects and holes are additionally introduced by reoxidation of this rGO using Hummers method (with reduced amount of $KMnO_4$ compared to standard procedure), thus providing an extremely defect-rich material.[32] Defects in our procedure are created in 3 steps. It is well known that some defects/holes are introduced in process of Hummers oxidation of graphite.[49, 50] On the second step, we explosively exfoliate hGO to produce rather defected rGO. The defects created in the exfoliation step

are mostly holes and point defects since carbon oxides are evolved in process of thermal annealing.[38] When rGO is oxidized again by Hummers procedure, we keep the holes of precursor rGO but also add new defects in process of oxidation. The increase in the number of defects can be followed by change in XPS spectra and increased signals from double bonded carbon(Fig. 8.3-8.6, Appendix).[32]

The graphene sheets simplified structure and defects (i.e. holes and vacancies, increasing on going from bGO to dGO) for the different graphene types herein considered are reported in Fig. 3.2.

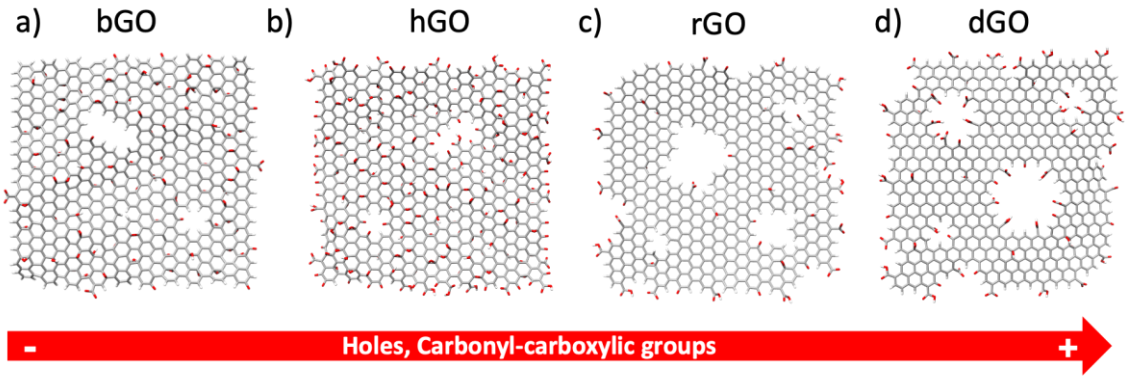

Fig. 3.2. *Models of the different graphene structures used in this work. Top view of a) Brodie GO (bGO), b) Hummer derived GO (hGO), c) reduced GO (rGO), d) defected GO (dGO). The models simplify the degree of holes and carbonyl-carboxylic defects of each type of graphene. Representative SEM-TEM images of dGO flakes and aggregates are shown in Fig. 8.2 Appendix.*

3.3.2 Characterization

The size of dGO (1:1) particles was analyzed using TEM and SEM. Full characterization (TGA, FTIR, XRD, AFM) was provide in a previous publication. [30, 32, 51]

Most of the particles were found to be in the range 30-100 nm but few particles of larger size were also detected (Fig. 8.2, Appendix). The particles tend to aggregate when precipitated even using diluted dispersions and individual flakes can be difficult to distinguish SEM.

The oxidation degree of dGO determined by XPS (Fig. 8.5, Appendix) was C/O=2.7 and confirmed using TGA recorded under nitrogen. The total weight loss over a temperature interval from ambient up to 700°C was about 55%, similar to standard hGO (~60%). However, standard hGO shows most of the weight loss in two sharp steps, first due to water desorption below 100°C (~8%) and second due to the removal of oxygen functional groups from the planar surface around 150-240°C (~30%). The TGA trace of dGO shows both steps typical for standard hGO

but only about 12% of weight is lost due to the removal of oxygen from the planar surface. The main weight loss (~24%) in dGO occurs gradually at temperatures above ~350°C which is usually assigned to the removal of oxygen groups (mostly carboxylic and carbonyls) attached to edges. dGO showed no peaks from (001) reflection in XRD providing evidence for strongly disrupted layer structure of individual flakes preventing it from ordered packing.

FTIR spectra of dGO showed much weaker peaks typically assigned to C-O-C and C-OH reflecting the extremely defect nature of this material and the absence of sufficient planar surface for these functional groups.

Brodie GO was prepared using 1 step oxidation using slightly modified procedure[15] and additional characterization of bGO is also available in reference [52].

Detailed characterization (TGA, FTIR, XRD, AFM) of this hGO batch was provide in a previous publication. [51]

Brodie graphite oxide generally shows smaller d(001), narrower and stronger diffraction peaks compared to hGO. The values of d(001) were found at ambient air conditions 6.34 Å and 7.8 Å for bGO and hGO respectively. Flake size was determined for bGO and hGO using dispersions deposited on Si surface and evaluated using AFM or SEM images. The size of bGO and hGO flakes is also very similar, typically in the range of few micrometers. However, when sonication is applied to prepare dispersions the size of flakes is reduced to average size of 0.2-0.3 micrometers independently on initial size.

TGA traces of bGO and hGO are distinctly different. The main de-oxygenation step is found at lower temperatures for hGO (maximum rate at 210˚C) and much sharper step at higher temperatures for bGO (255°C).

Smaller inter-layer distance and number of defects in bGO results in better layer packing and higher thermal exfoliation temperature.

FTIR of bGO shows absence of typical for hGO peak of sulphate group impurity and smaller intensity of C-OH and C=O peaks.

3.3.3 Adsorption kinetic and selectivity

Adsorption experiments were carried out by using dispersion of graphene nanosheets in tap water spiked with the mixture at 5ppm each of 8 ECs (Fig.8.1, Appendix). Results as removal percentage for each contaminant at contact time of 15 min, 1 h, 4 h and 24 h are shown in Fig. 3.3.

In all of the cases, removal was independent on the sorbent-sorbates contact time and similar values were observed at 15 min and 24 h. The only exception was observed for the removal of OFLOX by dGO which increased from 57% at 15 min to 72% at 24 h (Fig. 3.3c). Significant differences between GO samples in removal efficiency were observed only for two molecules: RhB and OFLOX, with higher removal of OFLOX for dGO (up to 72% at 24h) and RhB for rGO (up to 96% at 24h).

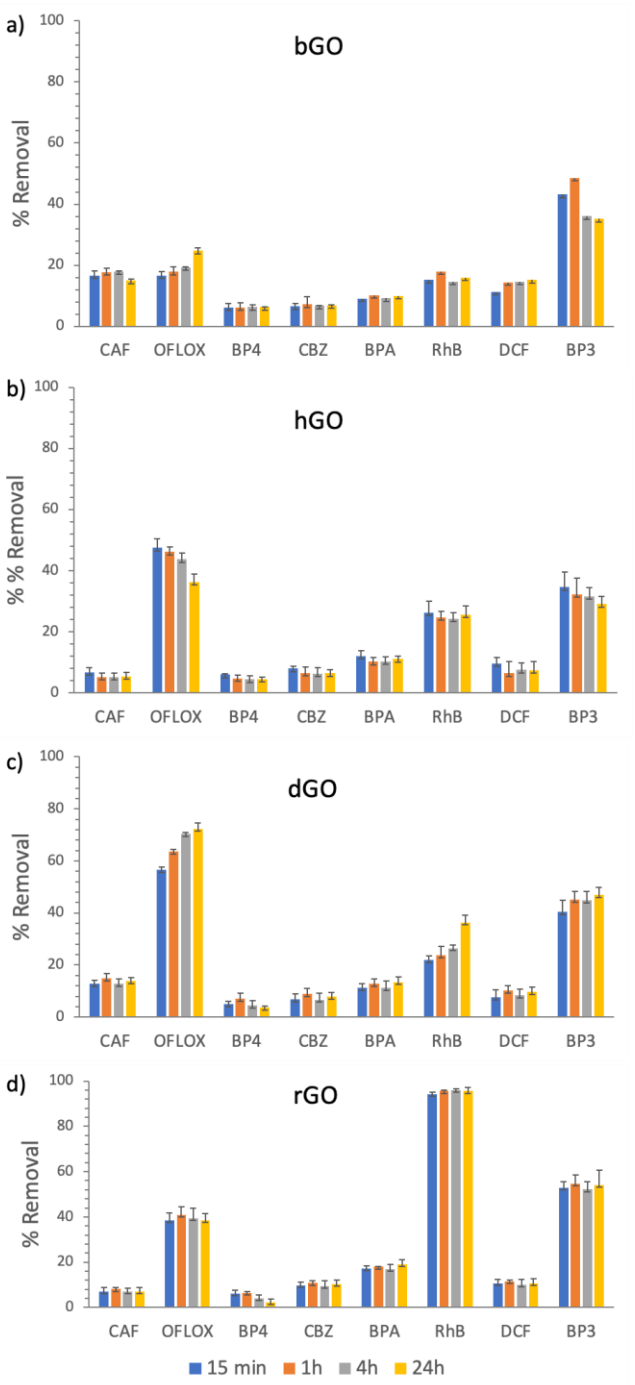

Fig. 3.3. *Removal % of the different GO samples at contact times 15 min,1 h, 4 h, 24 h for the mixture of selected ECs.*

3.3.4 Molecular Dynamic simulations

Molecular Dynamic (MD) simulations were carried out in order to explain the observed selectivity trend and get some insight on molecule-graphene interaction mechanisms, in relation to OFLOX and RhB. MD simulations could indeed reveal the most favorable adsorption sites[53] of the molecules on the different types of graphene oxide and determine quantitatively their binding energy.[54, 55]

3.3.4.1 Interactions of OFLOX and RhB with oxidized graphenes (bGO and hGO).

The calculated interaction energies of OFLOX and RhB with oxidized hGO and bGO were very similar (-26.5 and -26.1 kcal mol^{-1}, respectively), reflecting the close adsorption values experimentally observed (Fig. 3.3) and confirming that adsorption of OFLOX was slightly favored than that of RhB (Fig. 3.4) due to better electrostatic interactions with GO.

Indeed, even if the net charge of the two molecules is the same, the molecular electrostatic potential (MEP) of OFLOX shows a strong localization of the positive charge, while in RhB the positive charge is delocalized by resonance on the aromatic system (Fig 3.4c). Therefore, the electrostatic interactions of the negatively charged types of GO (bGO and hGO) are larger with OFLOX than with RhB. For the same reason, sorption of OFLOX on hGO was better than on bGO due to the larger number of carboxylic groups, negatively charged in aqueous solutions, present in hGO.[56]

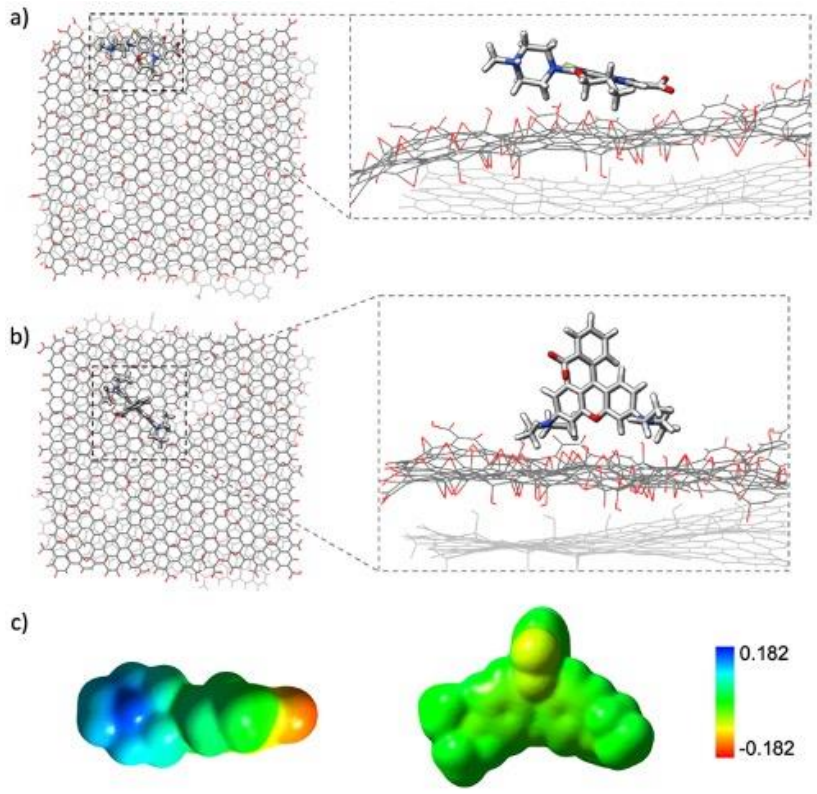

Fig. 3.4. *The adsorption of a) OFLOX and b) RhB on GO. Water molecules were omitted for clarity. c) Molecular electrostatic potential (MEP) surfaces of the OFLOX (on the left) and RhB (on the right) calculated using the RESP charges.*

3.3.4.2 Interactions of OFLOX and RhB with reduced graphene oxide (rGO)

In agreement with experimental results, showing higher affinity of rGO for RhB than for OFLOX, the calculated interaction energies of RhB and OFLOX on rGO were respectively -38.8 and -29.4 kcal mol^{-1}. The higher interaction of RhB with rGO, with respect to OFLOX, can be ascribed to the ability of the planar aromatic system of RhB to form π-π interactions with the extended sp^2-surface of the graphene sheet (Fig. 3.5).

For a deeper understanding of the observed selectivity, we also considered the change in solvent accessible surface area (ΔSASA) upon molecule adsorption, which can measure the surface complementarity between the planar structure of rGO and the two molecules. Upon binding ΔSASA, values were -98.5 ± 28.3 $Å^2$ for OFLOX and -130.3 ± 29.9 $Å^2$ for RhB, explaining the improved adsorption of RhB on rGO with respect to OFLOX.

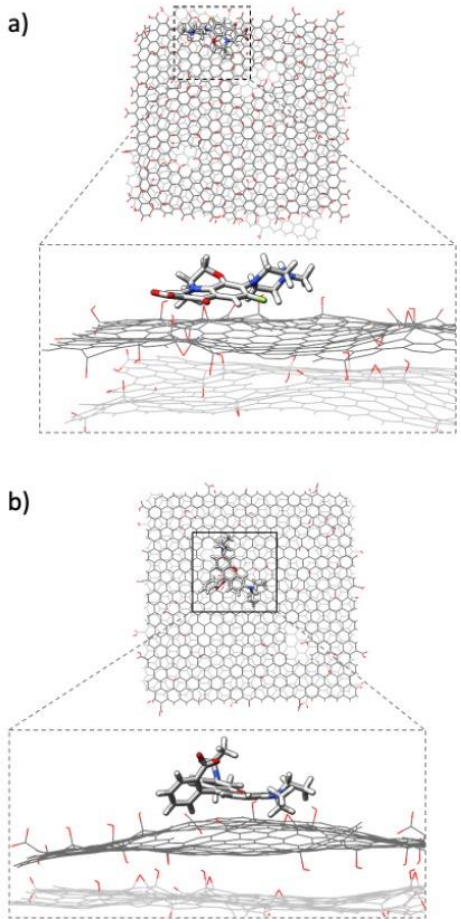

***Fig. 3.5**. Adsorption of a) OFLOX and b) RhB on rGO. Water molecules were omitted for clarity.*

3.3.4.3 Interactions of OFLOX and RhB with defective graphene oxide (dGO)

As shown in Fig. 3.3, the adsorption of OFLOX at 24 h was higher than that of RhB. The interaction energies of the molecules on dGO reproduced this trend since adsorption energy of OFLOX and RhB were respectively -32.0 and -30.6 kcal mol^{-1}. More importantly, the favorite adsorption site was different for the two molecules, indeed, while OFLOX can be trapped inside the holes present on the surface of graphene, RhB prefers a planar adsorption site lying on the basal plane of graphene sheet (Fig. 3.6).

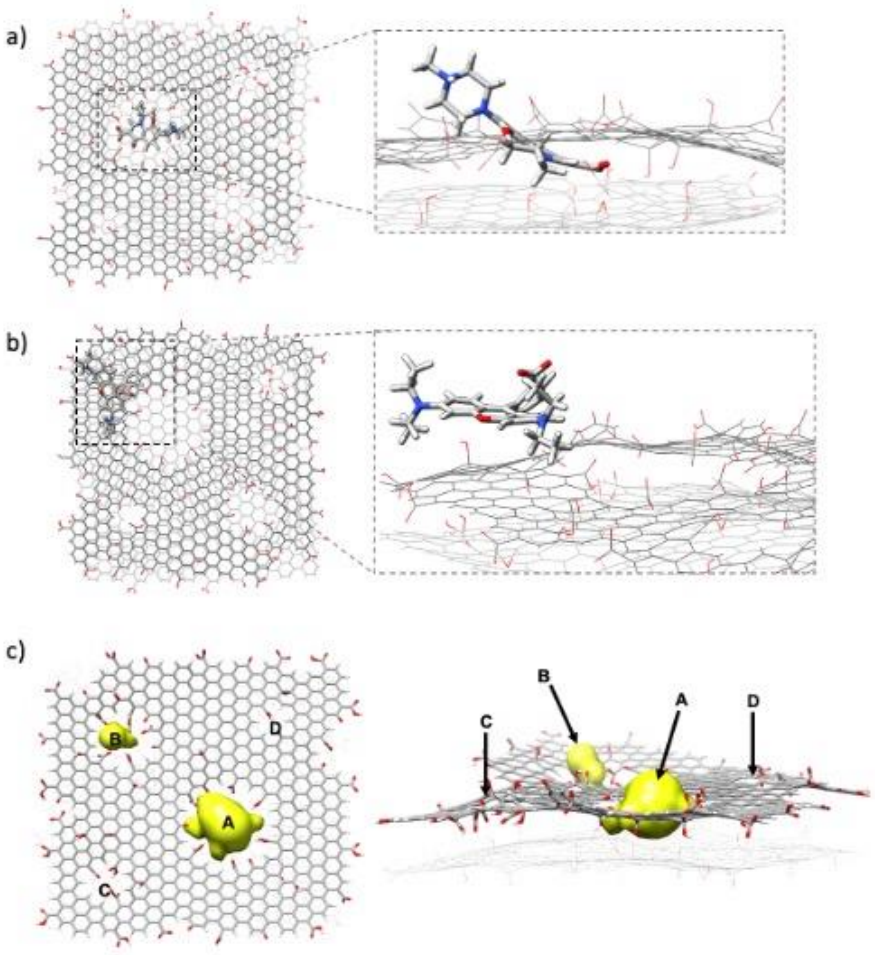

Fig. 3.6. *Adsorption of a) OFLOX and b) RhB on dGO. Water molecules were omitted for clarity. c) Molecular cavities determined by CHIMERA.*

In order to shed light on this behavior, a comparison between the dimension of the cavities formed by the graphene holes and the size of the molecules was carried out.

During the MD simulations, the holes present on the graphene sheets generated cavities characterized by a mean volume of 331.4 ± 22.4 $Å^3$ (Cavity A) and 79.5 ± 16.6 $Å^3$ (Cavity B) (Fig. 3.6). Given that the molecular volumes calculated for OFLOX and RhB are 284.4 ± 1.7 $Å^3$ and 388.5 ± 3.0 $Å^3$, it can be concluded that OFLOX fits with the larger cavities generated by the holes in dGO, while RhB is too large and interacts with the planar surface of graphene, explaining the observed higher selectivity of dGO for OFLOX. The driving force for the interaction between OFLOX and the holes is shape complementarity, as it is observed in the interactions between carbon nanomaterials and biomolecules.[57-61]

3.3.5 Adsorption isotherms and performances

Given the strong differences in adsorption selectivity of GO samples and their environmental concern, the maximum adsorption capacities (Qm) of OFLOX and RhB were investigated by dedicated adsorption isotherms experiments. Qm can give an estimation on the number of active sites where OFLOX or RhB can be adsorbed as well as the application potential of GO materials as sorbent for water purification. Moreover, given the strong selectivity of dGO observed for OFLOX we investigated the adsorption properties toward another fluoroquinolone antibiotic included in the EU watch list of priority contaminants, ciprofloxacin (CIPRO).[62] Two models were used for fitting the isotherms: i) the BET model considers a multilayer adsorption, where the molecule-molecule interaction is like molecule-substrate one; while ii) the Langmuir model considers only a single monolayer and a much stronger molecule-substrate interaction.

The results of the fitting are reported in in Appendix, (Fig. 8.7-8.9), while Table 3.1 summarizes the Qm obtained by the best fitting model as well as the estimation of C=O/O-C=O groups (that correlate with the number of holes and vacancies present in the graphene) determined by XPS. Isotherms of GAC for OFLOX and Methylene Blue (MB) and rGO with MB are reported in Appendix (Fig. 8.10 and 8.11).

Langmuir model was the best fitting for dGO toward all of the molecules, i.e., the molecule-substrate interaction is dominant on such 2D material. Additionally, the significantly higher Qm of OFLOX on dGO suggests a richer availability of adsorption sites on dGO respect to other materials.

The sorption capacity of three types of GO was correlated to their defect state and then compared to rGO (Fig. 3.7). According to our earlier studies,[32] the defect state of GO can be evaluated using C1s XPS spectra and relative number of carbon atoms functionalized with C=O/O-C=O groups as indicator. Such groups can be formed only on the edges of GO sheets and at-point defects. The edge atoms in GO sheets must also include edges of holes to explain relatively high abundance of C=O/O-C=O groups relative to the size of flakes. The relative number of C=O/O-C=O groups used as an indicator (Table 3.1), suggested the following trend of holes and vacancies abundance, i.e. bGO (1.6%) < hGO (8.3%) < dGO (18.4%). Accordingly, in dGO the high number of defects affects also the typical planar surface of GO nanosheets. The increase of holes and vacancies in

the set bGO-hGO-dGO correlates well with the increase of OFLOX, CIPRO and MB sorption capacity. On the other hand, there is no correlation between number of holes and vacancies and RhB sorption ability (Table 3.1). As discussed above, the driving force of the sorption of RhB by graphene sheets is due to π-π interactions.

Table 3.1. *Monolayer adsorption capacity (Qm) obtained from the fit of isotherms. A Langmuir, B BET, C from ref. [32]. *(C/O value disregarding oxygen from sulphate groups. Overall C/O=1.99). C=O was calculated from C 1s fit, considering as 100% the total amount of carbon atom present.*

Material→	hGO	bGO	dGO	rGO
C=O + O-C=O (%)	8.3 ±0.4	1.6 ±0.3	18.4 ±0.5	14.2 ±0.5
C/O	2.2*	2.6	2.7	6.7
OFLOX Qm (mg/g)	204 ±80 B	125 ±20 B	650 ±80 A	168 ±25 A
RhB Qm (mg/g)	439 ±100 B	246 ±50 B	381 ±30 A	244 ± 50B
CIPRO Qm (mg/g)	252 ± 100 B	126 ±20 A	319 ±100A	140 ± 20A
MB Qm (mg/g)	428 ±80 C	184 ±30 C	879 ±100C	177 ±40D

We suggest that the presence of holes and vacancies is the key parameter which provides increase of sorption for OFLOX, CIPRO and MB while the difference in oxidation degree and flake size are not decisive.

Another factor which strongly promotes the high sorption of certain molecules on GO samples (dGO, hGO, bGO) is their ability to swell in aqueous solutions. This was clearly demonstrated by the results obtained by using rGO (having the same holes and carboxylic groups of dGO) as sorbent.

Swelling enables excess of solvent between GO flakes and possibility to disperse GO on single-layered sheets in water. The high surface area of GO flakes is available for sorption because of the swelling which expands GO structure providing access into inter-layers for molecules and ions. It should be noted that BET surface area measured using analysis of gas sorption is not valid for solvent immersed GO. Gas sorption isotherms are recorded starting from vacuum conditions in powdered materials and gas molecules do not penetrate between GO sheets. That is why BET surface area of solid solvent free GO determined by gas sorption is rather small.

Using sorption of MB for estimation of surface area of graphite/graphene oxides is a common method already used in the 1960s,[63] re-introduced in modern

times for GO[64] and used in many studies.[65] Simple estimation of surface area values by sorption of MB were 466 m^2/g, 1086 m^2/g and 2233 m^2/g for bGO, hGO and dGO, respectively. It should be noted that this high below-surface area is not accessible for gases in water free powder GO materials. The N_2 sorption BET surface area of hGO, bGO and dGO is usually below 20 m^2/g, since GO in solid dry powder presents a compact layered structure inaccessible to molecules. That is in strong contrast to rGO, which exhibits moderately high surface area when tested by nitrogen sorption (~330 m^2/g), but it does not increase in solutions.

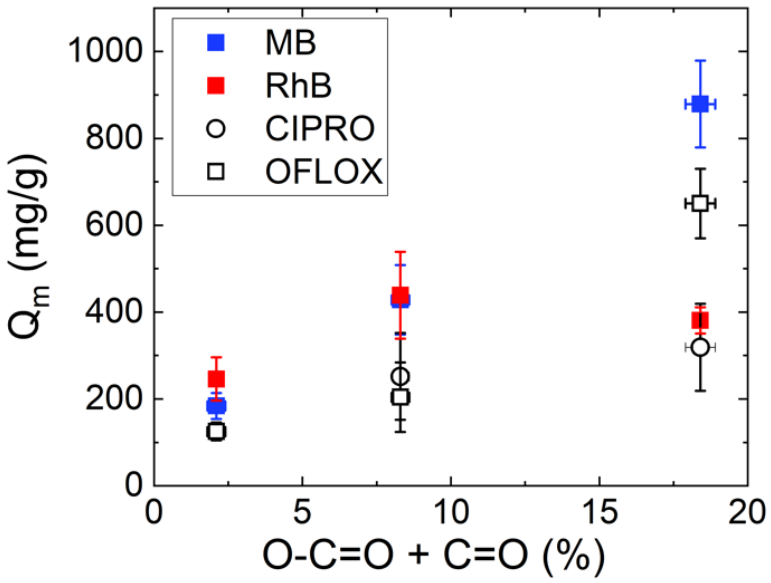

***Fig. 3.7**. Monolayer adsorption capacity (Qm) as a function of carboxylic and carbonyl defects (bGO: 1.6%, hGO: 8,3%, dGO: 18.4%).*

rGO is a hydrophobic material consisting of few layered graphene flakes in an essentially graphitic structure. In absence of swelling, only the outer surface of rGO flakes is available for sorption in aqueous solutions. As a result, the sorption of MB and OFLOX by rGO is limited by the external surface area of flakes despite high abundance of C=O groups, typical of the defected material. Note that rGO used in our study was produced by explosive thermal exfoliation, which is known to result in high abundance of defects and holes, as compared to chemically reduced GO and explains the relatively high relative number of C=O groups in this material. dGO is then produced by Hummers oxidation of rGO, this explaining why the number of edge carbon atoms (C=O) in rGO and dGO is similar, 14.2% to 18.4% respectively.

In view of the issues above, it can be concluded that most of the defects in dGO are created not by oxidation but were already present in the precursor rGO and formed during the process of thermal exfoliation. However, hydrophobic nature of rGO and absence of swelling limit the sorption only to the surface of flakes and prevents access to subsurface layers.

Remarkably, the maximum adsorption capacity of dGO for OFLOX (650 mg/g), and MB (879 mg/g) were higher than that of hGO (204 mg/g OFLOX), and 428 mg/g (MB) and significantly higher than those of Granular Activated Carbon (GAC), which is the industrial standard for adsorption technology, having Qm= 187 mg/g for MB, and 95 mg/g for OFLOX (Appendix, Fig. 8.10). Moreover, dGO efficiency was significantly higher than that of other nanosorbents for OFLOX removal including hydroxyapatite nanoparticles (Qm= 48.95 mg/g), rGO-MoS2 heterostructure (Qm= 37.31 mg/g) and zeolites (Qm= 31.32 mg/g).[66-68]

3.3.6 Recovery of dGO by ultrafiltration

Finally, to unravel the real application potential we tested the possibility to remove dGO sheets after use by ultrafiltration (UF) on commercial polysulfone (Medisulfone®, Medica spa) hollow fiber cartridges (D150 Ultra, Medica spa). Such filters are characterized by a cut-off of about 50 Å related to the minimum size of the fiber pores. In such filters, the fiber edges are closed, permitting a dead-end configuration that imposes a transmembrane flux through the fiber section, therefore retaining objects with size larger than that of the fiber pores. The minimum size of dGO flakes, estimated by AFM and SEM analyses was about 200 Å,[32] this would in principle enable full retention into Medisulfone® polymer pores.

In a typical experiment, a high concentrated dGO suspension (100 ppm, total volume 100 mL, tap water) was ultrafiltered (in-out transmembrane modality, i.e. the flow was pumped in the internal lume of the fibers at 5 mL/min, Fig. 3.8). The filtered solution (Fig. 3.8b) was clear, this suggesting successful dGO filtration. Moreover, the filtered solution was analyzed by UV-vis spectroscopy and compared to the starting dGO solution (about 100 ppm) and to standard solution of dGO in tap water at concentration in the range between 10-100 ppm. The spectra of the standards showed different baseline with intensity depending on the initial concentration (Fig. 3.8c). The baseline of dGO UF solution was much lower than that of the starting suspension (and superimposable with that of second control suspension at the same concentration of 100 ppm). Moreover, it was

comparable to the baseline of fresh tap water used also for suspension preparation. Collectively, these results confirm the successful retention of dGO by the ultrafilters.

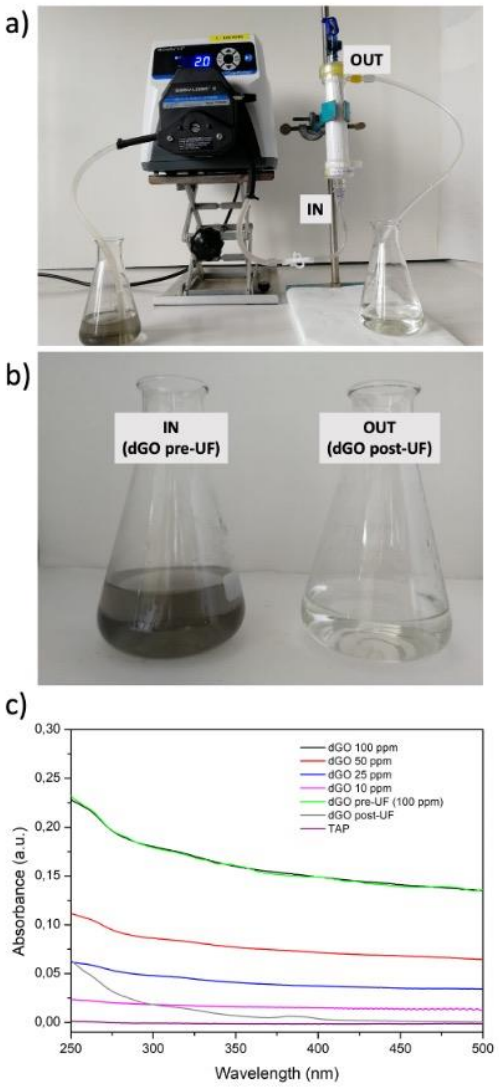

***Fig. 3.8**. a) Experimental set-up for ultrafiltration of dGO suspension by using commercial UF modules D150 ultra (Medica spa, cut-off 50 Å), b) dGO suspension before (about 100 ppm in tap water) and after filtration, c) UV-vis spectra of dGO standard solution and of pre-and post-filtered samples.*

3.4 Conclusions

In conclusion, we have shown that GO can be used as sorbent of a variety of organic emerging contaminants in tap water and that high selectivity and large uptakes in sorption of certain ECs (i.e. polar aromatic molecules such as OFLOX) can be achieved by design of GO with extremely defected structure.

Adsorption of the selected ECs occurred within 15 min with higher selectivity for oxidized GO toward OFLOX and BP3 while higher selectivity of rGO toward RhB dye was found.

Molecular dynamics modeling explained such different selectivity as the result of the shape complementarity between molecules and the different graphene nanosheets, i.e. planar RhB is favorably absorbed on rGO, while OFLOX is entrapped inside the holes generated by the defects due to size commensurability. MD simulations showed that planar molecules with delocalized surface charge are better adsorbed by reduced graphene oxide due to π-π interactions while positively charged aromatic molecules are mainly captured by electrostatic interactions.

Adsorption isotherms combined to XPS studies showed that the increase in defects state of GO is correlated with higher sorption capacity of OFLOX and CIPRO antibiotics and MB dye.

Remarkably, defect rich dGO showed an adsorption up to five times higher than that of the 'less defective' GO for OFLOX and of about three times higher for CIPRO, both active component of common antibiotics and of high environmental relevance. Such performance was six times higher than that of GAC, the industrial standard adsorption technology, and significantly higher than that of other nanomaterials already reported in literature. Finally, we demonstrate that dGO could be retained by commercial UF modules, this overcoming the risk related to secondary contamination by graphene nanosheets in treated water and opening interesting perspectives for exploitation of graphene nanosheets, such as our dGO in drinking water treatment.

3.5 References

1. https://sdgs.un.org/goals,
2. S. D. Richardson and S. Y. Kimura, *Analytical Chemistry*, 2020, **92**, 473-505.
3. N. Bolong, A. F. Ismail, M. R. Salim and T. Matsuura, *Desalination*, 2009, **239**, 229-246.
4. A. Pal, Y. He, M. Jekel, M. Reinhard and K. Y. Gin, *Environment international*, 2014, **71**, 46-62.
5. Y. Hou, S. Lv, H. Hu, X. Wu and L. Liu, *Applied Sciences*, 2021, **11**.
6. A. Abdelrasoul, H. Doan, A. Lohi and C.-H. Cheng, *ChemBioEng Rev*, 2015, **2**, 22-43.
7. S. Schulze, D. Zahn, R. Montes, R. Rodil, J. B. Quintana, T. P. Knepper, T. Reemtsma and U. Berger, *Water research*, 2019, **153**, 80-90.
8. P. Westerhoff, P. Alvarez, Q. Li, J. Gardea-Torresdey and J. Zimmerman, *Environ. Sci.: Nano*, 2016, **3**, 1241-1253.
9. D. W. Chang Min Park, Chunming Su, *Handbook of Nanomaterials for Industrial Applications Micro and Nano Technologies*

Recent Developments in Engineered Nanomaterials for Water Treatment and Environmental Remediation, , 2018.

10. K. Simeonidis, S. Mourdikoudis, E. Kaprara, M. Mitrakas and L. Polavarapu, *Environmental Science: Water Research & Technology*, 2016, **2**, 43-70.
11. S. T. Khan, F. Ahmad, M. Shahadat, W. U. Rehman and A. M. Khan, in *Environmental Nanotechnology for Water Purification*, 2020, DOI: https://doi.org/10.1002/9781119641353.ch6, pp. 151-186.
12. K. S. Ranjith, P. Manivel, R. T. Rajendrakumar and T. Uyar, *Chemical Engineering Journal*, 2017, **325**, 588-600.
13. Q. Cui, J. Xu, W. Wang, L. Tan, Y. Cui, T. Wang, G. Li, D. She and J. Zheng, *Science of The Total Environment*, 2020, **729**, 138892.
14. L. Chai, Y. Wang, N. Zhao, W. Yang and X. You, *Water research*, 2013, **47**, 4040-4049.
15. O. G. Apul, Q. Wang, Y. Zhou and T. Karanfil, *Water Res.*, 2013, **47**, 1648-1654.
16. S. Wang, H. Sun, H. M. Ang and M. O. Tadé, *Chemical Engineering Journal*, 2013, **226**, 336-347.
17. N. B. Singh, G. Nagpal, S. Agrawal and Rachna, *Environmental Technology & Innovation*, 2018, **11**, 187-240.
18. C. Backes, A. Abdelkader, C. Alonso, A. Andrieux-Ledier, R. Arenal, J. Azpeitia, N. Balakrishnan, L. Banszerus, J. Barjon, R. Bartali, S. Bellani, C. Berger, R. Berger, M. Bernal, C. Bernard, P. Beton, A. Beyer, A. Bianco and P. Bøggild, *2D Materials*, 2020, **7**, 022001.
19. S. Mantovani, S. Khaliha, L. Favaretto, C. Bettini, A. Bianchi, A. Kovtun, M. Zambianchi, M. Gazzano, B. Casentini, V. Palermo and M. Melucci, *Chem. Commun.*, 2021, **57**, 3765-3768.
20. A. Kovtun, A. Bianchi, M. Zambianchi, C. Bettini, F. Corticelli, G. Ruani, L. Bocchi, F. Stante, M. Gazzano, T. D. Marforio, M. Calvaresi, M. Minelli, M. L. Navacchia, V. Palermo and M. Melucci, *Faraday Discuss.*, 2021, **227**, 274-290.

21. R. Mailler, J. Gasperi, Y. Coquet, S. Deshayes, S. Zedek, C. Cren-Olivé, N. Cartiser, V. Eudes, A. Bressy, E. Caupos, R. Moilleron, G. Chebbo and V. Rocher, *Water research*, 2015, **72**, 315-330.
22. A. Iakunkov and A. V. Talyzin, *Nanoscale*, 2020, **12**, 21060-21093.
23. S. J. You, S. M. Luzan, T. Szabo and A. V. Talyzin, *Carbon*, 2013, **52**, 171-180.
24. A. Klechikov, J. H. Sun, I. A. Baburin, G. Seifert, A. T. Rebrikova, N. V. Avramenko, M. V. Korobov and A. V. Talyzin, *Nanoscale*, 2017, **9**, 6929-6936.
25. A. V. Talyzin, A. Klechikov, M. Korobov, A. T. Rebrikova, N. V. Avramenko, M. F. Gholami, N. Severin and J. P. Rabe, *Nanoscale*, 2015, **7**, 12625-12630.
26. P. Feicht, R. Siegel, H. Thurn, J. W. Neubauer, M. Seuss, T. Szabo, A. V. Talyzin, C. E. Halbig, S. Eigler, D. A. Kunz, A. Fery, G. Papastavrou, J. Senker and J. Breu, *Carbon*, 2017, **114**, 700-705.
27. A. V. Talyzin, G. Mercier, A. Klechikov, M. Hedenstrom, D. Johnels, D. Wei, D. Cotton, A. Opitz and E. Moons, *Carbon*, 2017, **115**, 430-440.
28. S. J. You, B. Sundqvist and A. V. Talyzin, *Acs Nano*, 2013, **7**, 1395-1399.
29. S. J. You, S. Luzan, J. C. Yu, B. Sundqvist and A. V. Talyzin, *J Phys Chem Lett*, 2012, **3**, 812-817.
30. A. S. Kuzenkova, A. Y. Romanchuk, A. L. Trigub, K. I. Maslakov, A. V. Egorov, L. Amidani, C. Kittrell, K. O. Kvashnina, J. M. Tour, A. V. Talyzin and S. N. Kalmykov, *Carbon*, 2020, **158**, 291-302.
31. A. V. Talyzin, G. Mercier, A. Klechikov, M. Hedenström, D. Johnels, D. Wei, D. Cotton, A. Opitz and E. Moons, *Carbon*, 2017, **115**, 430-440.
32. N. Boulanger, A. S. Kuzenkova, A. Iakunkov, A. Y. Romanchuk, A. L. Trigub, A. V. Egorov, S. Bauters, L. Amidani, M. Retegan, K. O. Kvashnina, S. N. Kalmykov and A. V. Talyzin, *ACS Appl. Mater. Interfaces*, 2020, **12**, 45122-45135.
33. J. Wang and S. Wang, *Journal of Environmental Management*, 2016, **182**, 620-640.
34. Y. Huang, J. C.-F. Law, T.-K. Lam and K. S.-Y. Leung, *Science of The Total Environment*, 2021, **755**, 142486.
35. J. L. Sotelo, G. Ovejero, A. Rodríguez, S. Álvarez, J. Galán and J. García, *Chemical Engineering Journal*, 2014, **240**, 443-453.
36. S. Valsecchi, M. Rusconi, M. Mazzoni, G. Viviano, R. Pagnotta, C. Zaghi, G. Serrini and S. Polesello, *Chemosphere*, 2015, **129**, 126-134.
37. A. V. Talyzin, T. Szabo, I. Dekany, F. Langenhorst, P. S. Sokolov and V. L. Solozhenko, *J Phys Chem C*, 2009, **113**, 11279-11284.
38. A. G. Klechikov, G. Mercier, P. Merino, S. Blanco, C. Merino and A. V. Talyzin, *Micropor Mesopor Mat*, 2015, **210**, 46-51.
39. R. M. B. D. M. Y. and P. A. K. M. Y. D.A. Case, W. Botello-Smith, D.S. Cerutti, T.E. Cheatham, III, T.A. Darden, R.E. Duke, T.J. Giese, H. Gohlke, A.W. Goetz, N. Homeyer, S. Izadi, P. Janowski, J. Kaus, A. Kovalenko, T.S. Lee, S. LeGrand, P. Li, C. Lin, T. Luchko, R. Luo, B. Madej and P. A. Kollman, *Journal*, Univ. California, San Fr., 2016.
40. W. Humphrey, A. Dalke and K. Schulten, *J. Mol. Graphics*, 1996, **14**, 33-38.
41. J. Wang, R. M. Wolf, J. W. Caldwell, P. A. Kollman and D. A. Case, *J. Comput. Chem.*, 2004, **25**, 1157-1174.
42. W. L. Jorgensen, J. Chandrasekhar, J. D. Madura, R. W. Impey and M. L. Klein, *The Journal of Chemical Physics*, 1983, **79**, 926-935.

43. T. Hou, J. Wang, Y. Li and W. Wang, *Journal of Chemical Information and Modeling*, 2011, **51**, 69-82.
44. S. Genheden and U. Ryde, *Expert Opinion on Drug Discovery*, 2015, **10**, 449-461.
45. R. A. Laskowski, *Journal of Molecular Graphics*, 1995, **13**, 323-330.
46. E. F. Pettersen, T. D. Goddard, C. C. Huang, G. S. Couch, D. M. Greenblatt, E. C. Meng and T. E. Ferrin, *J Comput Chem*, 2004, **25**, 1605-1612.
47. M. J. Frisch, G. W. Trucks, H. B. Schlegel, G. E. Scuseria, M. A. Robb, J. R. Cheeseman, G. Scalmani, V. Barone, G. A. Petersson, H. Nakatsuji, X. Li, M. Caricato, A. V. Marenich, J. Bloino, B. G. Janesko, R. Gomperts, B. Mennucci, H. P. Hratchian, J. V. Ortiz, A. F. Izmaylov, J. L. Sonnenberg, Williams, F. Ding, F. Lipparini, F. Egidi, J. Goings, B. Peng, A. Petrone, T. Henderson, D. Ranasinghe, V. G. Zakrzewski, J. Gao, N. Rega, G. Zheng, W. Liang, M. Hada, M. Ehara, K. Toyota, R. Fukuda, J. Hasegawa, M. Ishida, T. Nakajima, Y. Honda, O. Kitao, H. Nakai, T. Vreven, K. Throssell, J. A. Montgomery Jr., J. E. Peralta, F. Ogliaro, M. J. Bearpark, J. J. Heyd, E. N. Brothers, K. N. Kudin, V. N. Staroverov, T. A. Keith, R. Kobayashi, J. Normand, K. Raghavachari, A. P. Rendell, J. C. Burant, S. S. Iyengar, J. Tomasi, M. Cossi, J. M. Millam, M. Klene, C. Adamo, R. Cammi, J. W. Ochterski, R. L. Martin, K. Morokuma, O. Farkas, J. B. Foresman and D. J. Fox, *Journal*, 2016.
48. A. Ebadi, J. S. Soltan Mohammadzadeh and A. Khudiev, *Adsorption*, 2009, **15**, 65-73.
49. S. Eigler, C. Dotzer and A. Hirsch, *Carbon*, 2012, **50**, 3666-3673.
50. P. Feicht and S. Eigler, *Chemnanomat*, 2018, **4**, 244-252.
51. A. Nordenström, N. Boulanger, A. Iakunkov, G. Li, R. Mysyk, G. Bracciale, P. Bondavalli and A. V. Talyzin, *Nanoscale Adv.*, 2022, DOI: 10.1039/D2NA00362G.
52. J. Shayimova, R. R. Amirov, A. Iakunkov, A. Talyzin and A. M. Dimiev, *PCCP*, 2021, **23**, 17430-17439.
53. M. Calvaresi and F. Zerbetto, *J. Mater. Chem. A*, 2014, **2**, 12123.
54. M. Calvaresi, A. Bottoni and F. Zerbetto, *J. Phys. Chem. C*, 2015, **119**, 28077-28082.
55. M. Di Giosia, T. D. Marforio, A. Cantelli, F. Valle, F. Zerbetto, Q. Su, H. Wang and M. Calvaresi, *J. Colloid Interface Sci.*, 2020, **571**, 174-184.
56. A. M. Dimiev, L. B. Alemany and J. M. Tour, *Acs Nano*, 2013, **7**, 576-588.
57. M. Di Giosia, F. Zerbetto and M. Calvaresi, *Accounts of Materials Research*, 2021, DOI: 10.1021/accountsmr.1c00065.
58. M. Calvaresi, S. Furini, C. Domene, A. Bottoni and F. Zerbetto, *Acs Nano*, 2015, **9**, 4827.
59. M. Di Giosia, F. Valle, A. Cantelli, A. Bottoni, F. Zerbetto, E. Fasoli and M. Calvaresi, *Carbon*, 2019, **147**, 70-82.
60. M. Di Giosia, P. H. H. Bomans, A. Bottoni, A. Cantelli, G. Falini, P. Franchi, G. Guarracino, H. Friedrich, M. Lucarini, F. Paolucci, S. Rapino, N. A. J. M. Sommerdijk, A. Soldà, F. Valle, F. Zerbetto and M. Calvaresi, *Nanoscale*, 2018, **10**, 9908-9916.
61. M. Calvaresi and F. Zerbetto, *Acs Nano*, 2010, **4**, 2283.
62. L. de Pablo, M. L. Chávez and M. Abatal, *Chem. Eng. J.*, 2011, **171**, 1276-1286.
63. H. P. Boehm, A. Clauss, G. Fischer and C. Hofmann, *Proc. 5th Conf. on Carbon (Oxford: Pergamon)* 1962, 73-80.
64. P. Montes-Navajas, N. G. Asenjo, R. Santamaria, R. Menendez, A. Corma and H. Garcia, *Langmuir*, 2013, **29**, 13443-13448.

65. A. Nordenstrom, N. Boulanger, A. Iakunkov, I. Baburin, A. Klechikov, A. Vorobiev and A. V. Talyzin, *J Phys Chem C*, 2021, **125**, 6877-6885.
66. H. Wu, Y. Shi, X. Guo, S. Zhao, J. Du, H. Jia, L. He and L. Du, 2016, **39**, 4398-4407.
67. Z. Xu, X. Bai and Z. Ye, *Journal of Cleaner Production*, 2021, **291**, 125982.
68. D. N. R. de Sousa, S. Insa, A. A. Mozeto, M. Petrovic, T. F. Chaves and P. S. Fadini, *Chemosphere*, 2018, **205**, 137-146.

4 Graphene oxide nanosheets as sorbent

Graphene oxide nanosheets for drinking water purification by tandem adsorption and microfiltration

Adapted with permission from Sep.Purif.technol., 300, (2022), 121826, Elsevier
DOI 10.1016/j.seppur.2022.121826

4.1 Introduction

The removal of emerging contaminants (ECs) is a research and industrial priority, [1-4] requiring the urgent development of facile, sustainable, and highly efficient technologies in answer to the recently adopted European Drinking Water Directive 2020/2184 [5] and, more generally, to the United Sustainable Development Goal 6 'Ensure access to water and sanitation for all'. [6]

Graphene oxide (GO) and reduced graphene oxide (rGO) nanosheets have shown outstanding adsorption properties toward several organic and metal ion water contaminants, with superior performances with respect to other carbon-based nanomaterials. [7-16]

The outstanding performances of GO can be attributed to the high surface area, multiple surface functional groups as interaction-binding promoting sites, and good water dispersibility. [17, 18] Additionally, GO can be chemically manipulated in order to tailor its adsorption capability against pollutants. [14, 19-22] GO nanosheets have shown adsorption maximum capacity of about 570 mg/g [23] for methylene blue (MB), a dye, 550 mg/g for rhodamine B (RhB), another dye, and 356 mg/g for ofloxacin (OFLOX), a fluoroquinolone antibiotic. [24] Metal ions such as Cu (II), Zn (II) and Pb (II) are effectively removed as well, with a maximum capacity of 117 mg/g, 345 mg/g and 1119 mg/g respectively. [25] GO nanosheets have been also employed in combination with polymers like chitosan in the coagulation/flocculation process to remove turbidity and various contaminants. [26]

Perfluoroalkyl substances (PFAS) [27] are a family of persistent compounds used in many industrial processes and everyday products, including polymers, pharmaceuticals, adhesives, insecticides and fire retardants, that have been found around the world in groundwater, surface water and even drinking water, and are a source of potentially severe health risk. [28] Several cases of contamination have been discovered around the world and Italy hosts the third most important case,

in terms of extension of the polluted land: an area extending for almost 200 km^2 between the counties of Padua, Verona and Vicenza (Veneto Region, Northern Italy). High concentrations of several PFAS have been observed in 2013 in freshwater and groundwater. [29, 30] A significant social and scientific activity ended in the establishment of PFAS limits in drinking water in the recently adopted drinking water directive EU 2020/2184. [5]

Conventional purification technologies are partially ineffective in the removal of these substances from water and nanomaterials are expected to play a key role for enhanced purification from PFAS. [31-35] To date, only a few number of examples of treatment on PFAS by graphene materials has been reported, [31, 32, 36, 37] and most of them are limited to some specific molecules (e.g. perfluorooctanoic acid, PFOA, and perfluorooctanesulfonate, PFOS). [38-45]
Becanova et al [37] recently described the fabrication of graphene and benzylamine modified graphene monoliths and their use as passive samplers for preconcentration of a mixture of PFAS in contaminated sites. Longer chain ($C \geq 8$) perfluoroalkyl acids (PFAAs) were adsorbed more efficiently than shorter chain PFAAs, which were better removed only upon modification of the monoliths with benzylamine moieties. In general, 3D graphene materials, such as foams and aerogels, are preferred as adsorbing materials for purification purposes because of their ease of use and recovery, which can favour regeneration and reuse.[11, 46-50] For some specific contaminants, i.e. methylene blue and heavy metals, their performance has been found to be competitive with granular activated carbon (GAC, the industrial standard), but their fabrication generally requires freeze-drying or other demanding processing that may limit future scale up.

Here, we demonstrate that commercial GO and rGO 2D-nanosheets can be used without any additional processing for adsorption of contaminants from water and then easily removed from the treated water by combining an innovative two step method consisting of adsorption in batch and microfiltration (MF) on polyethersulfone hollow fiber (PES-HF) modules (Plasmart 100 module, Medica Spa). Such modules have a filtering surface of about 0.1 m^2, cut off of 1.000 KDa (inner diameter ~280-300 µm, outer diameter ~360-400 µm) and are a well-established technology for plasmapheresis (i.e. plasma purification) and drinking water disinfection, due to their removal of bacteria and microorganisms, with log retention LRV= 9 (i.e. 99,99999999% retention). [51] We demonstrate that PES-HF

modules retain GO/rGO nanosheets quantitatively after the adsorption of microcontaminants from tap water. We studied GO and rGO having different surface chemistry and charge, to gain an insight on adsorption mechanisms. The capacity of the procedure (from now on GO+MF) is demonstrated on OFLOX and MB, since they have strong affinity with GO but are not retained by PES-HF modules (neither by adsorption on PES polymer nor by physical filtration through the membrane porosity). [52] Moreover, we demonstrate the suitability of this procedure for the removal of a mixture of fourteen selected PFAS in tap water at the maximum concentration so far found in contaminated sources.

4.2 Experimental

4.2.1 Materials

OFLOX and MB were purchased from Merck, Germany, and used without further purification (Fig. 8.1, Appendix). PFAS standard (CH_3CN:H_2O 9:1, 200 µg/mL) were purchased from Agilent Technologies (Santa Clara, CA, US).(Fig. 8.12, Appendix) All the experiments on PFAS were carried out by using polypropylene vials. GO was purchased from Layer One (previously called Abalonyx) and used without further purification (graphene oxide powder <35 mesh, product code 1.8, XPS: O/C ratio 0.39 ± 0.01, C 70.1 ± 0.9%, O 27.2 ± 0.9%, N 0.2 ± 0.1%, S 1.0 ± 0.1%, Si 0.8 ± 0.1%, Cl 0.7 ± 0.1%; Mn, a typical residue from synthesis, below 0.1%).[53] rGO was purchased from Layer One and used without further purification (rGO powder, fully reduced, carbon content of about 98.5-99% weight). GAC was purchased from CABOT Norit Spa (Ravenna, Italy, Norit GAC 830 AF, MB index min 240 mg/g, BET surface area >1˙000 m^2/g, see Table 8.2, Appendix).[54] In order to remove sub-millimetric particles (namely separating powder from granules), GAC was washed with deionized water at a mild flux, then dried overnight in an oven at 40 °C. Plasmart 100 MF module (Versatile® PES hollow fibers, membrane area filtering surface 0.1 m^2, pore average size 100-200 nm) were provided by Medica Spa (Medolla, Italy).[36]

4.2.2 Preparation of GO/rGO starting suspension and nanosheets morphology characterization

Typically, each batch of GO/rGO starting suspension consisted of a 2 mg/mL dispersion in deionized water (total volume 50 mL and total GO/rGO content 100 mg). The dispersion was sonicated for 4 h. The morphology of isolated GO

deposited on silicon was studied by atomic force microscopy (AFM). Data were acquired in tapping mode employing a NTEGRA microscope of NT-MDT and rectangular silicon probes (RTESPA-300, Bruker, k = 40 N/m, ω = 300 kHz). Image processing and particle shape analysis was performed using SPIP software. XPS spectra were acquired by hemispherical analyser (Phoibos 100, Specs, Germany), calibrated on Au 4f7/2 peak at 84.0 eV and using a Mg Kα excitation. AFM on rGO was not performed since rGO consists of larger aggregates rather than nanosheets. Aggregation experiments were carried out starting from this suspension and diluting it in Milli-Q water.

Scanning electron microscopy (SEM) analysis were performed on GO and rGO both in Milli-Q water and tap water and SEM imaging were acquired with ZEISS LEO 1530 FEG. For the adsorption tests, the starting solution was diluted with tap water spiked with contaminants.

Size distribution of GO/rGO aggregates in tap water was obtained by Laser Granuloumeter Saturn II (Micromeritics, Norcross, GA, USA). The quantitative study of lateral sizes was performed using percentile analysis. [55]

4.2.3 GO/rGO loading capacity of MF modules

100 mL of GO/rGO starting suspension was filtered at 50 mL/min with a Cole-Parmer Masterflex® peristaltic pump on Plasmart 100 module in OUT-IN modality. This procedure was repeated with new batches of GO/rGO under the same conditions until saturation was reached (i.e. module clogging). The same protocol was applied also to determine the capacity of IN-OUT filtration modality.

4.2.4 Pores size and distribution of MF modules

The size of pores of PES-HF was obtained by using a liquid-liquid displacement porosimeter Poroliq1000 (Porometer, Germany-Belgium). The single fibre was sealed in loop shape with epoxy resin onto an inox stainless steel sample holder. Isobutanol-water was used as the wetting liquid, while water saturated with isobutanol was used as the displacement liquid. Through-pores size distribution was determined by using the Young – Laplace equation. A contact angle of 40 ° was measured for PES-HF with an OCA Dataphysics instrument.

4.2.5 GO/rGO release experiments

The presence of GO and rGO in filtered water after the tandem GO/rGO+MF experiments was checked by UV-vis analysis in comparison to the spectra of standard suspensions at known concentrations and total organic carbon (TOC)

analysis in comparison to tap water. UV-Vis was performed by Cary 3500 UV-vis spectrophotometer (Agilent Technologies, Santa Clara, CA, USA).

4.2.6 Adsorption-microfiltration procedure optimization

In a typical experiment, GO starting suspension (total amount of GO 80 mg, total volume 40 mL) was added to a solution of OFLOX or MB in tap water (30 mg of OFLOX/MB in 60 mL, i.e. 0.5 mg/mL) and stirred for 30 min in darkness. The suspension obtained in this way was then filtered through a MF module, OUT-IN modality, at 55 mL/min using a Cole-Parmer Masterflex® peristaltic pump. The maximum amount of OFLOX or MB removed by a single MF module was estimated by repeating the procedure with a new batch of GO+OFLOX/MB suspension until clogging of the module was reached. Method optimization was made at different initial concentration of OFLOX, and 300 mg/L was selected as case study due to detection limit of the instrument.

4.2.7 High performance liquid chromatography analyses

HPLC analyses of the selected contaminants were performed on a Dyonex Ultimate 3000 system equipped with a diode array detector. 200 µL samples were used as sources for the automated injection. The chromatographic separation was performed on a reverse phase Zorbax XDB-C8 column (4.6 × 150 mm, 5 µm) at flow rate of 1.0 mL/min, detection at λmax of each analyte, linear gradient TFA 0.05% aqueous solution/acetonitrile from 80:20 to 0:100. In each experiment, the removal of each analyte was determined by comparison with that of the initial untreated solution. The results are expressed as the mean of two independent experiments ± SD.

4.2.8 Regeneration experiments

GO/rGO regeneration: GO starting suspension (total amount of GO=200 mg, volume=100 mL) was added to a solution of MB (300 mg/L, total volume = 250 mL) and stirred for 30 min. In the case of rGO, basing on adsorption isotherms studies previously reported,[17] a solution of MB at 100 mg/L was added, and total volume of 250 mL was used. After this time, GO/rGO was centrifuged (18˙000 rpm, 5 min), washed with 200 mL of ethanol for three times, filtered on a fritted-disc Büchner funnel, dried under vacuum and reused for a second adsorption cycle. This process was subsequently repeated in order to perform a third and last cycle.

Module regeneration: GO/rGO starting suspension (about 2 g/L) was added to an equal amount of tap water to induce flocculation and stirred for 30 min. The

suspension was then filtered at 50 mL/min with a Cole-Parmer Masterflex peristaltic pump on a Plasmart 100 module in OUT-IN modality. GO was then extracted from the module through the application of alternated water (200 mL/min) and compressed air flows (4 bar) in IN-OUT modality and simple mechanical shaking of the module. In this way, 1.1 g of GO was collected (i.e. 75% of the original amount). The recollected GO was then dispersed again in water and used for additional two cycles with an additional drop of GO maximum loading of about 35%. Similarly, rGO was extracted by flowing water at 200 mL/min without the need of compressed air, in IN-OUT modality. In this way, 1.3 g of rGO were recollected) i.e. >90% of the original amount). The recollected rGO was used for additional cycle and recollected with yield higher than 90% in each run.

4.2.9 Core-shell HF-GO module fabrication and use for comparative GO+MF and microfiltration experiments

The core shell PES-GO hollow fibers module was prepared by filtering 25 mL of the starting GO suspension through the module OUT-IN at 1 bar and then performing a thermal annealing at 80 °C for 12 h. [52] After that, the filtering-annealing cycle was repeated, giving the final device. Finally, 100 mg of GO were loaded and fixed on the outer wall of the fibers. Filtration experiments were performed in the same OUT-IN modality (tap water 100 mL, OFLOX 20 mg, contact time 30 min, flow rate 55 mL/min).

4.2.10 PFAS kinetic experiments

A standard solution of the fourteen PFAS in methanol was prepared starting from the commercial mixture (final concentration: 5 mg/L). GO powder (25 mg) was sonicated in 2.5 mL of distilled water for 2 h, then 22.5 mL of tap water were added (pH = 6.9). The suspension was spiked with 50 µL of the mixture of fourteen PFAS and the final concentration of each contaminant was 10 µg/L in a total volume of 25 mL. After a variable contact time (10 min, 30 min, 4 h and 24 h) on a rotary shaker, the samples were centrifuged 10 min at 10˙000 rpm and the amount of PFAS in filtered water was determined by UPLC-MS/MS. The same procedure was applied to rGO (pH of the suspension was 7.2) and GAC (pH of the suspension was 7.3). In the case of GAC, no sonication was performed.

4.2.11 PFAS removal experiments

A standard solution of the fourteen PFAS in methanol was prepared starting from the commercial mixture (final concentration: 5 mg/L). GO or rGO (25 mg,

Abalonyx, rGO 99% reduced) were sonicated in 2.5 mL of distilled water for 2 h, then 22.5 mL of tap water were added (pH = 6.9). The suspension was spiked with 50 µL of the mixture of fourteen PFAS and the final concentration of each contaminant was 10 µg/L in a total volume of 25 mL. After 30 min of contact time on a rotary shaker the suspension was filtered in a OUT-IN modality at 55 mL/min using a Cole-Parmer Masterflex® peristaltic pump. The concentration of PFAS in filtered water was checked by UPLC-MS/MS.

4.2.12 UPLC-MS/MS method for PFAS quantification

Analysis on PFAS were performed by using a UPLC-MS/MS Waters ACQUITY UPLC H-Class PLUS – XEVO TQS Micro mass detector. The chromatographic separation was performed on a reverse phase Waters Acquity UPLC CSH Phenyl-Hexyl (2.1 x 100 mm, 1.7 µm) and Waters Isolator Column 2.1x50 mm, column temperature 34 °C, linear gradient from 100:0 to 5:95 mobile phase A (MeOH: aqueous NH_4OAc 2 mM 95:5)/mobile phase B (NH_4OAc 2 mM in MeOH), flow rate 0.3 mL/min. The mobile phase composition varied according to the gradient program reported in Table 8.3, Appendix. Mass details and limits of quantitation (LOQ) for each analyte are reported in Table 8.4, Appendix.

The calibration curves were calculated by using the average value of 2 subsequent UPLC-MS/MS injections. Calibration curve solutions (0.1, 0.5, 1.0, 2.5, 5.0, 10) were freshly prepared diluting methanolic PFAS stock solution with laboratory phase A and injected before each analytical batch. Regression equations of calibration curves were linear in the range of 10-0.01 or 0.05 or 0.1 mg/L depending on the analyte (Table 8.4, Appendix). The results are expressed as the mean of 2 ± SD. Laboratory drinking water was checked for PFAS contamination and no PFAS were detected above LOD value.

4.3 Results and Discussion

4.3.1 GO/rGO aggregates size analysis and microfiltration

A GO suspension was prepared by dispersion of GO powder in deionized water and sonication for 4 h.

Atomic force microscopy (AFM) analysis revealed a percentage of monolayers > 99.0% with a median size (D50) of about 170 nm (Fig. 4.1a). Moreover, the 90% of GO nanosheets (D90) have a lateral size lower than 600 nm

(Fig. 8.13 and Table 8.5, Appendix). However, if the suspension was directly prepared in tap water under the same conditions, the dispersion was not stable, and flocculation could be observed after a few minutes (Fig. 4.1b).

Scanning electron microscopy (SEM) images of the GO suspension in tap water dropped on silicon substrate confirm the presence of aggregates, contrasting with the almost uniform distribution of single flakes of GO in Milli-Q water (Fig. 8.14, Appendix). The size of GO aggregates was analyzed by laser diffraction particle size analyzed (LG) since, given their intrinsic limits, AFM (size ≤100 μm) and dynamic light scattering (DLS, size ≤10 μm) attempts failed. The size distribution percentiles obtained was D10 = 8 μm, D50 = 41 μm and D90 = 64 μm (see also Table 8.5, Appendix).

PES-HF mean pore size measured by porosimeter analysis (Fig. 4.1c, 4.1d) was in the in the range of 200-250 nm with the minimum pore size close to 100 nm. Therefore, the size of aggregates was at least two orders of magnitude higher than the pore size of PES-HF, meaning that the sheets would be retained by microfiltration on MF modules in dead-end filtration modality, i.e. with flow passing through the membrane porous wall (OUT-IN modality). Permeability curve and repeated measurements are reported in Fig. 8.13c, 8.13d, Appendix.

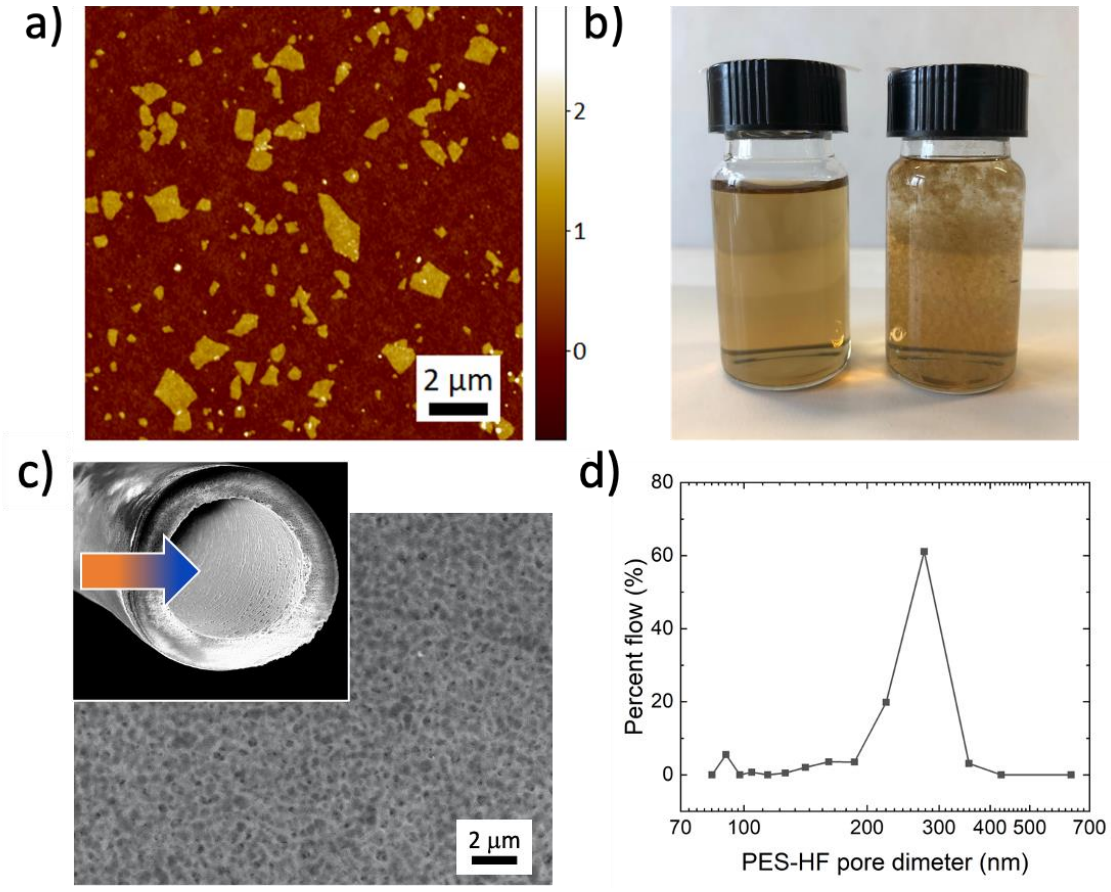

Fig. 4.1. *a) AFM image of GO nanosheets deposited from deionized water on silicon. b) GO dispersion in Milli-Q water (left) and tap water (right) after 30 min at concentration 0.1 mg/mL showing flocculation in tap water. c) Pores on the PES-HF fiber surface, the inset shows a PES-HF single fiber used for microfiltration and of the flow pathway in the OUT-IN modality. The fluid enters from the external wall of the hollow fibers and passes through the section to enter the fiber lume (lume diameter 300 µm. d) Pore size distribution measured with a Liquid-Liquid Displacement Porosimeter, from the pressure value of bubble point at 0.18-0.25 bar.*

In the same conditions, a rGO suspension was prepared and analyzed. As expected from the high reduction state of rGO, the suspension was less stable and faster precipitation of rGO was also observed in this case. The lateral size distribution was D10 = 6 µm, D50 = 16 µm and D90 = 32 µm (LG), slightly lower that GO, but of the same order of magnitude. GO and rGO have extremely different chemical structures, GO is highly oxidised, with O/C ratio of 0.4, with C-O functionalities representing almost 50% of all carbon atoms. In contrast, rGO is a fully reduced material, where 99% of atoms are carbon and only 1% oxygen atoms, as revealed by XPS analysis (Fig. 8.15, Appendix).

Flocculation of GO in tap water has been already observed and ascribed to the effect of ions type and valence and to ionic strength that are almost negligible in deionized water.[56, 57]

The exfoliated starting GO suspension in deionized water was then diluted with tap water to induce flocculation and then filtered until clogging of the MF module, and consequent drop of flow rate (from 50 mL/min to 15 mL/min), was reached. A maximum GO capacity of about 1.4 g was estimated for the MF module.

The opposite transmembrane filtration modality (IN-OUT), with the fluid entering the fiber lume and passing through the section to the external wall, was also considered. In this case, a maximum GO loading capacity of 800 mg was estimated, about half of the capacity of the OUT-IN modality. The higher value observed for the OUT-IN modality can be likely ascribed to the higher dead volume of the outer inner-fiber space. OUT-IN modality was selected as the ideal configuration and used for the following water purification experiments. Almost similar behaviour was observed for rGO with higher loading (about 1.7 g) in the OUT-IN modality.

Fig. 4.2 shows the comparison between high-speed centrifugation and microfiltration procedures on GO and rGO. Increasing centrifugation time up to 30 min at the maximum speed did not affect the precipitation yield. It can be clearly seen that centrifugation leads to uncomplete precipitation, in particular in the case of rGO. As a result, reiterated centrifugations are required, while in the case of MF treatment a clear solution is observed after a single step. Beside the highest operational simplicity of MF, the module have standard cut-off, ensuring that protocol reproducibility is independent from the operators, treatment time and scale.

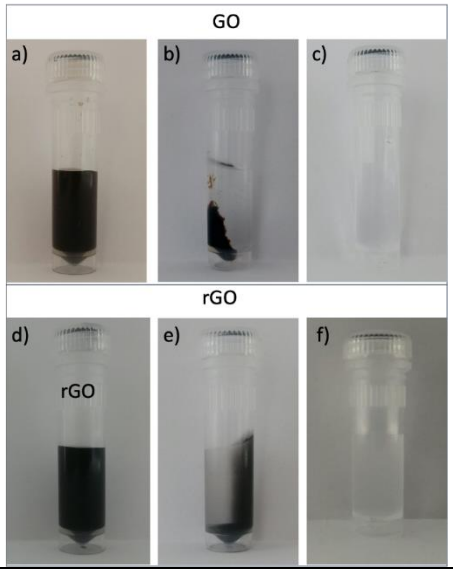

Fig. 4.2. *A suspension of GO or rGO in deionized water was diluted with tap water, as for water treatment experiments, then centrifugated at 10˙000 rpm for 10 min or microfiltered. Top: GO suspension before centrifugation (a), after centrifugation (b), and after MF (c). Bottom: rGO suspension before centrifugation (d), after centrifugation (e), and after MF (f).*

Standard chemical potability of treated water in accordance with current EU regulation (D. Lgs. 31/01) was confirmed for treated water (Table 8.6, Appendix).[57] The analysis also confirmed the absence of secondary contamination by metal ions that could be released from GO nanosheets (i.e. manganese-containing chemicals are used during GO synthesis). Moreover, in order to check the presence of possible release of GO from the module, we performed UV-vis analysis on treated water (after concentration by rotary evaporation) and compared the spectra to those of GO suspensions at concentrations in the range of 2.5-10 mg/L (Fig. 8.16,Appendix). After filtration, the sample was clear and no traces of GO in filtered water, within the LOD of the method (~2.5 mg/L), were found in the UV-vis spectrum. This finding was in good agreement with the total organic carbon (TOC) measurements, being 3 mg/L for GO+MF solution and 2 mg/L for pristine tap water (Table 8.6, Appendix). rGO retention was tested as well, comparing the UV-vis analysis of a suspension of rGO 1 mg/mL, before and after filtration on MF module, with a standard solution of rGO 5 mg/L and no evidence of rGO was found in treated water (Fig. 8.16, Appendix).

Noteworthy, GO/rGO could be recovered after use allowing regeneration and reuse. By inverting the flow direction through the MF cartridge, GO/rGO detached from the HF surface and pores cavities. A volume of water from 200 to 350 mL per gram of rGO/GO was required to yield a recovery of about 80%.

4.3.2 Optimization of the adsorption-microfiltration procedure

After establishing the capability of MF modules to retain GO nanosheets, adsorption experiments were performed for the removal of OFLOX and MB in spiked tap water by exploiting the experimental setup shown in Fig. 4.3. OFLOX was selected as a reference substance due to its strong affinity for GO (maximum adsorption capacity of GO nanosheets >300 mg/g of GO),[24, 58] quick equilibrium time,[59-61] and ease of detection. MB was selected since it is the standard contaminants used for adsorption tests on carbon materials.

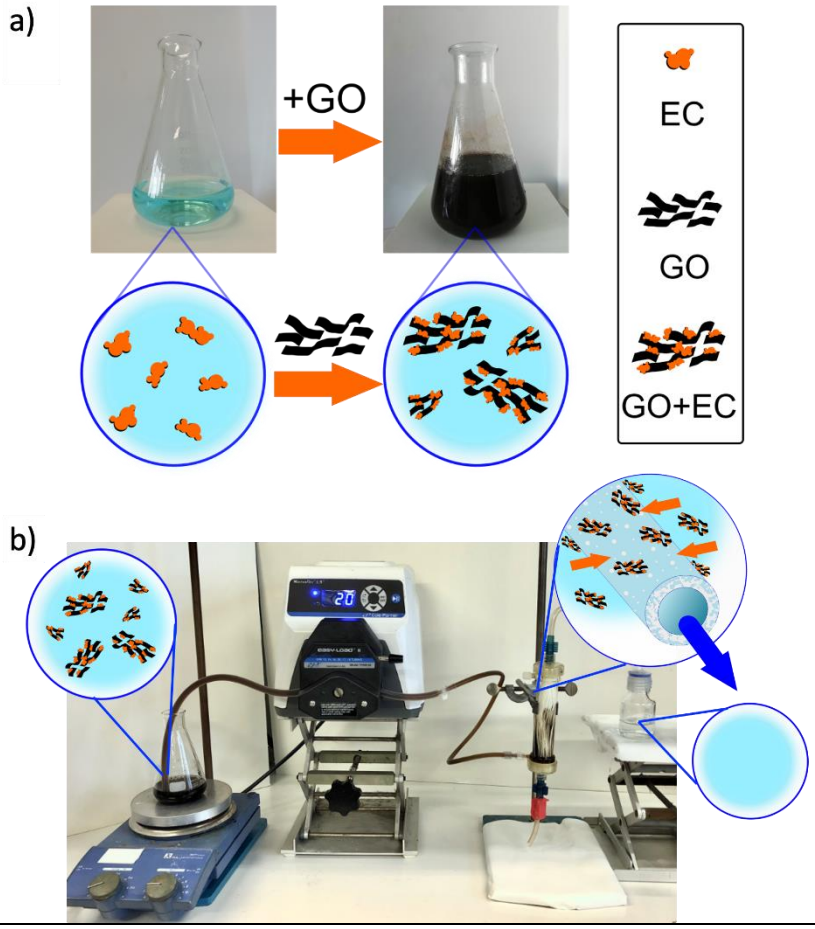

Fig. 4.3. *a) Adsorption: GO nanosheets are introduced in tap water spiked with OFLOX or MB and the solution is stirred at room temperature for 30 min in darkness; b) filtration: the suspension is filtered through the MF module in OUT-IN transmembrane modality.*

Firstly, we excluded any possible contribution of PES-HF to the adsorption of OFLOX[52] and MB. Then we performed removal experiments on OFLOX and MB. We found that the removal of OFLOX at initial concentration in the range 25-300 mg/L, was independent on the initial concentration, with values ranging between 99.8% and 86.8% (Fig 4.4). In order to facilitate the analytical detection, we performed all the subsequent experiments at an initial concentration of 300 mg/L.

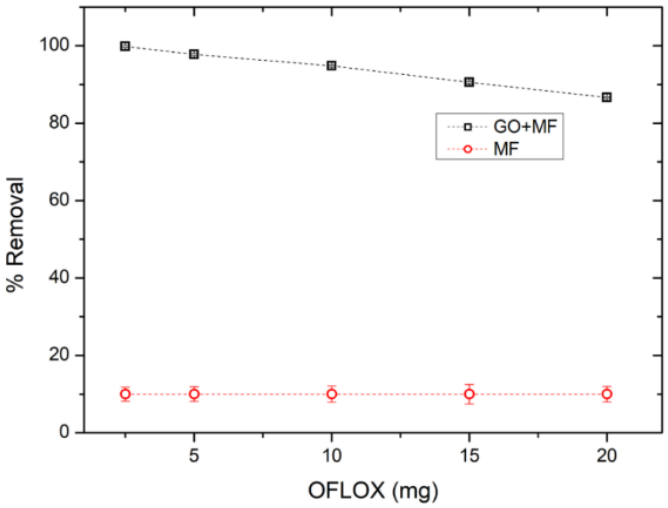

Fig. 4.4. *Removal of OFLOX at different initial concentrations using adsorption with GO followed by microfiltration through a MF module (GO+MF) vs removal by a plain PES MF module (MF, no GO). Experimental conditions were: GO 100 mg; contact time 30 min; flow rate 55 mL/min; total treated volume 100 mL. Each experiment was performed with a new MF module.*

In a typical experiment, a sample of tap water spiked with OFLOX or MB was added to the starting GO suspension, stirred for 30 min in darkness, then filtered through a MF module and the amount of OFLOX or MB in filtered water quantified by HPLC (OFLOX) or UV-vis (MB) analyses.

The maximum amount of OFLOX removed by a single MF module was then estimated by repeating the GO+MF experiments on the same MF module until clogging was reached, filtering at each repetition a new aliquot of GO and OFLOX solution (300 mg/L) . In these conditions, we were able to remove about 240 mg of OFLOX per gram of GO (60% of removal each repetition) and 356 mg for MB per gram of GO by using a single MF module (Fig. 4.5). It should be noted that the maximum adsorption capacity estimated at the equilibrium by adsorption isotherms of granular activated carbon (GAC), the industrial benchmark for

adsorption on OFLOX and MB, are 95 mg/g and 187 mg/g respectively,[17] and that less than 5% of removal was observed for GAC after 30 min treatment.

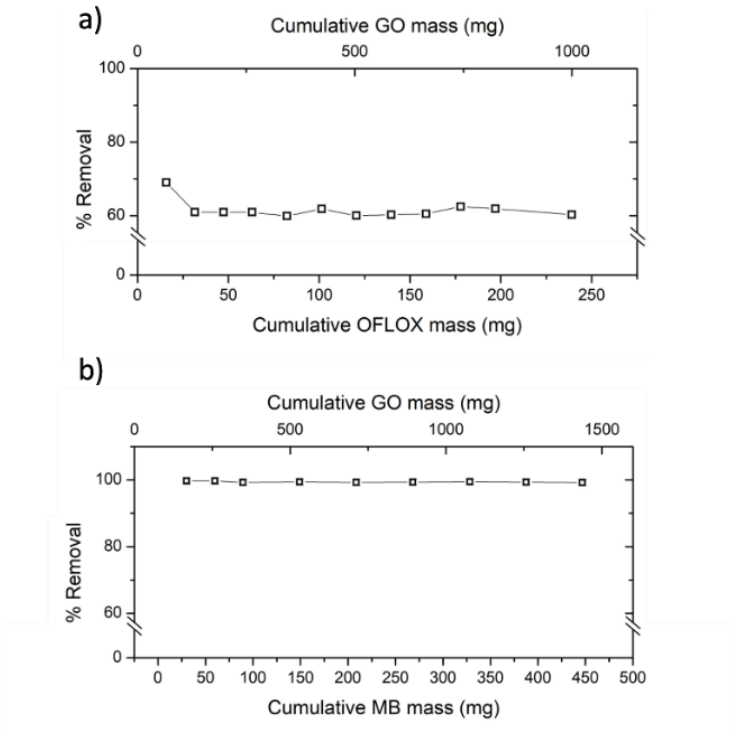

Fig. 4.5. *Estimation of maximum mass removal for a) OFLOX and b) MB. Each adsorption experiment was performed on the same MF module until clogging was reached. Experimental conditions for each repetition were: OFLOX/MB 30 mg, GO 80 mg; contact time 30 min; flow rate 55 mL/min; treated volume 100 mL.*

4.3.3 Regeneration of exhausted GO/rGO nanosheets

After recovering of exhausted GO/rGO materials, regeneration possibility was also investigated and the whole procedure is schematized in Fig. 4.6. To this aim, after adsorption of MB, recollected sheets were washed with ethanol (about 10 mL of ethanol per mg of MB), recovered by centrifugation and final filtration, dried and reused in a second run of adsorption. In the case of GO, a drop of removal from 99% →90%→ 70% was observed on going from the first to the third run, likely due to loss of material during each washing/filtration phases. Nevertheless, it should be pointed out that in this experiment a very high concentration of MB was used in order to saturate GO (i.e. 75 mg MB in 250 mL of water, 300 mg/L). Similar trend was observed for rGO.

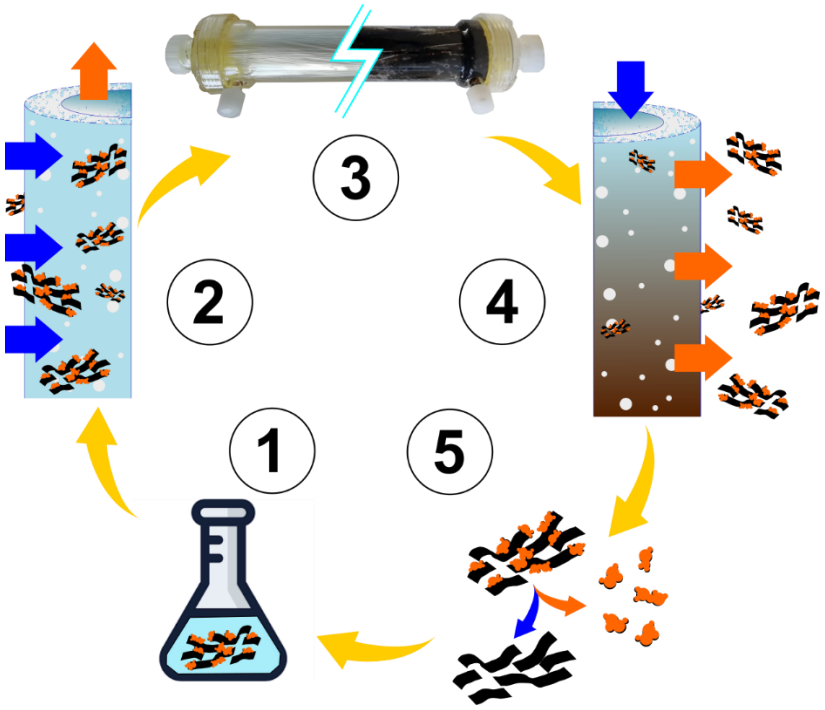

***F*ig. 4.6.** Regeneration scheme of exhausted GO/rGO and saturated filter. 1) GO/rGO is added to polluted water and stirred for 30 min in order to perform the adsorption, 2) exhausted GO/rGO is filtered in OUT-IN modality through a MF module, 3) this two-steps procedure is repeated until the clogging of the module occurs, 4) GO/rGO is recollected from the filter through the use of water and compressed air fluxes in IN-OUT modality, 5) contaminants are extracted from GO/rGO by washing with ethanol three times, thus regenerating the adsorbing material. Regenerated GO/rGO and MF module are then ready for further adsorption cycles.

4.3.4 Two step GO+MF vs one step PES-GO core shell HF

The performance of the procedure GO+MF was finally compared to that obtained by using a core-shell PES-GO hollow fibers (HF-GO) module, having a multilayer GO coating fixed to the PES fiber wall. We recently demonstrated that adsorption of organic contaminants in core-shell HF-GO modules occurs by intercalation of the molecules in between overlapped GO layers. [52] The core-shell HF-GO module was created by fixing 100 mg of GO on the outer wall of the fibers and the comparative experiments were performed at an OFLOX initial concentration of 200 mg/L. Fig. 4.7a and 4.7b describe the two different processes: i) GO nanosheets adsorb OFLOX and the GO sheets are then filtered on MF module in OUT-IN modality (Fig. 4.7a), ii) OFLOX spiked water is filtered on a core-shell HF-GO module having the same overall amount of GO pre-immobilized on the fiber surface outer wall in OUT-IN modality (i.e. the flow is forced to pass the GO multilayer, Fig. 4.7b). In the first case, the adsorption process mainly relies on the interactions of OFLOX molecules with the functional groups on GO nanosheets, including π-π interactions, H bonds and hydrophobic interactions. In the latter

case, adsorption occurs through the interplay of surface interactions and intercalation.[52]

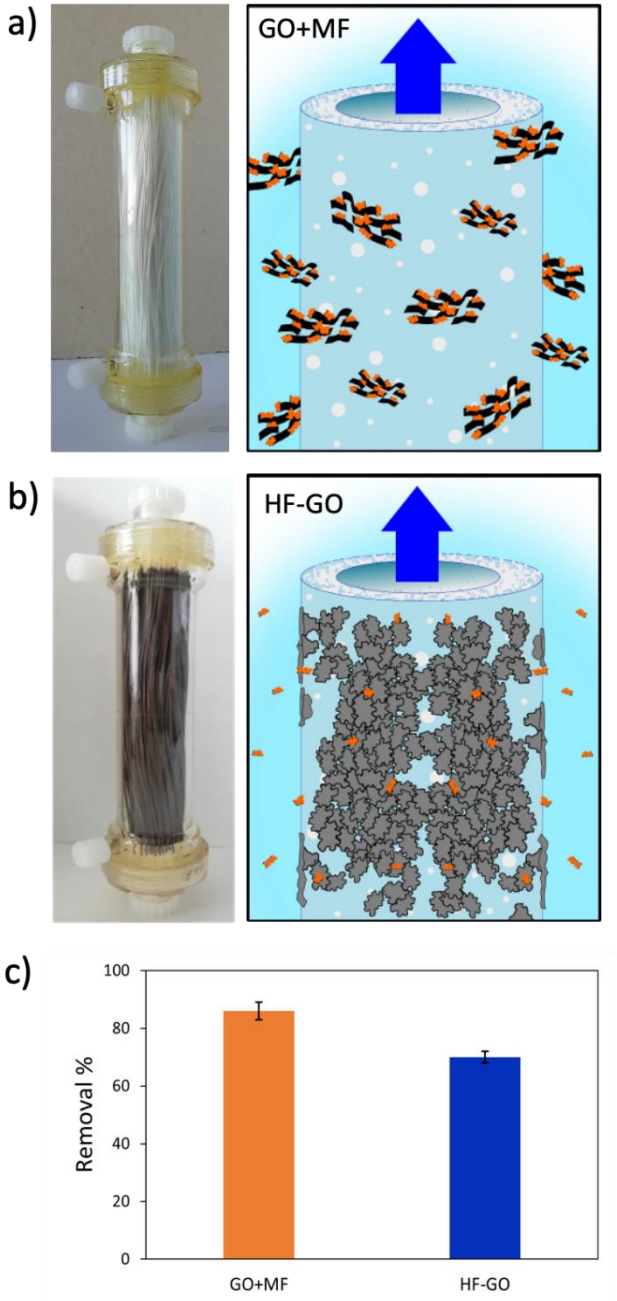

Fig. 4.7. *Comparison between GO+MF procedure here proposed and MF on GO coated HF fibers. a) MF module used for the adsorption-microfiltration process and sketch of the working mechanism, b) core-shell HF-GO module (left) and sketch of the working mechanism. Intercalation of OFLOX between the overlapped GO sheets in the multilayer has been already demonstrated.* [52] *c) Comparison between purification performances of adsorption performed by monolayer GO followed by microfiltration (GO+MF; orange bar) and simultaneous adsorption-microfiltration performed by GO multilayer (HF-GO; blue bar). Experiments repeated twice on two different modules.*

The removal efficiency estimated by UV-vis analysis for the GO+MF procedure was 86% (174 mg/g), and 70% (140 mg/g) for the core-shell HF-GO module (Fig. 4.7c), meaning that intercalation of molecules in GO multilayers overcomes the loss of surface area of the monolayer nanosheets. However, GO+MF procedure can be reiterated many times with almost the same performance (Fig. 4.5a) until saturation of the MF module by GO and allow regeneration of both GO and MF cartidge and reuse for three consecutive cycles. On the other hand, the core-shell HF-GO module performance drops from 70% to 21% after the second step.

4.3.5 Application of GO/rGO+MF to PFAS removal from tap water

The optimized procedure was then exploited for the removal of a mixture of PFAS of different alkyl chain length (3 ≤CF_2 ≤13) from spiked water at the maximum concentrations detected in contaminated groundwaters (i.e.10 µg/L) in Veneto Region (Italy) [29]. GO and rGO performances vs GAC are summarized in Fig. 4.8 . Adsorption tested on GO nanosheets (Fig. 4.8a, grey bars) showed increasing removal with the increase of alkyl chain length for molecules ending with a carboxylic group, i.e. perfluorobutanoic acid (PFBA, 3 CF_2, <5%), perfluorononanoic (PFNA, 8 CF_2, <20%), perfluorotridecanoic acid (PFTrDA, 12 CF_2, >99%). Higher performances were observed for sulfonated compounds rather than for carboxylic analougues, and on the increase of chain length, i.e. perfluorobutanesulfonic acid (PFBS, 4 CF_2 <5%), perfluorooctanesulfonic acid (PFOS, 8 CF_2 = 43%). After the MF step (Fig. 4.8a, yellow bar), removal was significantly higher for all compounds (PFBS increased from <5% to 91%) thanks to the contribution of the PES-HF to the adsorption. It can also be seen that rGO was more effective than GO (Fig. 4.8b; orange bars) in PFAS removal with increasing performance on increasing PFAS chain length, i.e. 21% for PFBA (3 CF_2), 61% perfluoropentanoic acid (PFPeA, 4 CF_2), 95% perfluorohexanoic acid (PFHxA, 5 CF_2). Sulfonated compounds are better removed than carboxylic molecules, i.e. 96% PFBS (4 CF_2) vs 61% PFPeA (4 CF_2). No significant contribution of the MF step on the removal efficiency was observed, as shown by the comparison with the experiment including the MF step (Fig. 4.8b, blue bars) and with rGO adsorption alone (Fig. 4.8b, orange bars).

The lower performance of GO with respect to rGO on both short chain and long chain sulfonated and carboxylic compounds could be likely ascribed to the different surface charge of GO and rGO. Indeed, the Z potential of GO was -43.5

mV (tap water, after 2 h sonication) while that of rGO was -35.3 mV. The more negative surface charge of GO leads to a higher repulsive electrostatic interactions with PFAS molecules, which are mostly present in solution as dissociated anions at neutral pH (such as in our experimental conditions). [62, 63] On the other hand, the enhancement of performance on increasing the perfluoralkyl chain length can be related to the higher hydrophobicity of the PFAS molecules with octanol-water partition coefficient (log Kow) values in the range 2.3-8.9 (PFBA, 3 CF_2, and PFTeA, 13 CF_2, respectively) as already reported in literature,[31] showing that hydrophobic interactions, rather than electrostatic ones, dominated PFAS adsorption onto GAC.

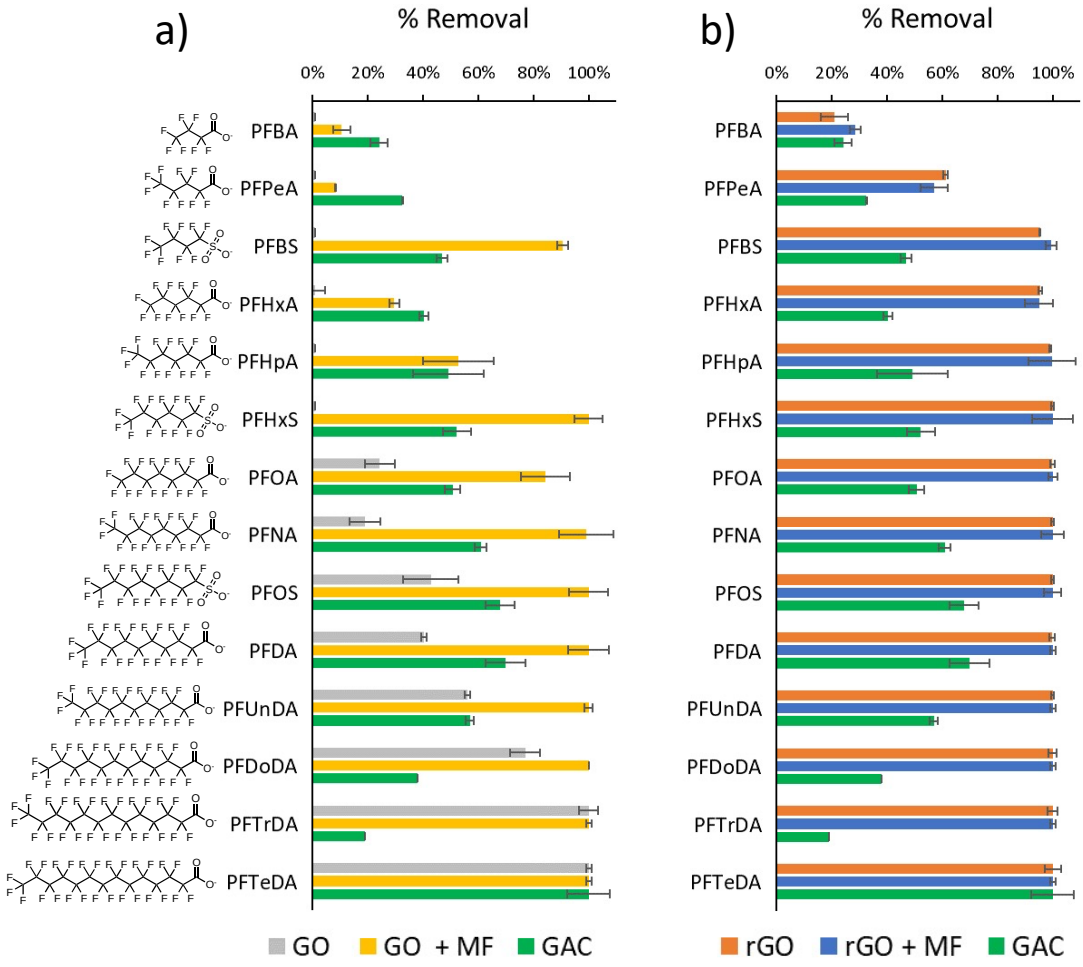

Fig. 4.8. *Removal of PFAS by a) GO after 30 min of adsorption (GO, grey bars) and after adsorption and microfiltration (GO+MF, yellow bars), and b) by rGO after 30 min of adsorption (rGO, orange bars), after adsorption and microfiltration (rGO+MF, blue bars) and after adsorption on GAC (green bars). PFAS initial concentration 10µg/L each.*

The performance of were compared to that of GAC,[64, 65] the standard adsorber used for PFAS removal in real potabilization plant. The MF+GO procedure removes about 72 µg/g of PFAS (total µg of PFAS per gram of sorbent), while the

MF+rGO removed about 138 µg/g of PFAS (total µg of PFAS per gram of sorbent), while GAC after 30 min of contact time removed 44 µg/g of PFAS (total µg of PFAS per gram of sorbent; this last value increases up to 96.3 µg/g after 24 h), highlighting the higher suitability of rGO with respect to GO and the higher performance of both GO/rGO+MF procedure with respect to GAC for PFAS adsorption.

It is noteworthy that dedicated kinetic experiments highlighted the superior performance of rGO that, in just 10 min rather than 24 h required to GAC, expressed most of its adsorption potential (Fig. 8.17 and Table 8.7, Appendix) with PFAS removals up to 3-5 times higher than GAC.

4.4 Conclusions

In conclusion, we presented a new methodology based on tandem adsorption on flocculated GO/rGO nanosheets and microfiltration, requiring only a few minutes to remove organic contaminants from drinking water. According to standard Italian regulation, potability was confirmed for GO/rGO+MF treated tap water and no evidence of graphene nanosheets release was found. The procedure exploited commercial GO and rGO nanosheets and commercially available hollow fiber microfiltration modules. The efficacy of the procedure on the removal of several classes of emerging contaminants (including OFLOX, a fluoroquinolone antibiotic) and PFAS was higher than that estimated for GAC adsorption under the same experimental conditions, in only few minutes of treatment.

The procedure has been here demonstrated for the removal of organic contaminants but it could be extended to the removal of metal cations, such as copper and lead, whose high performance adsorption of graphene has been widely demonstrated. [25] It provides a complementary purification technology to the current standard adsorption on GAC for the removal of contaminants that are not efficiently removed by GAC. Moreover, synergy between graphene and hollow fiber MF modules could be exploited to combine depuration and sanitation in a single device. Indeed, MF modules, even Plasmart modules herein described, are already used as last step of purification in point of use devices for final disinfection of treated water. To this aim, automatization and prototyping of graphene addiction are ongoing in our lab.

4.5 References

1. B. Petrie, R. Barden and B. Kasprzyk-Hordern, *Water Res.*, 2015, **72**, 3-27.
2. R. Tröger, H. Ren, D. Yin, C. Postigo, P. D. Nguyen, C. Baduel, O. Golovko, F. Been, H. Joerss, M. R. Boleda, S. Polesello, M. Roncoroni, S. Taniyasu, F. Menger, L. Ahrens, F. Yin Lai and K. Wiberg, *Water Res.*, 2021, **198**, 117099.
3. K. E. Murray, S. M. Thomas and A. A. Bodour, *Environ. Pollut.*, 2010, **158**, 3462-3471.
4. R. Meffe and I. de Bustamante, *Sci. Total Environ.*, 2014, **481**, 280-295.
5. H. R. Mortaheb, M. Baghban Salehi and M. Rajabzadeh, *Journal of Industrial and Engineering Chemistry*, 2021, **99**, 407-421.
6. Z. Xu, T. Wu, J. Shi, K. Teng, W. Wang, M. Ma, J. Li, X. Qian, C. Li and J. Fan, *J. Membr. Sci.*, 2016, **520**, 281-293.
7. N. Baig, Ihsanullah, M. Sajid and T. A. Saleh, *J. Environ. Manage.*, 2019, **244**, 370-382.
8. G. Ersan, O. G. Apul, F. Perreault and T. Karanfil, *Water Res.*, 2017, **126**, 385-398.
9. L. Jiang, Y. Liu, S. Liu, G. Zeng, X. Hu, X. Hu, Z. Guo, X. Tan, L. Wang and Z. Wu, *Environ. Sci. Technol.*, 2017, **51**, 6352-6359.
10. T. A. Tabish, F. A. Memon, D. E. Gomez, D. W. Horsell and S. Zhang, *Sci. Rep.*, 2018, **8**, 1817.
11. N. Yousefi, X. Lu, M. Elimelech and N. Tufenkji, *Nat. Nanotechnol.*, 2019, **14**, 107-119.
12. R. L. White, C. M. White, H. Turgut, A. Massoud and Z. R. Tian, *J. Taiwan Inst. Chem. Eng.*, 2018, **85**, 18-28.
13. S. Z. N. Ahmad, W. N. Wan Salleh, A. F. Ismail, N. Yusof, M. Z. Mohd Yusop and F. Aziz, *Chemosphere*, 2020, **248**, 126008.
14. S. Mantovani, S. Khaliha, L. Favaretto, C. Bettini, A. Bianchi, A. Kovtun, M. Zambianchi, M. Gazzano, B. Casentini, V. Palermo and M. Melucci, *Chem. Commun.*, 2021, **57**, 3765-3768.
15. K. Balasubramani, N. Sivarajasekar and M. Naushad, *J. Mol. Liq.*, 2020, **301**, 112426.
16. I. Anastopoulos, I. Pashalidis, A. G. Orfanos, I. D. Manariotis, T. Tatarchuk, L. Sellaoui, A. Bonilla-Petriciolet, A. Mittal and A. Núñez-Delgado, *J. Environ. Manage.*, 2020, **261**, 110236.
17. S. Khaliha, T. D. Marforio, A. Kovtun, S. Mantovani, A. Bianchi, M. L. Navacchia, M. Zambianchi, L. Bocchi, N. Boulanger, A. Iakunkov, M. Calvaresi, A. V. Talyzin, V. Palermo and M. Melucci, *FlatChem*, 2021, **29**, 100283.
18. W. Peng, H. Li, Y. Liu and S. Song, *J. Mol. Liq.*, 2017, **230**, 496-504.
19. M.-P. Wei, H. Chai, Y.-L. Cao and D.-Z. Jia, *J. Colloid Interface Sci.*, 2018, **524**, 297-305.
20. J. Geng, Y. Yin, Q. Liang, Z. Zhu and H. Luo, *Chem. Eng. J.*, 2019, **361**, 1497-1510.
21. D. R. Dreyer, S. Park, C. W. Bielawski and R. S. Ruoff, *Chemical Society Reviews*, 2010, **39**, 228-240.
22. S. Guo, Y. Nishina, A. Bianco and C. Ménard-Moyon, *Angew. Chem. Int. Ed.*, 2020, **59**, 1542-1547.
23. S. Khaliha, Unpublished results.
24. A. Kovtun, M. Zambianchi, C. Bettini, A. Liscio, M. Gazzano, F. Corticelli, E. Treossi, M. L. Navacchia, V. Palermo and M. Melucci, *Nanoscale*, 2019, **11**, 22780-22787.

25. F. Perreault, A. Fonseca de Faria and M. Elimelech, *Chem. Soc. Rev.*, 2015, **44**, 5861-5896.
26. E. F. Aboelfetoh, A. E. Aboubaraka and E.-Z. M. Ebeid, *J. Environ. Manage.*, 2021, **288**, 112481.
27. J. Glüge, M. Scheringer, I. T. Cousins, J. C. DeWitt, G. Goldenman, D. Herzke, R. Lohmann, C. A. Ng, X. Trier and Z. Wang, *Environmental Science: Processes & Impacts*, 2020, **22**, 2345-2373.
28. E. Panel o. C. i. t. F. Chain, D. Schrenk, M. Bignami, L. Bodin, J. K. Chipman, J. del Mazo, B. Grasl-Kraupp, C. Hogstrand, L. Hoogenboom, J.-C. Leblanc, C. S. Nebbia, E. Nielsen, E. Ntzani, A. Petersen, S. Sand, C. Vleminckx, H. Wallace, L. Barregård, S. Ceccatelli, J.-P. Cravedi, T. I. Halldorsson, L. S. Haug, N. Johansson, H. K. Knutsen, M. Rose, A.-C. Roudot, H. Van Loveren, G. Vollmer, K. Mackay, F. Riolo and T. Schwerdtle, *EFSA J.*, 2020, **18**, e06223.
29. R. O. f. E. HO (World Health Organization), 2017., *Keeping our Water Clean: The Case of Water Contamination in the Veneto Region, Italy (Copenhagen).* .
30. S. Valsecchi, M. Rusconi, M. Mazzoni, G. Viviano, R. Pagnotta, C. Zaghi, G. Serrini and S. Polesello, *Chemosphere*, 2015, **129**, 126-134.
31. C. Wu, M. J. Klemes, B. Trang, W. R. Dichtel and D. E. Helbling, *Water Res.*, 2020, **182**, 115950.
32. E. Gagliano, M. Sgroi, P. P. Falciglia, F. G. A. Vagliasindi and P. Roccaro, *Water Res.*, 2020, **171**, 115381.
33. T. Jin, M. Peydayesh and R. Mezzenga, *Environ. Int.*, 2021, **157**, 106876.
34. P. J. J. Alvarez, C. K. Chan, M. Elimelech, N. J. Halas and D. Villagrán, *Nat. Nanotechnol.*, 2018, **13**, 634-641.
35. P. Alipour Atmianlu, R. Badpa, V. Aghabalaei and M. Baghdadi, *J. Environ. Chem. Eng*, 2021, **9**, 106514.
36. S. Lath, D. A. Navarro, D. Losic, A. Kumar and M. J. McLaughlin, 2018, **15**, 472-480.
37. J. Becanova, Z. S. S. L. Saleeba, A. Stone, A. R. Robuck, R. H. Hurt and R. Lohmann, *Environ. Sci.: Nano*, 2021, **8**, 2894-2907.
38. C. Zhao, J. Fan, D. Chen, Y. Xu and T. Wang, *Nano Res.*, 2016, **9**, 866-875.
39. N. B. Saleh, A. Khalid, Y. Tian, C. Ayres, I. V. Sabaraya, J. Pietari, D. Hanigan, I. Chowdhury and O. G. Apul, *Environ. Sci. Water Res. Technol.*, 2019, **5**, 198-208.
40. D. Barker, A. Fors, E. Lindgren, A. Olesund and E. Schröder, *The Journal of Chemical Physics*, 2020, **152**, 024704.
41. L. Liu, Y. Liu, B. Gao, R. Ji, C. Li and S. Wang, *Crit. Rev. Environ. Sci. Technol.*, 2020, **50**, 2379-2414.
42. S. Deng, Q. Zhang, Y. Nie, H. Wei, B. Wang, J. Huang, G. Yu and B. Xing, *Environ. Pollut.*, 2012, **168**, 138-144.
43. Q. Yu, S. Deng and G. Yu, *Water Res.*, 2008, **42**, 3089-3097.
44. C. T. Vu and T. Wu, *Environ. Sci. Water Res. Technol.*, 2020, **6**, 2958-2972.
45. P. McCleaf, S. Englund, A. Östlund, K. Lindegren, K. Wiberg and L. Ahrens, *Water Res.*, 2017, **120**, 77-87.
46. Z. Bano, S. A. Mazari, R. M. Y. Saeed, M. A. Majeed, M. Xia, A. Q. Memon, R. Abro and F. Wang, *J. Water Process Eng.*, 2020, **36**, 101404.
47. Z. Sun, S. Fang and Y. H. Hu, *Chem. Rev.*, 2020, **120**, 10336-10453.
48. Y. Shen, Q. Fang and B. Chen, *Environ. Sci. Technol.*, 2015, **49**, 67-84.
49. Y. Lin, Y. Tian, H. Sun and T. Hagio, *Chemosphere*, 2021, **270**, 129420.

50. R. Mohd Firdaus, N. Berrada, A. Desforges, A. R. Mohamed and B. Vigolo, *Chemistry – An Asian Journal*, 2020, **15**, 2902-2924.
51. P. Srivastava, B. Singh and M. Angove, *J. Colloid Interface Sci.*, 2005, **290**, 28-38.
52. A. Kovtun, A. Bianchi, M. Zambianchi, C. Bettini, F. Corticelli, G. Ruani, L. Bocchi, F. Stante, M. Gazzano, T. D. Marforio, M. Calvaresi, M. Minelli, M. L. Navacchia, V. Palermo and M. Melucci, *Faraday Discuss.*, 2021, **227**, 274-290.
53. P. Zhang, J.-L. Gong, G.-M. Zeng, C.-H. Deng, H.-C. Yang, H.-Y. Liu and S.-Y. Huan, *Chem. Eng. J.*, 2017, **322**, 657-666.
54. W. C. Chong, Y. L. Choo, C. H. Koo, Y. L. Pang and S. O. Lai, *AIP Conf. Proc.*, 2019, **2157**, 020005.
55. J. F. a. K. Kenney, E. S., *Percentile Ranks 3.6 in Mathematics of Statistics, Pt. 1*, 3rd ed. Princeton, NJ: Van Nostrand pp. 38-39, 1962., 1962.
56. C.-J. Shih, S. Lin, R. Sharma, M. S. Strano and D. Blankschtein, *Langmuir*, 2012, **28**, 235-241.
57. I. Chowdhury, M. C. Duch, N. D. Mansukhani, M. C. Hersam and D. Bouchard, *Environ. Sci. Technol.*, 2013, **47**, 6288-6296.
58. M. Zambianchi, M. Durso, A. Liscio, E. Treossi, C. Bettini, M. L. Capobianco, A. Aluigi, A. Kovtun, G. Ruani, F. Corticelli, M. Brucale, V. Palermo, M. L. Navacchia and M. Melucci, *Chem. Eng. J.*, 2017, **326**, 130-140.
59. P. Bradder, S. K. Ling, S. Wang and S. Liu, *Journal of Chemical & Engineering Data*, 2011, **56**, 138-141.
60. Q. Kong, X. He, L. Shu and M.-s. Miao, *Process Saf. Environ. Prot.*, 2017, **112**, 254-264.
61. A. Molla, Y. Li, B. Mandal, S. G. Kang, S. H. Hur and J. S. Chung, *Appl. Surf. Sci.*, 2019, **464**, 170-177.
62. Ş. I. Voicu, F. Aldea and A. Nechifor, *Rev. Chim.*, 2010, **61**, 817-821.
63. K.-U. Goss, *Environ. Sci. Technol.*, 2008, **42**, 5032-5032.
64. M. Elabadsa, M. Varga and V. G. Mihucz, *Microchem. J.*, 2019, **150**, 104079.
65. R. Desmiarti, Y. Trianda, M. Martynis, A. Viqri, T. Yamada and F. S. Li, *Int. J. Technol.*, 2019, **10**, 1488-1497.

5 Graphene-composite for water treatments

Graphene oxide-polysulfone hollow fibers membranes with synergic ultrafiltration and adsorption for enhanced drinking water treatment

Adapted with permission J. Membr. Sci, 658, (2022), 120707; Elsevier

DOI 10.1016/j.memsci.2022.120707

5.1 Introduction

Polysulfone (PSU) porous membranes are well-known and used membranes for micro and ultrafiltration for hemodialysis and water disinfection purposes. [1-4] Their wide range of applications relies on the structure versatility of such membranes, with morphology and porosity that can be tuned by the choice of several parameters including processing solvent/ non solvent, coagulation temperature, casting solution composition and humidity.[5-7] In recent years, aiming at membranes with enhanced mechanical properties, biofouling resistance and multifunctionality, doping of PSU membranes (mainly flat membranes) with nanomaterials have been widely investigated.[8]

Carbon-based nanomaterials such as carbon nanotubes (CNT), nanofibers and graphene-reinforced membranes have been fabricated by phase inversion processes adapted to integrate such nanomaterials.[9] It has been shown that doping of PSU with carbon nanotubes of different structure (single, multiwalled) and functionalization (i.e. amine, azide, carboxylic groups) increases water permeability (up to ~600 $Lm^{-2}h^{-1}$),[10] improves tensile strength and modulus, increases materials crystallinity and thermostability[11] and enhanced rejection of NaCl solution.[12] With the advent of graphene 2D materials, having higher processability and lower costs than CNT, graphene doped membranes have been also realized[13, 14] and have shown improved thermal and mechanical properties,[15] [16] ion exchange capability[17] and arsenate rejection capability (just to mention few)[18], than undoped analogues.

Adsorption properties were observed for these membranes.[19, 20] For instance Badrinezhad et al demonstrated methylene blue adsorption from water with removal efficiency of about 80% by 0,75% doped PSU membranes[21] and desorption of about 40% which was lower than that observed in graphene free

membranes. The fabrication of PSU-GO adsorptive membranes with 5% in weight of GO content was repeated and demonstrated the ability of this membranes to adsorb selected emerging contaminants (ECs) in mixture in tap water with significant enhancement of removal of hydrophilic molecules including ofloxacin antibiotic, carbamazepine and diclofenac.[22]

On this line, here we report the fabrication of PSU hollow fiber (PSU-HFs) membranes through an ad hoc developed industrial pilot plant (Medica spa, production capacity 200000 Km/yr) doped with GO at different loadings (PSU-GO HFs). We investigated the structural, filtration and adsorption properties of modules realized by the newly developed HFs aimed at their exploitation for the fabrication of multifunctional modules for point of use (POU) drinking water treatment.

POU drinking water treatment systems are installed on the water supply lines ahead of water taps, and/or dispensers to provide on-site water purification. A wide range of POU technologies have emerged in recent years including adsorption membrane filtration and disinfection that are combined in a specific sequence to form a POU system. These systems are exploited to adjust water taste and odour and are expected to remove hazardous contaminants such as ECs[23-28] not completely removed during drinking water treatment such as perfluoroalkyl chain substances (PFAS).[29-36]

Polysulfone hollow fiber (PSU-HFs) membranes consist of hollow fibers with surface pores and macro voids of porosity in the range 5-10 nm that have been recently introduced in the POU water purification market for water disinfection, i.e. removal of bacteria, viruses and endotoxins capability. PSU-HFs modules are exploited as last treatment step after adsorption and/or ion exchange and/or reverse osmosis steps to remove pathogens.[37, 38] Aiming at simplified and more efficient POU systems,[39] here we propose adsorptive PSU-GO HFs based modules for combined ultrafiltration and adsorption of different water pollutants, both organics and heavy metals. Previous studies on PSU-HFs doped with carbon nanoparticles and prepared by phase inversion DMF→water showed adsorptive capability toward benzene, phenol and toluene from aqueous solution[40] with adsorption capacity (Q_{max}) of the membranes increasing with carbon nanoparticle concentration in the range 50-60 mg/g. Zahri et al [41] reported PSU-graphene oxide hollow fiber membranes prepared by phase inversion from a mixture DMAC, THF

and EtOH to water and demonstrated gas separation properties with CO_2/N_2 and CO_2/CH_4 selectivity enhancement by 158% and 74% respectively with respect to neat PSU membranes. More recently, Sainath et al further enhance the CO_2/CH_4 gas separation performance of PSU-GO HFs by zeolitic imidazolate nanoparticles inclusion.[42]

However, at the best of our knowledge no examples of PSU-GO HFs for combined adsorption and ultrafiltration for the removal of pollutants in mixture in tap water have been reported. Here, we consider selected organic and heavy metal contaminants of concern recently revised in the drinking water directive EU 2020/2184,[43] including perfluoroalkyl substances (PFAS)[29-34] Pb and Cr[44, 45] and studied their adsorptive removal by the newly developed PSU-GO HF modules.

Moreover, to evaluate safe use of the proposed filters for drinking water filtration, we tested the release of GO nanosheets from such modules through Surface Enhanced Raman Spectroscopy (SERS) method, allowing state of the art limit of quantification of GO in water down to 0.1 ppb.

5.2 Experimental

5.2.1 Materials

GO powder was purchased from Abalonyx (AS, Norway) and used without further purification (graphene oxide dry powder <35 mesh, product code 1.8, XPS: O/C ratio 0.39 ± 0.01, C 70.1 ± 0.9%, O 27.2 ± 0.9%, N 0.2 ± 0.1%, S 1.0 ± 0.1%, Si 0.8 ± 0.1%, Cl 0.7 ± 0.1%, Mn below 0.1%). Standard PSU HFs (Medisulfone®) and PSU Ultrafiltration modules were provided by Medica Spa.

5.2.2 Porosity

PSU HFs and PSU-GO 3.5% HFs have been analyzed for pore size and pore distribution through liquid-liquid-displacement-porometer (LLDP), Poroliq TM1000 (Porometer, Germany-Belgium). PSU HFs porosity was measured after spinning without glycerinization, since glycerin impairs the porometer measurement. PSU-GO 3.5% HFs were analysed after mild glycerinization, extensive water washing and air-drying at room temperature, to remove any glycerin residual. Fibers to be analyzed by LLDP were prepared by horizontally placing one or more hollow fibers into the holder and sealing with a bicomponent glue the fibers' edges; measurement occurred in out-in modality. Isobutanol saturated with water was the wetting liquid and the water saturated with butanol was the displacement liquid.

5.2.3 HF spinning and module assembling

The dope solution is prepared adding PSU granules to a GO solution in NMP, obtained after 24-36 h of sonication, at room temperature (25°C). PSU is mixed with the GO solution (ratio 1→5% w/w PSU/GO, polymer concentration range 10-20% PSU-GO/NMP), alternating propeller immersion mixing and sonication, while viscosity is checked periodically. The resulting dope solution is extruded with a lab scale benchtop spinning plant, with a maximum dope solution capacity of 3 kg at room temperature (Fig. 8.18, Appendix). During extrusion in the spinneret, the dope solution enters in contact with a precipitation solution composed of water and NMP. The PSU-GO HF then freely fall in a coagulation bath, are collected by a bobbin system, moved into a washing bath, and finally collected onto a collection wheel. Fibers are stocked in bundles and then kept in water for solvent extraction and glycerinization, and ultimately dried at open air. 1 kg of material corresponds approximately to 20 km of fibers.

Lab-scale modules of standard PSU Medisulfone® and PSU-GO HF were prepared, containing different GO loadings (Fig. 5.1). Small bundles of closed fibers are obtained cutting the dried stocked bundles with a hot wire. Fibers are then potted in polyurethane resin at the edges inside a module scaffold and then centrifuged. The potting is ultimately cut (to open the fibers) and headers were welded.

Filtering surface (FS) of the modules was 0,025 m^2 (standard PSU HF) or 0.015 m^2 (PSU-GO HF) and they were assembled into a cartridge of 5 mL dead volume. For characterization at tap POU, modules with U-shaped fibers were prepared with FS 0.28 m^2; U-shaped modules can be directly connected to the tap, working with tap water pressure (3 bar; mean flow rate 5 L/min).

5.2.4 Ciprofloxacin adsorption experiments

The adsorption capacity of PSU-GO HFs containing different GO loadings was tested under dynamic conditions by filtering tap water spiked with ciprofloxacin (Fig. 8.1, Appendix). In a typical experiment, 5 mg/L CIPRO tap water solution was filtered in dead end in-out transmembrane modality on PSU-GO HFs module at a constant flow of 5 mL/min. Fractions each 200 mL were collected and analysed by UV-vis analysis (Agilent Cary 3500) to determine CIPRO concentration. The filtration experiments were carried out until the removal was below 2%. The experiments were repeated in triple by using new modules for each repetition.

5.2.5 Cut-off determination by dextrans filtration

Fluorescent dextrans at different molecular weight (MW) were used as tracers for cut-off determination. Fluorescein isothiocyanate dextran 4 kDa, 10 kDa, 20 kDa, 40 kDa, 70 kDa were purchased from Merck. A solution of each tracer in *N*-propyl-gallate was prepared at a concentration of 5 mg/mL. Lab-scale modules of PSU and PSU-GO 3.5% HFs were tested, (three modules for each tracer). The modules were pre-rinsed with water and the tracer solution was filtrated in dead end in-out modality at constant pressure. The filtrate was collected in sequential fraction of 500 µL volume each. A total of 12-14 fractions were collected for each module. Samples were analyzed by a fluorometer (Fluoroskan, ThermoFisher Scientific) at the excitation wavelength of 484 nm and emission wavelength of 538 nm. Experiments were repeated in triple by using each time a new module.

5.2.6 PFAS removal experiments and analysis

Tap water spiked with a mixture of fourteen PFAS C_3-C_{13} (Fig. 8.12, Appendix) was prepared and filtered (dead end, in-out) at 5 mL/min using a Cole-Parmer Masterflex® peristaltic pump on the selected PSU HFs, PSU-GO 3.5% HFs and GAC modules, previously washed with 2 L of MilliQ water. GAC was tested for comparison. The concentration of each contaminant was 0.5 µg/L in a total volume of 1 L. The concentration of PFAS in filtered water was analyzed by UPLC-MS/MS.

5.2.7 UPLC-MS/MS method for PFAS quantification

Analysis on PFAS were performed also by using a UPLC-MS/MS Waters ACQUITY UPLC H-Class PLUS – XEVO TQS Micro mass detector. 0.5 mL samples were used as sources for the automated injection. The chromatographic separation was performed on a reverse phase Waters Acquity UPLC CSH Phenyl-Hexyl (2.1 x 100 mm, 1.7 µm) and Waters Isolator Column 2.1x50 mm, column temperature 34 °C, linear gradient from 100:0 to 5:95 mobile phase A (MeOH: aqueous NH_4OAc 2 mM 95:5)/mobile phase B (NH_4OAc 2 mM in MeOH), flow rate 0.3 mL/min. The mobile phase composition varied according to the gradient program reported in Table 8.3, Appendix. Mass details and limits of quantification (LOQ) for each analyte are reported in Table 8.4, Appendix.

The calibration curves were calculated by using the average value of 2 subsequent UPLC-MS/MS injections. Calibration curve solutions (0.1, 0.5, 1.0, 2.5, 5.0, 10) were freshly prepared diluting methanolic PFAS stock solution with laboratory phase A and injected before each analytical batch. Regression equations of

calibration curves were linear in the range of 10-0.01 or 0.05 or 0.1 mg/L depending on the analyte (see Table 8.4, Appendix). The results are expressed as the mean of 2 ± SD. Laboratory drinking water was checked for PFAS contamination: no PFAS were detected above LOD value.

5.2.8 Heavy metals removal experiments and analysis

Mineral water spiked with a mix of heavy metals and metalloids (Pb, Cu, Cd, Ni, Cr(III), As(V), V and U) at a final concentration of 100 µg/L each was prepared starting from individual 1 g/L stock solutions (ICP-MS standards, VWR). Spiked mineral water was filtered on selected modules (PSU HFs, PSU-GO 3.5% HFs and GAC), previously washed with 1 L of MilliQ water. Flow was set at 5 mL/min and 3 L of water were treated, then flow was incremented to 40 mL/min and two more liters treated for a preliminary evaluation of performance under different flow conditions of the selected modules. Samples were collected every 200 mL. Each fraction was immediately acidified with 1% HNO_3 Suprapur (Sigma-Aldrich) and solutions were analyzed by ICP-MS (Model 5800, Agilent).

At the end of the filtration experiment, the mobility of adsorbed contaminants was tested by passing three fractions of 50 mL MilliQ water at 20 mL/min in-out mode, and two more fractions of 50 mL in reverse out-in flow. Concentration was measured as described above and percentage of release respect to total adsorbed was calculated. Module filling material weight was 0.2, 0.26 and 1.5 g for PSU HFs, PSU-GO 3.5% HFs and GAC, respectively. All tests were carried out in duplicate and reported as mean value with standard deviation.

5.2.9 Potability of filtered water

Chemical and biological parameters included in the Italian D.Lgs 31/01 (implementation of 98/83/EU Directive) were tested in tap water before and after in-out filtration through PSU-GO 5% module with U-shaped fibers of FS 0.28 m^2 at 5 L/min, total volume 100 L.

5.2.10 GO release tests by SERS

PSU HFs and PSU-GO 3.5% HFs modules were washed with 2 L of hot MilliQ water (80 °C) in dead end in-out configuration at 50 mL/min using a Cole-Parmer Masterflex® peristaltic pump, to remove glycerin. Thereafter, 500 mL, were recirculated for 2 h at 250 mL/min. The flow used was significantly higher than the maximum one that the module is supposed to ensure to guarantee porosity and filtration capacity (i.e. max flow 50 mL/min). This flow may cause mechanical

stress of the hollow fibers, with possible release of GO from the fibers. Same procedure was performed on PSU-GO HFs. Samples were analyzed using surface-enhanced Raman spectroscopy (SERS). [46]

The SERS-active substrate was prepared in the following way: gold nanoparticles (AuNPs; 20 µL of a 10.7 nM solution) were deposited dropwise on a Si/SiO_2 substrate. Subsequently, 120 drops (1200 µL) of analytical solution were added to the center of the SERS substrate. The sample was analyzed by SERS detection using an InVia Renishaw microspectrometer equipped with a 532 nm point-based laser. The power density was kept below 10% and a 1 s acquisition time was employed to avoid laser heating effects. SERS measurements were acquired for 400 μm^2 surfaces located in the middle of the drops with an average of 3000 spectra measurements. The baseline was removed using Windows®-based Raman Environment (WiRE) software. The 3000 spectra were then averaged to give a single spectrum for each replica, using a program generated in MATLAB R2020a with our own code. The spectrum of AuNPs was used as the control and was subtracted in all the samples to avoid the interferences.

The calibration curve was built using the intensity of the D peak, as analytical signal, for the concentration range 0.1-10 µg/L. The practical limit of quantification (P-LOQ), which is defined as the minimum level at which GO can be measured in water samples with accuracy higher of 80% and relative standard deviation (RSD) lower than 10%, was 0.1 ppb.

5.3 Results and Discussion

5.3.1 PSU-GO HFs modules fabrication and characterization

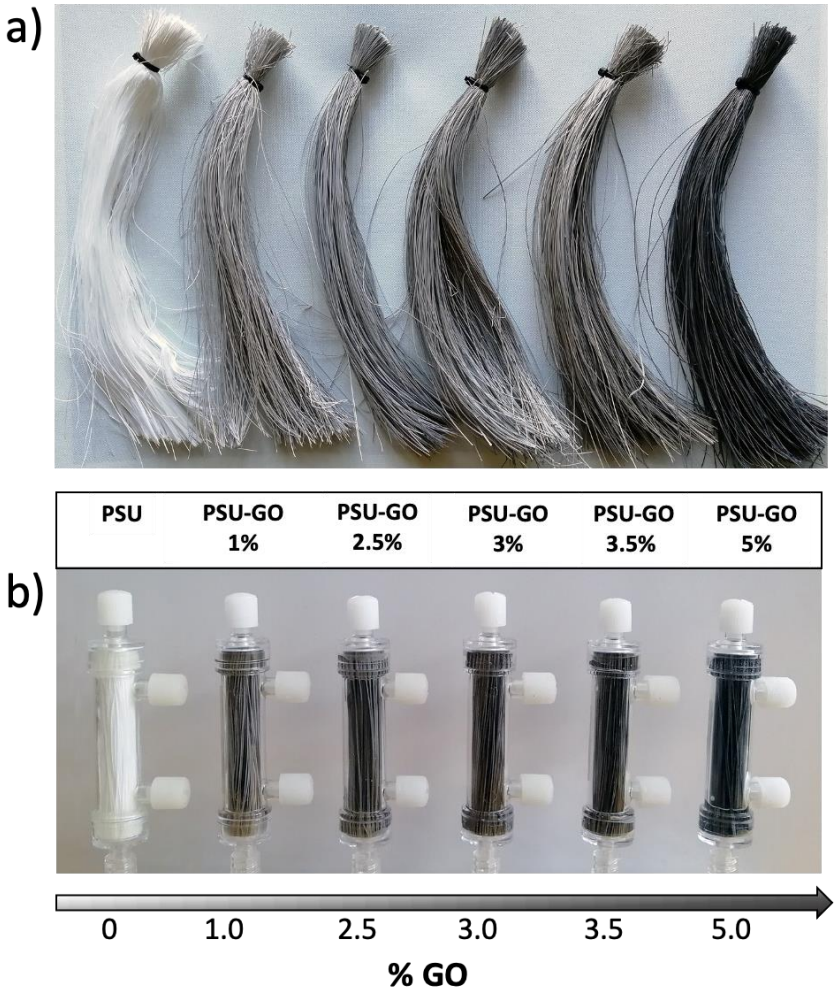

Fig. 5.1. *a) PSU HFs and b) filtration modules, with different amounts of GO (w/w). From left to right: pristine PSU; PSU-GO 1%; PSU-GO 2.5%; PSU-GO 3%; PSU-GO 3.5%; PSU-GO 5%. Cartridge size are 6.5 cm length, 1.5 cm diameter, 4.5 ml dead volume.*

Hollow fibers of PSU-GO at 1%, 2.5%, 3%, 3.5% and 5% w/w (GO:PSU) were obtained by phase inversion procedure (NMP→water) of a GO:PSU casting solution (PSU/NMP 10-20% w/w, PSU/GO 1-5% w/w) at room temperature, through a pilot spinning line by using the pre-industrial pilot line shown in Fig. 8.18, Appendix. The membranes were then assembled in prototype modules of filtering surface 0.015 m^2 that were then used for the following performance tests. The maximum flow rate acceptable for these cartridges was about 100 mL/min. Membranes and corresponding modules are shown in Fig. 5.1.

The pore average size and pore distribution of PSU and PSU-GO HFs were analyzed by porometer (pore distribution through LLDP (Liquid-Liquid-Displacement-Porometer, details in materials and methods).

The size of through-pores of PSU and PSU-GO fibres was considered as the MFP (Mean Flow Pore Size) which represents the pore range with an amount of 50 % of the total flow (point of intersection of LLDP- and Half-Perm-Curve) and results are reported in Table 5.1.

PSU-GO HFs showed average pore size of 13 nm, i.e. higher than that determined for standard PSU HFs (6 nm), this being likely due to the slightly different extrusion conditions exploited for PSU-GO spinning.

Table 5.1. *Diameters of through-pores (nm) obtained by using Liquid-Liquid-Displacement-Porometer.*

	Small pore size	Mean Flow Pore	Maximum pore size
PSU	6.2 ±0.3	6.4 ±0.4	6.5 ±0.3
PSU-GO 3.5%	11 ±1	13 ±2	22 ±6

The morphology of PSU-GO fibers resembles that of the pristine PSU HFs with wall section thickness of about 50 mm, lume diameter of 250-300 mm and outer porosity of 5-10 mm (Fig.5.2).

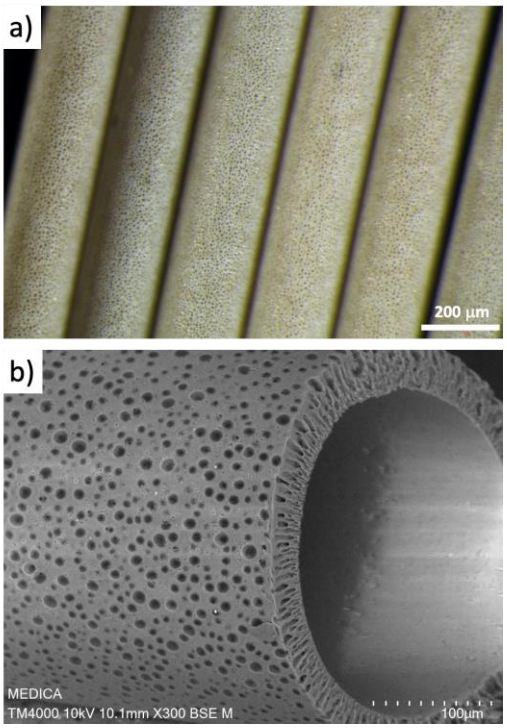

Fig. 5.2. *PSU-GO HFs morphology. a) Optical microscopy image of fibers, b) HF wall and section.*

The cross-section SEM images of PSU-GO HFs as a function of the GO loadings, at 1%, 3.5% and 5% loading are shown in Fig. 5.3. PSU-GO HFs show the typical hollow fiber structure, with extended finger-like pores and a thin sponge-like layer beneath it. An average wall thickness of ca. 45 ± 5 μm and inner diameter of ca. 220 ± 20 μm was observed for all the samples together with a slight increase in the micro-void size is observed on increasing GO loading. Some large GO flakes can be seen exposed at the outer surface of the pores (Fig. 5.3f, representative SEM image of PSU-GO 1%) in accordance with the contact angle measurements (Fig. 8.19, Appendix), showing a decrease from 60.1±4.1 ° for PSU to 53.1±2.1° for PSU-GO 3.5%, indicating a slight enhancement of the surface hydrophilicity.

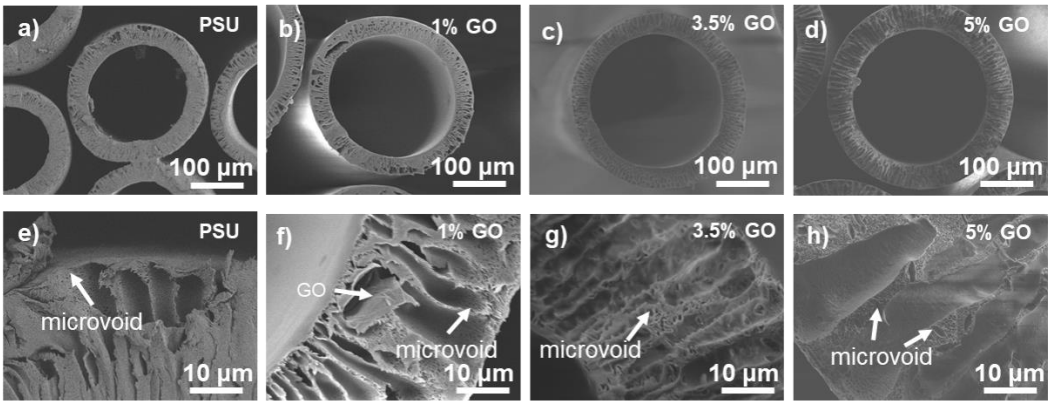

Fig. 5.3. *Low and high magnification SEM cross-section images of a,e) bare PSU, b,f) PSU-GO 1%, c,g) PSU-GO 3.5%, d,h) PSU-GO 5% HFs.*

Raman spectra of GO and PSU-GO HFs are showed in Fig. 5.4 and Fig. 8.20, Appendix. The spectrum of PSU (Fig. 8.20a, Appendix) showed main peaks located at around 790, 1146, 1584, 1605, and 3068 cm^{-1}, correlated to the asymmetric C-S-C, asymmetric C-O-C vibration, aromatic ring chain vibration, and C-H vibration, respectively. The broad peak at around 2900 cm^{-1}, can be ascribed to the PSU methyl bonds. The Raman spectrum of GO showed two characteristic peaks at 1350 and 1596 cm^{-1} (Fig. 5.4a), corresponding to the D band (defects or disorders) and G band (pristine sp^2 carbon atoms) of GO. No overlap between the D band from GO and other characteristic peaks of PSU were observed this allowing the identification of GO distribution on PSU-GO composites by Raman mapping. Raman mapping and depth profiling techniques are shown in Fig. 5.4b and Fig. 8.20, Appendix. All tested PSU-GO samples, including 1%, 3.5% and 5% GO loading amount, showed GO almost homogeneous distribution inside the hollow fiber section. As expected, PSU-GO 5% revealed the highest D peak

intensity (5x10^4 CCD cts). Meanwhile, GO flakes on PSU-GO 3.5% showed the best integration with the finger-like PSU matrix structure, according to the D peak distribution of GO from the relative z-stack imaging (Fig. 5.4b).

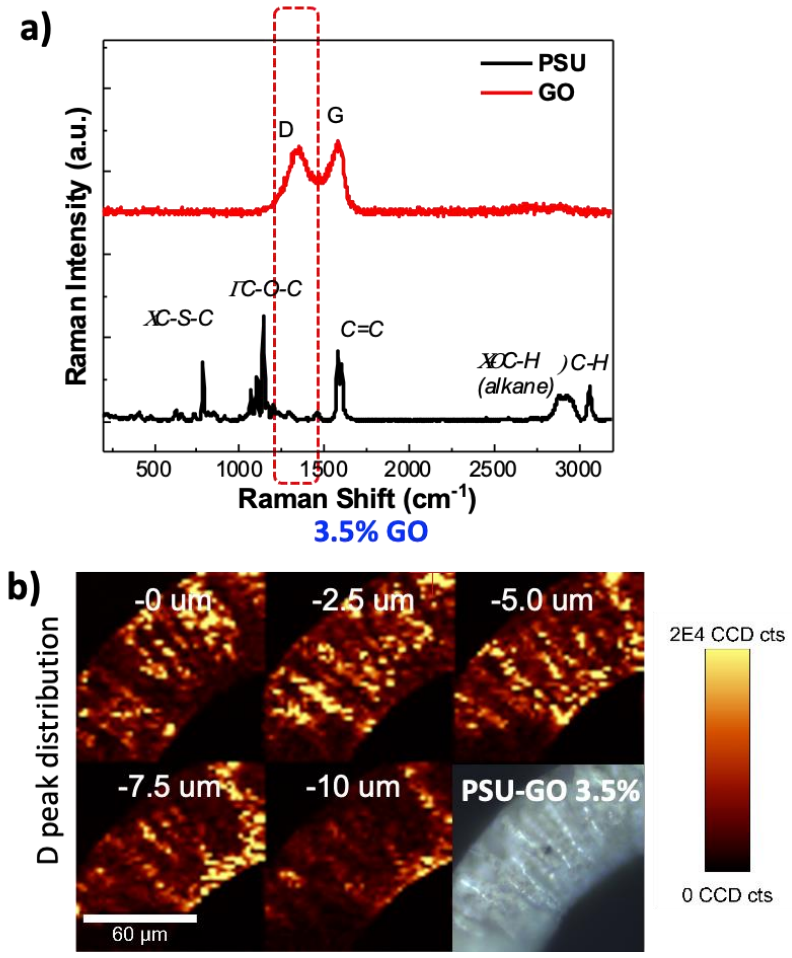

Fig. 5.4. *a) Raman spectra of GO and PSU; b) Z stack of Raman maps and the relative optical image of PSU-GO 3.5% HFs, constructed by mapping the D-band region.*

5.3.2 Tailoring of GO loading in PSU-GO HFs

Ciprofloxacin (CIPRO), a fluoroquinolone antibiotic, is strongly adsorbed by GO [47] but it is not removed by PSU HFs, thus we here exploited CIPRO removal from water to study its adsorption as a function of GO loading amount in order to optimize the hollow fibers composition. Tap water spiked with CIPRO was filtered through modules of PSU-GO HFs (Fig. 5.5a), dead-end transmembrane modality (in-out), at low flow rate (5 mL/min) until breakthrough was reached (about 3L filtered). We estimated the maximum adsorption capacity (Qmax) as milligrams of CIPRO removed per gram of composite by the plateau of the loading curves. As shown by Fig. 5.5b the performances were independent from the initial concentration of CIPRO in the range 0.5-5 mg/L. CIPRO spike at 5 mg/L was

chosen to enable fast detection by UV, the low flow rate was selected to reach the highest contact time allowed in flow experiments and establish the highest removal capacity of the modules.

The overall trend of adsorption capacity Qmax on increasing GO doping amount (0%-5%) is shown in Fig. 5.5c (and Fig 8.21, Appendix), with Qmax increasing from 0.25 mg/g to about 6 mg/g from PSU HFs (0% GO) to PSU-GO 5% HFs. No significant advantage was observed by increasing GO amount from 3.5% to 5%, this highlighting PSU-GO 3.5% as the best compromise between performance and costs, mainly affected by GO doping amount.

The maximum adsorption capacity of GO for CIPRO estimated by isotherm curve is about 250 mg/g of GO at the equilibrium time (24 h).[47] In our experimental conditions, the contact time at 5 mL/min is about 35 s., thus far from the equilibrium conditions, the maximum adsorption capacity expressed in mg removed/g of total GO was 168 mg/g of GO (PSU-GO 3,5%), which is close to the value at the equilibrium (250 mg/g), this indicating that the flow rate does not significantly affect the total removal capacity of PSU-GO HFs filters.

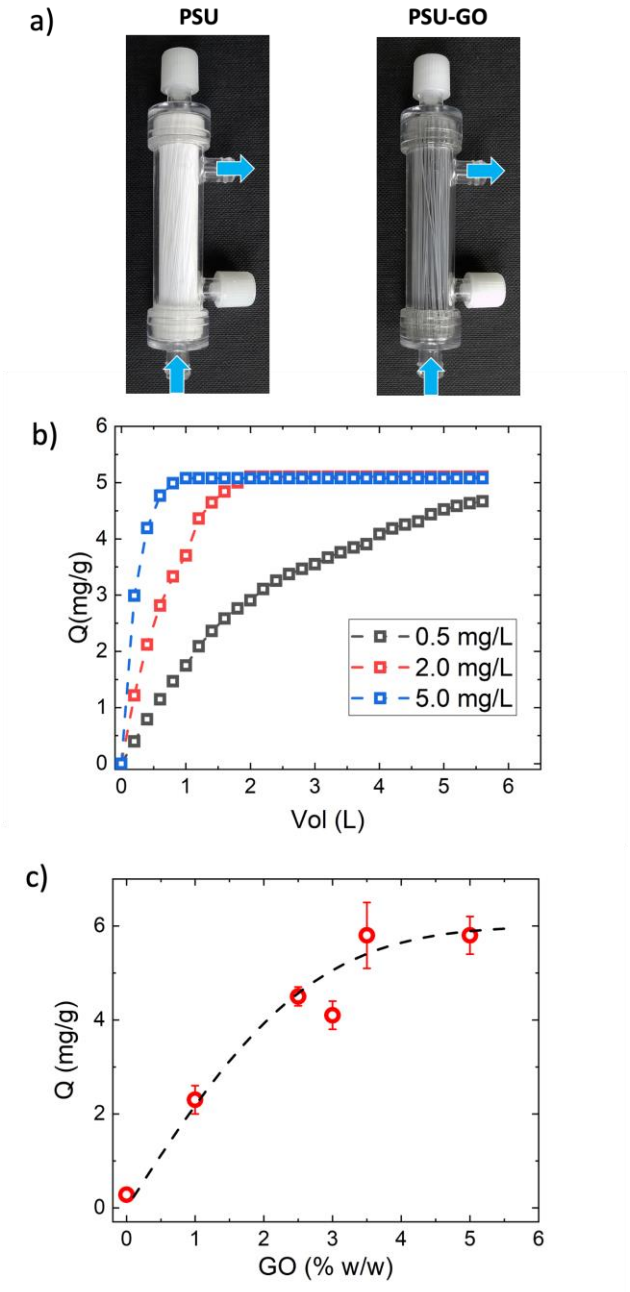

Fig. 5.5. *a) From left to right, modules of PSU HFs, and PSU-GO 3.5% HFs. The arrow indicates water in and out pathways (i.e. dead end transmembrane in-out modality for PSU HFs and PSU-GO HFs,). b) Adsorption capacity as a function of the initial CIPRO concentration on PSU-GO 3.5% HFs. c) maximum adsorption capacity estimated by the loading curves (Fig. 8.21, Appendix),* C_{IN} *CIPRO=5 mg/L, treated volume 3 L, flow rate 5 mL/min.*

5.3.3 Molecular Weight Cut-Off (MWCO) and ultrafiltration of PSU-GO HFs

The MWCO of PSU-GO 3.5% HFs, taken as reference, was determined by fluorescent dextrane filtration experiments. Fluorescein isothiocyanate (FITC) dextranes of different MW were filtered over PSU and PSU-GO HFs in dead end in-out modality. The MWCO of HFs is conventionally defined as the MW of the molecule with 90% retention. Fig. 5.6a shows the trend of retention vs FITC-

Dextrane MW and a MWCO of 15 kDa, and 62 kDa are estimated for PSU and PSU-GO 3.5% HFs, respectively, in line with the porometer determination. Nevertheless, permeability of PSU and PSU-GO HFs (UF coefficient) were almost comparable. Indeed, ultrafiltration coefficients estimated by flowing pure water through the filters and measuring pressure and ultrafiltration rate, were similar, i.e. 7.6±1.0 (PSU) and 10.1±1.7 (PSU-GO) (Fig. 5.6b)

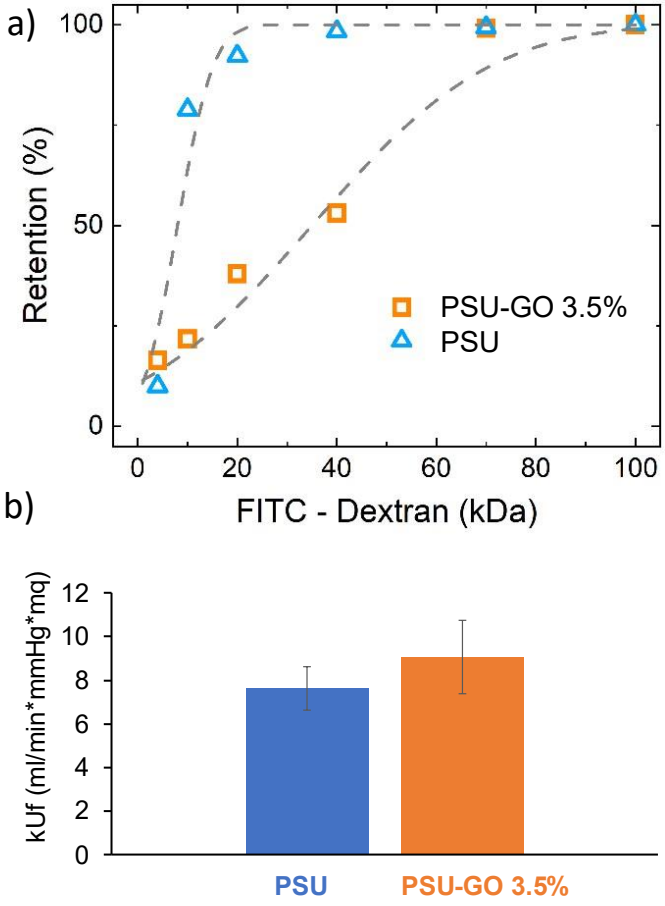

Fig. 5.6. *Ultrafiltration range flow rate of PSU and PSU-GO 3.5% HFs. a) Retention of FITC-Dextran, b) Ultrafiltration coefficients of PSU and PSU-GO 3.5% HFs.*

5.3.4 Removal of PFAS and heavy metals

Tap water (pH 7, 1L) spiked with a mixture of fourteen PFAS (0.5 µg/L each) of different molecular size (C_3 - C_{13}, Fig. 5.7) and end-substitution (sulphonates or carboxylates) was filtered through PSU, PSU-GO HFs 3.5%, and GAC for comparison. All modules showed higher removal toward long chain molecules (C_8-C_{13}). PSU-GO showed higher removal for sulphonated PFAS respect to carboxylate analogues of same length (i.e. C_6: 99% for PFHxS vs 79% for PFHpA, or C_4:35% for PFBS vs 4% for PFPeA). Fig. 5.7 shows the removal efficiencies normalized to the amount of adsorbing material in each module, expressed as

mass of PFAS removed per gram of sorbent material. The adsorption capacity of PSU and PSU-GO HFs was significantly higher than that of GAC for almost all PFAS. The total amount of PFAS removed by PSU-GO 3.5% was up to seven times more efficient than GAC.

According to previous studies [48-51], the two most important factors driving PFAS adsorption are hydrophobic interactions and electrostatic interactions. Fig. 5.7c shows, for PSU and PSU-GO 3.5% HFs, the trend of PFAS removal with *n*-octanol/water partition coefficient ($\log K_{OW}$), which grows linearly with PFAS molecular weight.

It can be observed that PFAS with $\log K_{OW}$ in the range 4.5-6.5 are better removed by PSU-GO HFs than PSU HFs, and that the same removal is observed for $\log K_{OW}$ higher than 6.5. This effect emerges despite the higher hydrophilicity of PSU-GO with respect to PSU, as shown also by contact angle measurements (Fig. 8.19, Appendix). The slightly higher hydrophilicity of PSU-GO seems particularly beneficial to the adsorption of short chain PFAS, ($4<\log K_{OW}<5$). Fig. 5.7c shows that in the $\log K_{OW}$ range 4.5-6-5, the higher is the hydrophilicity of the PFAS, the higher is the gap between the removal value for PSU and for PSU-GO HFs. This evidence suggests that repulsive electrostatic interactions are less relevant than hydrophobic interactions. On the other hand, experiments at higher PFAS initial concentration (10 µg/L rather than 0.5 µg/L; Fig. 8.22, Appendix) show a significant similar performance between PSU HFs and PSU-GO HFs. At higher concentration, it has been shown that PFAS can aggregate into micelles [52], this would enhance the role of electrostatic rather than hydrophobic interactions as sorption driving forces. Overall, this evidence suggests a delicate interplay between hydrophobic and electrostatic interactions, which govern PFAS adsorption in this system. The overall proposed mechanism for PFAS adsorption in PSU-GO HFs modules is summarized in Fig. 5.10.

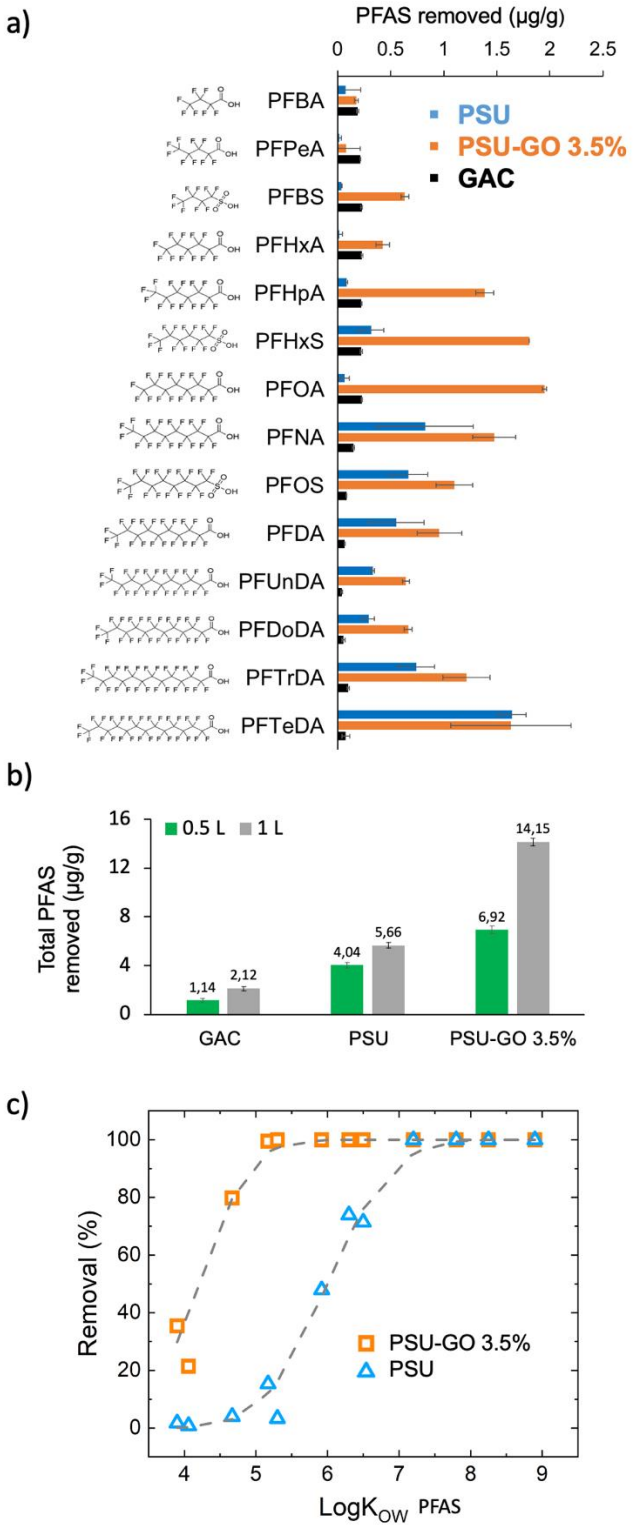

Fig. 5.7. *a) Removal of a mixture of fourteen PFAS in tap water, total volume=1 L, C_{IN}= 0.5 µg/L, flow rate= 5 mL/min in µg/g of PSU HFs (blue, total mass of composite 260 mg), PSU-GO 3.5% HFs (orange, total mass of composite 270 mg), and GAC (black, total mass 2.4 g). b) Total amount of PFAS removed µg/g after 0.5 L (green) and 1 L (grey) filtered. c) Removal of PFAS mixture in tap water vs the PFAS LogK_{OW} of PSU HFs (blue) and PSU-GO 3.5% HFs (orange).*

The removal of heavy metals and metalloids mix (As(V), Cd, Cr(III), Cu, Ni, Pb, U, and V) at 100 µg/L in mineral water (pH 7.5) was also tested. After treating 3 L of

contaminated water, different affinities of metals towards the proposed materials were highlighted. The adsorption capacity of PSU, PSU-GO 3.5% HFs and GAC expressed as micrograms of contaminant removal normalized to gram of sorbent in the module, toward metal ions and metalloids is shown in Fig. 5.8. PSU-GO 3.5% HFs outperform GAC in the removal of Cr(III), Cu and Pb.

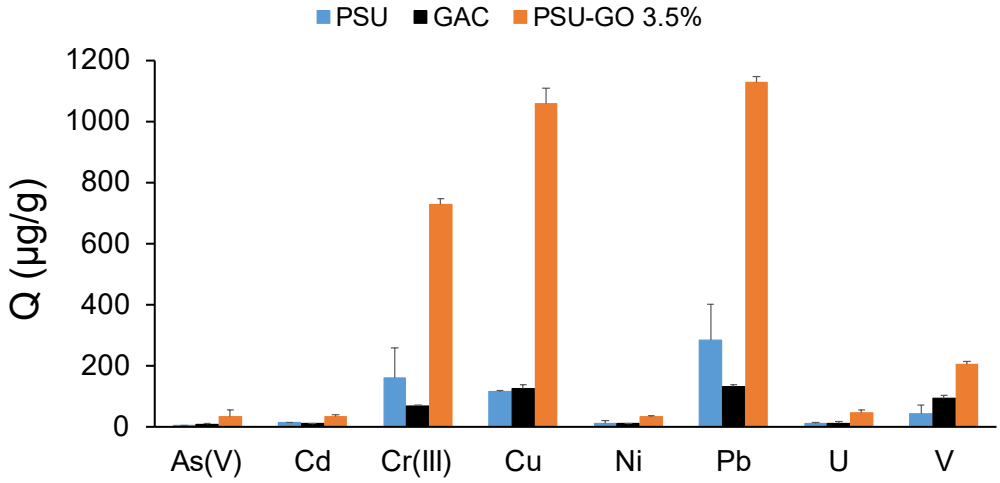

Fig. 5.8. *Adsorption capacity Q (µg/g) towards a mixture of different heavy metals and metalloids. Three different adsorption materials were compared: PSU HFs (blue, left) and PSU-GO 3.5% HFs (orange, right), and GAC granules (black, middle). Flow rate 5 mL/min and total filtered volume 3 L, C_{IN}= 100 µg/L each.*

The plotting of removal efficiency vs treated volume (Fig. 5.9) shows that removal of Pb and Cu follows a similar trend, with initial removal capacity close to 100% for PSU-GO 3.5% HFs and final removal capacity of 50-60%. On the other hand, a constant removal of about 50% was observed for Cr(III). In the case of Pb and Cu, GAC removal capacity was about 10-20% lower for the first 2 L treated, then performance was similar to PSU-GO 3.5% HFs while negligible adsorption on neat PSU HFs was found for all the heavy metals and metalloids. Interestingly, as observed for ciprofloxacin removal, the observed PSU-GO HFs performances were independent on the flow rate (changing flow from 5 mL/min to 40 ml/min) as instead observed in the case of GAC (Fig. 8.23, Appendix) whose removal became lower than 20%.

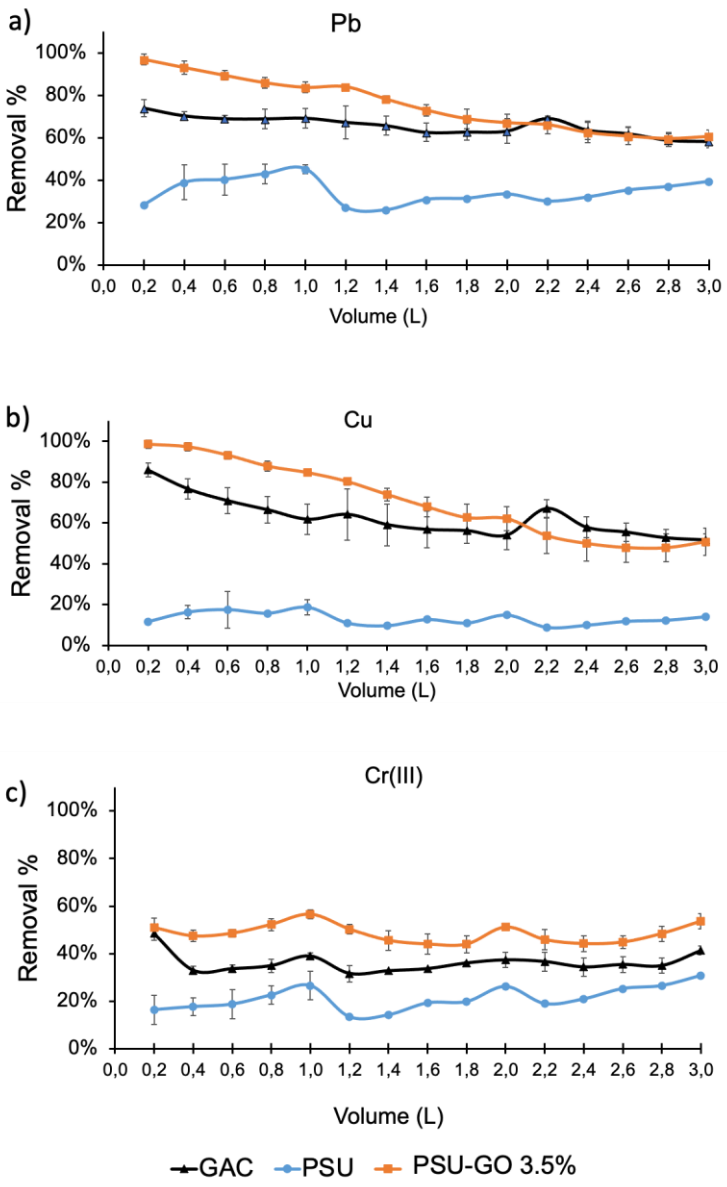

Fig. 5.9 *Removal efficiency as function of treated volume (L) of a) Pb^{2+}, b) Cu^{2+}, c) $Cr(OH)_2^{+}$/$Cr(OH)^{2+}$.Three different adsorption materials were compared. PSU HFs (blue) and PSU-GO 3.5% HFs (orange) and GAC (black) granules. Flow rate 5 mL/min and total filtered volume 3 L.*

Different studies proved higher Cu and Pb adsorption, if compared to other heavy metals, onto negatively charged surfaces with exposed –OH and –O groups as in our case, i.e. adsorption on GO. [53-57] The adsorption passes through two different mechanisms: 1) exchange reaction onto permanent negatively charged sites, that involves not hydrolyzed cations. 2) surface complexation at variable charged hydroxyl edges, that follows selective adsorption, according to the tendency of different metals to hydrolyze.[54]

Cu and Pb hydrolyze more readily than Ni and Cd, and hence are more likely to interact with a hydroxylated surface, while Ni and Cd do not compete

effectively for variable surface charges, due to their lower tendency to form hydrolysis products. Consequently, Ni and Cd adsorption is more restricted to permanent charge sites, especially in a competitive environment, such as a mix of metals. Previous studies [57-60] demonstrate that the overall metal affinities for goethite were generally found to follow the order Cr > Cu > Pb > Zn > Cd > Co > Ni > Mn > Ca > Mg, which was consistent with electronegativity or hydrated radii of the cations.

Overall, removal experiments on CIPRO, PFAS and metal ions suggest a removal mechanism based on the interplay of electrostatic interactions, hydrophobic interactions and π-π stacking between GO and the contaminants. Heavy metals are removed with higher performances than PFAS, likely thanks to the predominant surface complexation mechanisms favored also by positive electrostatic interaction with the negatively charged GO flakes. A schematic representation of adsorption mechanism for organics and heavy metals is depicted in Fig. 5.10.

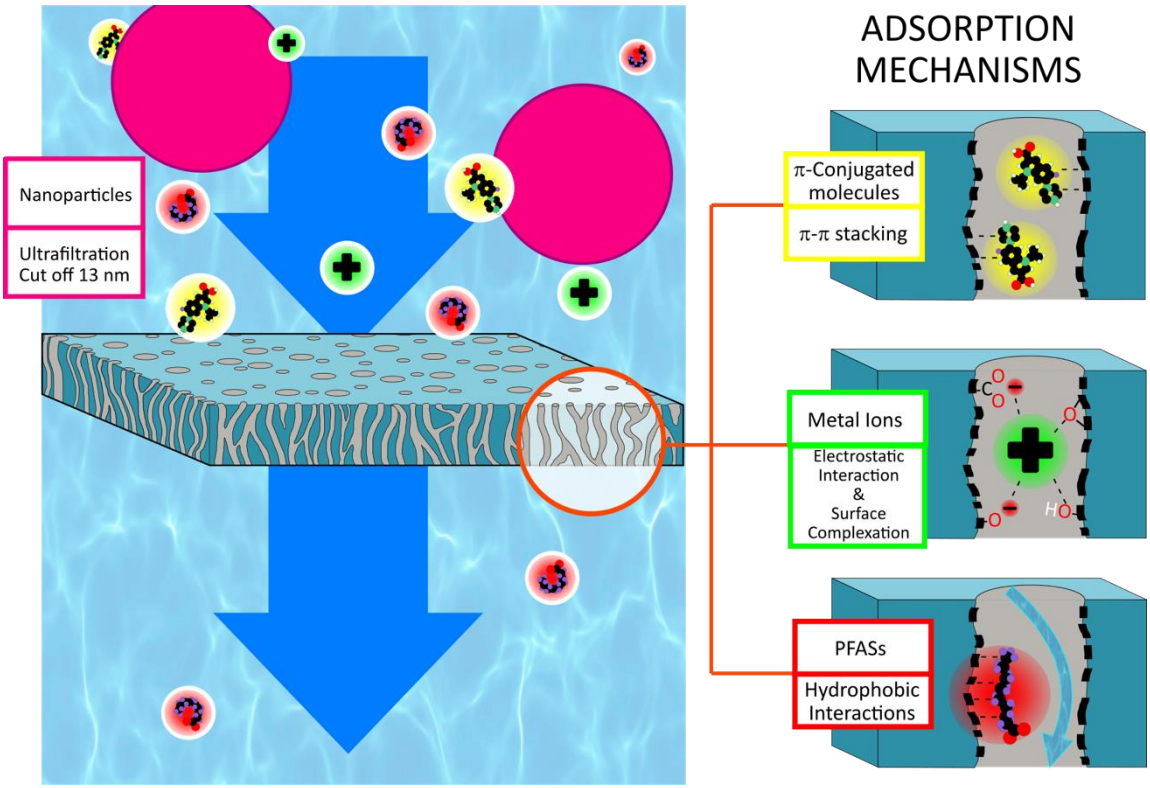

Fig. 5.10. *Sketch of the adsorption mechanisms of pollutants on PSU-GO: π-conjugated molecules are adsorbed through π-π stacking, metal ions through electrostatic interactions and surface complexation, and PFAS through hydrophobic interactions.*

5.3.5 Water potability and GO release test by Surface-Enhanced Raman Spectroscopy (SERS)

Chemical and biological water potability was verified on tap water before and after filtration as listed in Table 8.8, Appendix. In addition, to validate the safety of use of the PSU-GO HFs modules, we studied possible release of GO nanosheets during water purification. To this aim, we exploited a method, recently developed by some of us, [46] able to detect and quantify GO in water samples at ultra-trace levels using surface-enhanced Raman spectroscopy (SERS). The methodology is based on the deposition of water GO dispersions on a SERS active substrate based on gold nanoparticles.

The optimized analytical protocol was applied to the detection and quantification of GO in tap water samples filtered through PSU HFs and PSU-GO 3.5% HFs modules. Water (1L) was filtered at a flow of 250 mL/min, i.e. 2.5-fold higher the maximum operating flow for PSU HFs prototype cartridges in Fig. 5.1b. Fig. 5.11 shows the spectra of the filtered sample as it and after fortification. Our methodology predicted a concentration of 0.10 µg/L (in agreement with the experimental spike), with a relative standard deviation (RSD) below 4, in accordance with previously RSD of the method. Calibration curve based on intensity at 1350 cm^{-1} is reported in the inset of Fig. 5.11 (spectra in Fig. 8.24, Appendix). From these results, it is evident that the filtered water through PSU-GO HF does not contain GO under the limit of detection.

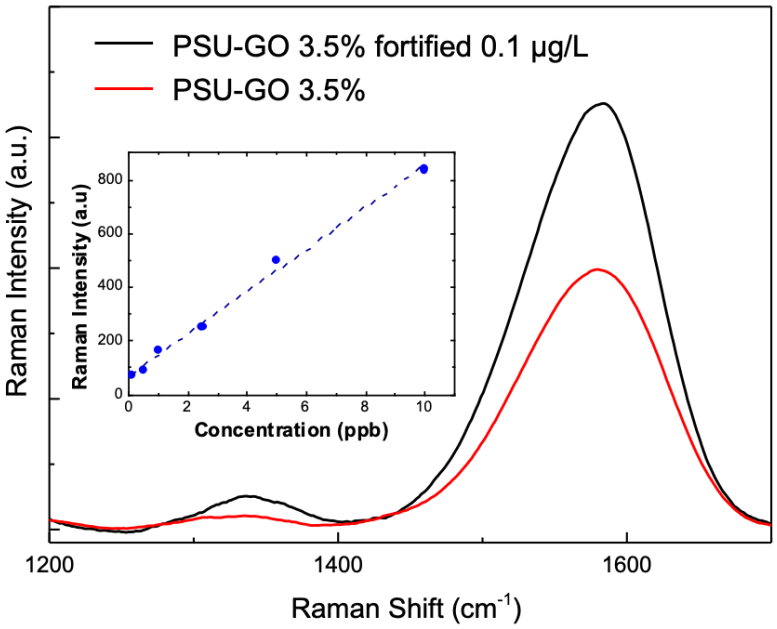

Fig. 5.11. *SERS spectra for PSU-GO 3.5% (red) and PSU-GO 3.5% fortified 0.1 µg/L (black). The inset shows the calibration curve based on the intensity at 1350 cm^{-1}.*

To the best of our knowledge, this is the first case of study on release from PSU-graphene composite with a limit of quantification below the mg/L limit, typically achieved by UV-vis or TOC analyses. [61]

5.3.6 Preliminary real conditions POU test

For validation of PSU-GO 3,5% HFs modules we performed a removal test in a pilot connected to the tap working with a reservoir allowing us to spike water before treatment with the PSU-GO modules. Module with U-shaped bundles (0.28 m^2 fig. 11a, b) were produced since they are the standard POU module structure proposed by the producer (Medica spa). The amount of GO estimated in these modules was about 210 mg on a total HF weight of 6 g. For validation, tap water (100 L) was spiked with CIPRO (at 1 mg/L) and operated at about 2.5 bar (2 L/min). 5 L samples were collected and at each sampling the inlet solution was also collected and checked by HPLC-UV analysis. Fig. 5.12 shows the overall set-up (a) the module structure (b) and U-shape membranes inside the module (c). An initial removal of about 65% was found which decrease to about 30% after 40 L. Despite the observed removal decay, the total mass of removed CIPRO in 100 L normalized to the amount of GO in the module, was about 110 mg removed per g of GO, compared to the 168 mg/g GO obtained in lab scale prototypes tested at 5

mL/min (Fig. 8.21, Appendix). The estimated contact time of real size U-shaped module at 2 L/min is 10-fold lower than the one of lab scale prototypes tested at 5 mL/min, meaning that the removal of CIPRO by GO mediated adsorption is only partly affected by contact time (and/or flow rate).

It should be remarked that for this experiment we used a ppm spike of CIPRO which is far from the environmentally occurring concentration of CIPRO (ng-mg/L). This preliminary study on real size devices suggested that for POU applications, GO distribution and availability seem to affect the adsorption capacity more than flow rate. The removal decay could be likely enhanced by improving the distribution of GO nanosheets within the composite and by reducing their aggregation which likely limits the exposed surface area and the overall adsorption.

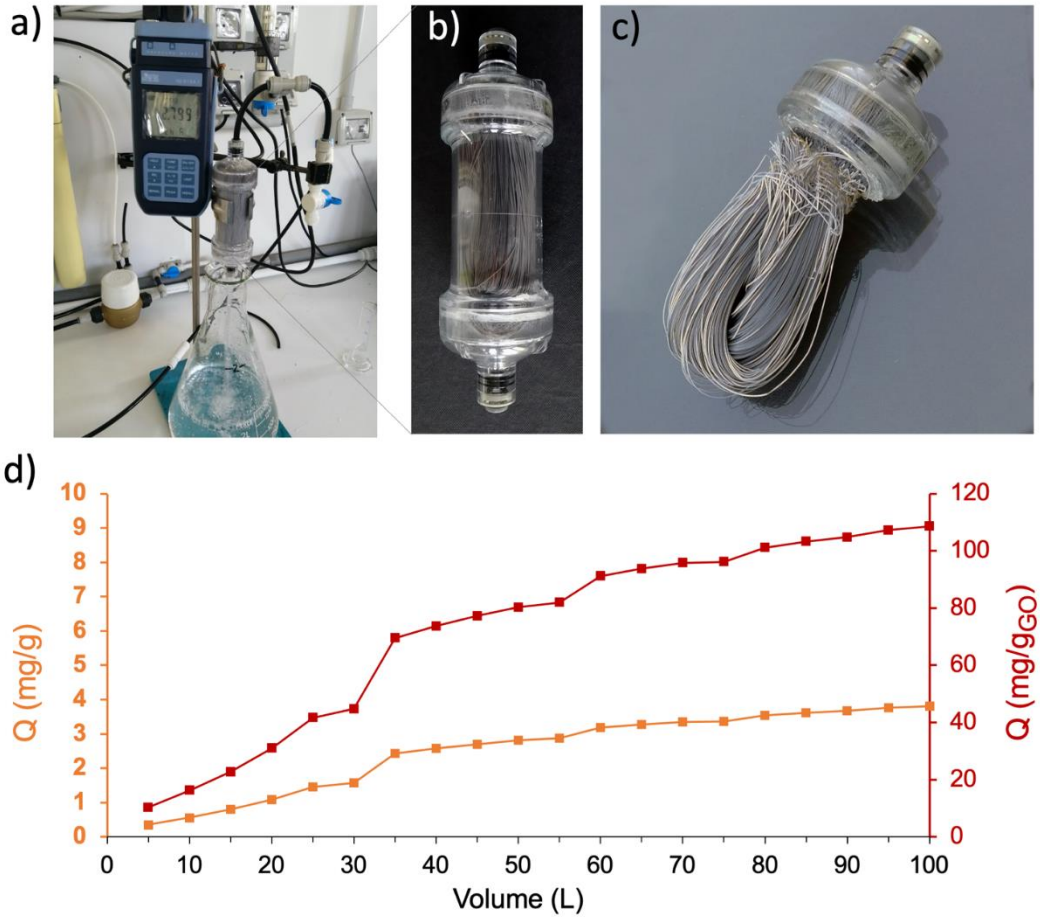

Fig. 5.12. *a) PSU-GO 3.5% cartridge (FS 0,28m^2, U-shaped HFs) connected at the tap (at 2.8 bar as shown by the manometer). Composite weight in each module about 6 g, with 210 mg of GO. b) zoom of the cartridge and c) of the U shape assembled fibers. d) Removal trend of CIPRO (spike at 1 mg/L).*

5.4 Conclusions

A new class of GO enhanced ultrafiltration modules produced with a semi-industrial pilot plant, has been herein described. We demonstrated that PSU-GO HFs modules preserve ultrafiltration properties of commercial PSU HF modules, but also exhibited the adsorption properties typical of GO nanosheets. PSU-GO HFs have been proved superior to both pristine PSU HFs and GAC, the industrial standard sorbent, in the removal of several classes of water contaminants. In particular, PSU-GO removal of ciprofloxacin antibiotic, Pb, Cu, and Cr(III); and perfluoroalkyl substances (PFAS, C4-C13) from real tap water matrix, were higher than that of GAC with a performance much less affected by the operational flow rate and negligible release at higher flow rate compared to for GAC. Higher selectivity for short chain PFAS with respect to GAC was observed. The importance of removing PFAS with $\log K_{OW}$ higher that 5 was pointed out by the Stockholm Convention on Persistent Organic Pollutants, [62] since that value is the threshold for bio-accumulation and bio-concentration. Preliminary tests on POU real scale filters for tap water purification at tap operational conditions (pressure-flow rate) demonstrated comparable performance of small prototype working at low flow rate (5mL/min) for CIPRO. Such capacity, as expected was lower than that of graphene nanosheets dispersion due to reaggregation of GO sheets in the composite. The absence of GO secondary contamination in after-treatment water has been verified through SERS experiments with a limit of detection of 0.1 µg/L and prove the safe use of these devices for water treatment. Some challenges are still to be tackled to exploit the full potential of this material, as compared to purely adsorption filters, to optimize the set-up to create more favorable kinetic conditions for the adsorption, to minimize the reaggregation of GO nanosheets to enhance their distribution and exposure of such sheets to the outer pore surface. Studies in these directions are currently in progress.

5.5 References

1. T. A. Tweddle, O. Kutowy, W. L. Thayer and S. Sourirajan, *Ind. Eng. Chem. Prod. Res. Dev.*, 1983, **22**, 320-326.
2. T. Sewerin, M. G. Elshof, S. Matencio, M. Boerrigter, J. Yu and J. de Grooth, *Membranes*, 2021, **11**, 890.
3. M. Mondal and S. De, *Chem. Eng. J.*, 2016, **285**, 304-318.
4. A. L. Ahmad, M. Sarif and S. Ismail, *Desalination*, 2005, **179**, 257-263.
5. J. Gao, K. Y. Wang and T.-S. Chung, *J. Membr. Sci.*, 2020, **603**, 118022.
6. A. Abdelrasoul, H. Doan, A. Lohi and C.-H. Cheng, *ChemBioEng Rev*, 2015, **2**, 22-43.
7. W.-P. Zhu, S.-P. Sun, J. Gao, F.-J. Fu and T.-S. Chung, *J. Membr. Sci.*, 2014, **456**, 117-127.
8. T. A. Otitoju, A. L. Ahmad and B. S. Ooi, *RSC Advances*, 2018, **8**, 22710-22728.
9. A. Pandele, O. Serbanescu and Ş. I. Voicu, *Coatings*, 2020, **10**, 609.
10. S. Mangukiya, S. Prajapati, S. Kumar, V. K. Aswal and C. N. Murthy, *J. Appl. Polym. Sci.*, 2016, **133**.
11. K. Matsumoto, T. Takahashi, S. Ishii and M. Jikei, *Int. J. Soc. Mater. Eng. Resour.*, 2014, **20**, 77-81.
12. M. Amini, M. Jahanshahi and A. Rahimpour, *J. Membr. Sci.*, 2013, **435**, 233-241.
13. T. Hwang, J.-S. Oh, W. Yim, J.-D. Nam, C. Bae, H.-i. Kim and K. J. Kim, *Sep. Purif. Technol.*, 2016, **166**, 41-47.
14. O. Kwon, Y. Choi, E. Choi, M. Kim, Y. C. Woo and D. W. Kim, 2021, **11**, 757.
15. M. Ionita, A. M. Pandele, L. Crica and L. Pilan, *Composites Part B*, 2014, **59**, 133-139.
16. N. Meng, Z. Wang, Z.-X. Low, Y. Zhang, H. Wang and X. Zhang, *Sep. Purif. Technol.*, 2015, **147**, 364-371.
17. L. Liu, C. Tong, Y. He, Y. Zhao and C. Lü, *J. Membr. Sci.*, 2015, **487**, 99-108.
18. R. Rezaee, S. Nasseri, A. H. Mahvi, R. Nabizadeh, S. A. Mousavi, A. Rashidi, A. Jafari and S. Nazmara, *J. Environ. Health Sci. Engineer.*, 2015, **13**, 61.
19. Z.-Q. Huang and Z.-F. Cheng, *J. Appl. Polym. Sci.*, 2020, **137**, 48579.
20. L. Qalyoubi, A. Al-Othman and S. Al-Asheh, *Case Stud. Chem. Environ. Eng.*, 2021, **3**, 100086.
21. L. Badrinezhad, S. Ghasemi, Y. Azizian and A. Nematollahzadeh, *Polym. Bull.*, 2018, **75**, 469-484.
22. M. Zambianchi, M. Durso, A. Liscio, E. Treossi, C. Bettini, M. L. Capobianco, A. Aluigi, A. Kovtun, G. Ruani, F. Corticelli, M. Brucale, V. Palermo, M. L. Navacchia and M. Melucci, *Chem. Eng. J.*, 2017, **326**, 130-140.
23. L. Jiang, Y. Liu, S. Liu, G. Zeng, X. Hu, X. Hu, Z. Guo, X. Tan, L. Wang and Z. Wu, *Environ. Sci. Technol.*, 2017, **51**, 6352-6359.
24. B. S. Rathi, P. S. Kumar and P.-L. Show, *J. Hazard. Mater.*, 2021, **409**, 124413.
25. R. Meffe and I. de Bustamante, *Sci. Total Environ.*, 2014, **481**, 280-295.
26. K. E. Murray, S. M. Thomas and A. A. Bodour, *Environ. Pollut.*, 2010, **158**, 3462-3471.
27. B. Petrie, R. Barden and B. Kasprzyk-Hordern, *Water Res.*, 2015, **72**, 3-27.
28. R. Tröger, H. Ren, D. Yin, C. Postigo, P. D. Nguyen, C. Baduel, O. Golovko, F. Been, H. Joerss, M. R. Boleda, S. Polesello, M. Roncoroni, S. Taniyasu, F. Menger, L. Ahrens, F. Yin Lai and K. Wiberg, *Water Res.*, 2021, **198**, 117099.

29. E. Gagliano, M. Sgroi, P. P. Falciglia, F. G. A. Vagliasindi and P. Roccaro, *Water Res.*, 2020, **171**, 115381.
30. J. Glüge, M. Scheringer, I. T. Cousins, J. C. DeWitt, G. Goldenman, D. Herzke, R. Lohmann, C. A. Ng, X. Trier and Z. Wang, *Environmental Science: Processes & Impacts*, 2020, **22**, 2345-2373.
31. L. Liu, Y. Liu, B. Gao, R. Ji, C. Li and S. Wang, *Crit. Rev. Environ. Sci. Technol.*, 2020, **50**, 2379-2414.
32. P. McCleaf, S. Englund, A. Östlund, K. Lindegren, K. Wiberg and L. Ahrens, *Water Res.*, 2017, **120**, 77-87.
33. N. B. Saleh, A. Khalid, Y. Tian, C. Ayres, I. V. Sabaraya, J. Pietari, D. Hanigan, I. Chowdhury and O. G. Apul, *Environ. Sci. Water Res. Technol.*, 2019, **5**, 198-208.
34. S. Valsecchi, M. Rusconi, M. Mazzoni, G. Viviano, R. Pagnotta, C. Zaghi, G. Serrini and S. Polesello, *Chemosphere*, 2015, **129**, 126-134.
35. V. Franke, P. McCleaf, K. Lindegren and L. Ahrens, *Environ. Sci. Water Res. Technol.*, 2019, **5**, 1836-1843.
36. D. Lu, S. Sha, J. Luo, Z. Huang and X. Zhang Jackie, *J. Hazard. Mater.*, 2020, **386**, 121963.
37. C. K. Pooi and H. Y. Ng, *npj Clean Water*, 2018, **1**, 11.
38. M. Peter-Varbanets, C. Zurbrügg, C. Swartz and W. Pronk, *Water Res.*, 2009, **43**, 245-265.
39. P. Westerhoff, P. Alvarez, Q. Li, J. Gardea-Torresdey and J. Zimmerman, *Environ. Sci.: Nano*, 2016, **3**, 1241-1253.
40. R. Mukherjee and S. De, *Sep. Purif. Technol.*, 2016, **157**, 229-240.
41. K. Zahri, K. C. Wong, P. S. Goh and A. F. Ismail, *RSC Advances*, 2016, **6**, 89130-89139.
42. K. Sainath, A. Modi and J. Bellare, *J. Membr. Sci.*, 2020, **614**, 118506.
43. https://eur-lex.europa.eu/legal-content/EN/TXT/?uri=CELEX%3A32020L2184 , 2020
44. W. Peng, H. Li, Y. Liu and S. Song, *J. Mol. Liq.*, 2017, **230**, 496-504.
45. S. Z. N. Ahmad, W. N. Wan Salleh, A. F. Ismail, N. Yusof, M. Z. Mohd Yusop and F. Aziz, *Chemosphere*, 2020, **248**, 126008.
46. E. Briñas, V. Jehová González, M. A. Herrero, M. Zougagh, Á. Ríos and E. Vázquez, 2022.
47. S. Khaliha, T. D. Marforio, A. Kovtun, S. Mantovani, A. Bianchi, M. L. Navacchia, M. Zambianchi, L. Bocchi, N. Boulanger, A. Iakunkov, M. Calvaresi, A. V. Talyzin, V. Palermo and M. Melucci, *FlatChem*, 2021, **29**, 100283.
48. M. Ateia, A. Maroli, N. Tharayil and T. Karanfil, *Chemosphere*, 2019, **220**, 866-882.
49. C. T. Vu and T. Wu, *Environ. Sci. Water Res. Technol.*, 2020, **6**, 2958-2972.
50. T. Jin, M. Peydayesh and R. Mezzenga, *Environ. Int.*, 2021, **157**, 106876.
51. T. Jin, M. Peydayesh, H. Joerss, J. Zhou, S. Bolisetty and R. Mezzenga, *Environ. Sci. Water Res. Technol.*, 2021, **7**, 1873-1884.
52. S. Kancharla, R. Jahan, D. Bedrov, M. Tsianou and P. Alexandridis, *Colloids Surf., A*, 2021, **628**, 127313.
53. L. de Pablo, M. L. Chávez and M. Abatal, *Chem. Eng. J.*, 2011, **171**, 1276-1286.
54. P. Srivastava, B. Singh and M. Angove, *J. Colloid Interface Sci.*, 2005, **290**, 28-38.
55. K. Lackovic, M. J. Angove, J. D. Wells and B. B. Johnson, *J. Colloid Interface Sci.*, 2003, **257**, 31-40.

56. M. Shi, X. Min, Y. Ke, Z. Lin, Z. Yang, S. Wang, N. Peng, X. Yan, S. Luo, J. Wu and Y. Wei, *Sci. Total Environ.*, 2021, **752**, 141930.
57. P. Trivedi, L. Axe and J. Dyer, *Colloids Surf., A*, 2001, **191**, 107-121.
58. P. Zhang, J.-L. Gong, G.-M. Zeng, C.-H. Deng, H.-C. Yang, H.-Y. Liu and S.-Y. Huan, *Chem. Eng. J.*, 2017, **322**, 657-666.
59. W. C. Chong, Y. L. Choo, C. H. Koo, Y. L. Pang and S. O. Lai, *AIP Conf. Proc.*, 2019, **2157**, 020005.
60. X. Wang, Z. Chen and S. Yang, *J. Mol. Liq.*, 2015, **211**, 957-964.
61. A. Kovtun, A. Bianchi, M. Zambianchi, C. Bettini, F. Corticelli, G. Ruani, L. Bocchi, F. Stante, M. Gazzano, T. D. Marforio, M. Calvaresi, M. Minelli, M. L. Navacchia, V. Palermo and M. Melucci, *Faraday Discuss.*, 2021, **227**, 274-290.
62. H. Fiedler, R. Kallenborn, J. d. Boer and L. K. Sydnes, *Chem. Int.*, 2019, **41**, 4-11.

6 Graphene oxide modification for tailored adsorption capacity

Amino acid-driven adsorption of emerging contaminants in water by modified graphene oxide nanosheets

Adapted with permission Environ. Sci. Water Res. Technol., 2023, 9, 1040; RSC
DOI https://doi.org/10.1039/D2EW00871H;
Adapted with permission Chem.com., 2022, 58, 9766; RSC
DOI https://doi.org/10.1039/d2cc03256b

The full description of the synthesis and characterization can be found at a dedicated link in the published version of the articles. Herein, my main focus is on the contribution I made to the publication.

6.1 Introduction

In the last decades, contamination of water sources has become more frequent all over the world. A great variety of pollutants, such as pharmaceuticals, personal care products, plastics, and additives, among the others,[1-5] are not satisfyingly removed from water sources by conventional water treatment technologies. In the worst cases, this includes even drinking water.[6, 7] This issue calls for the urgent development of new technology for detection, early warning, and remediation of those contaminants with proved eco- and human toxicity (such as perfluoroalkyl substances or bisphenol A).[8-11]Adsorption is the most promising strategy to enable the capture of emerging contaminants.[12-14]

Among the new sorbents emerging in literature for water applications, graphene oxide (GO) is particularly advantageous as a sorbent. It can be exploited as a standalone material[15-19] or as an additive of polymeric membranes, in order to develop adsorptive membranes (i.e. membranes with synergic adsorption and filtration capability).[20-24]

Graphene oxide (GO) nanosheets have shown outstanding adsorption performances in terms of kinetic and adsorption capacities toward PFAS, methylene blue, and ofloxacin. For example, a maximum adsorption capacity of 356 mg/g of ofloxacin[25] was found for GO, i.e. an adsorption capacity 3.5 times higher than that of granular activated carbon (GAC), the industrial sorbent

benchmark.[17] Adsorption maximum capacity of methylene blue for GO was found to be two times higher than that reported for activated carbon.[17] High adsorption efficiency was also demonstrated for reduced GO (rGO) at short contact time (30 min), with values exceeding 99% for carboxylate and sulphonate PFAS with fluoroalkylchain length from CF_4 to CF_{13}.[18]

However, a full understanding of the relationships between structure and sorption selectivity/efficiency is needed to maximize the impact of graphene in water treatment. This requires an extensive investigation on different types of graphene nanosheets and a wide library of contaminants. Indeed, the adsorption strongly depends on the interplay of surface area, surface chemistry, and morphology of the sorbent, and on the chemical structure of the targeted contaminants, which can change dramatically, even within the same family of contaminants (i.e. drugs, dyes, personal care products).[16]

For instance, the role of oxidation degree in GO has been recently demonstrated by the synthesis of highly defected GO (i.e. GO with a prominent number of holes and defects on the surface).[17, 26-28] The number of carbonyl and carboxylic groups, mainly located at the defect edges, increased directly with the number of holes.[17]

The key role of surface chemistry on the adsorption properties is also proved by the studies of selectivity and efficiencies of functionalized graphene-based sorbents, in comparison with unmodified graphene.[16, 29]

Losic et al.[29] recently summarized the results on different graphenic materials and rationalized the adsorption performance in relation with surface area, pore size, type of functional groups, C/O, C/N, and C/S atomic ratios of the graphenic sorbents. For example, sulphonated graphene nanosheets showed enhanced removal of methylene blue with respect to graphene, thanks to the enhanced electrostatic interaction promoted by SO_3H groups.[30] Amino-functionalized graphene oxide (AGO) aerogels showed enhanced electrostatic interactions toward negatively charged perfluorooctanoic acid (PFOA),[31] with respect to unmodified GO and consequent high removal (>99%) of PFOA from water. GO-based silica coated magnetic nanoparticles functionalized with 2-phenylethylamine (PEA) proved to be good sorbent for organophosphorus pesticides in water thank to the various chemical groups on the nanocomposite

surface allowing hydrogen bonding and π–π interactions with electronegative atoms (P, N, and S) of the pesticides.[32]

Here, we report on the synthesis and structure-sorption properties relationship of amino acids-functionalized GO. Amino acids are convenient building blocks to tune the surface chemistry of GO nanosheets thanks to their availability, small size, and large chemical variety. They can be covalently grafted on GO by following different routes, including amination or C-N coupling[33-36] with the epoxide or carboxylic functional groups, which are abundantly available on the surface of GO nanosheets. Previous studies reported the successful use of amino acid-modified GOs (both covalently and not covalently bound) for the removal of metals,[37-39] organic dyes,[40, 41] and antibiotics.[42]

Starting from this evidence and aiming at a rational understanding of the adsorption mechanism, here we report on the synthesis of L-Lysin, L-glutamic and L-methionine- modified GO (GO-Lys, GO-Glu, GO-Met).[43] Their structural characterization and the investigation on the role of the amino acid in the adsorption properties were also deeply studied. The three selected amino acids have side chain of similar length but strongly different chemical properties. Indeed, they are characterized by different charges at neutral pH (Glu: negative, Met: neutral, Lys: positive) and by different pendant groups, i.e. carboxylic (Glu), thioether (Met) or amine (Lys), enabling different type of intermolecular interactions. The structure-adsorption properties relationships in amino acid modified graphenic materials were investigated by combined theoretical and experimental approach, which includes adsorption kinetic and selectivity test, molecular dynamic simulations, and adsorption isotherms.

6.2 Experimental

6.2.1 Materials

Graphene oxide (GO) and reduced graphene oxide 80% (rGO) were purchased by Layer One (S-126/36) and used without further purification. L-methionine methyl ester, L-lysine, L-glutamic acid monosodium salt monohydrate, ofloxacin (OFLOX), diclofenac (DCF), benzophenone-4 (BP4), carbamazepine (CBZ), bisphenol A (BPA), benzophenone-3 (BP3), rhodamine B (RhB), and caffeine (CAF) were purchased by Sigma-Aldrich and used without any further purification. Sodium hydroxide was purchased from Carlo Erba. LC-MS grade acetonitrile was

purchased from Sigma-Aldrich in the highest available purity and used without any further purification. Plasmart 100 microfiltration modules (Versatile™ PES hollow fibers, cut off 150 nm, filtering surface 0.1 m^2, pore size 100-200 nm) were provided by Medica s.p.a. (Medolla, Italy).[44]

6.2.2 Synthesis of GO-amino acid and purification

A basic solution of amino acid (L-Lysine, L-glutamic or L-methionine methyl ester) was prepared and then added to GO suspension. by adding 930 mg of amino acid and 381 mg of NaOH in milliQ water (13 mL). The mixture was irradiated with microwaves for 3 h and the crude was purified by microfiltration on commercial Versatile™ PES modules, (Plasmart 100 module, Medica s.p.a). The full description of the synthesis can be found in the published version of the article.[43, 45] The structures of the obtained amino acid-modified graphene oxide (GO) and the microfiltration (MF) purification procedure are schematically depicted in Fig. 6.1 and 6.2, respectively.

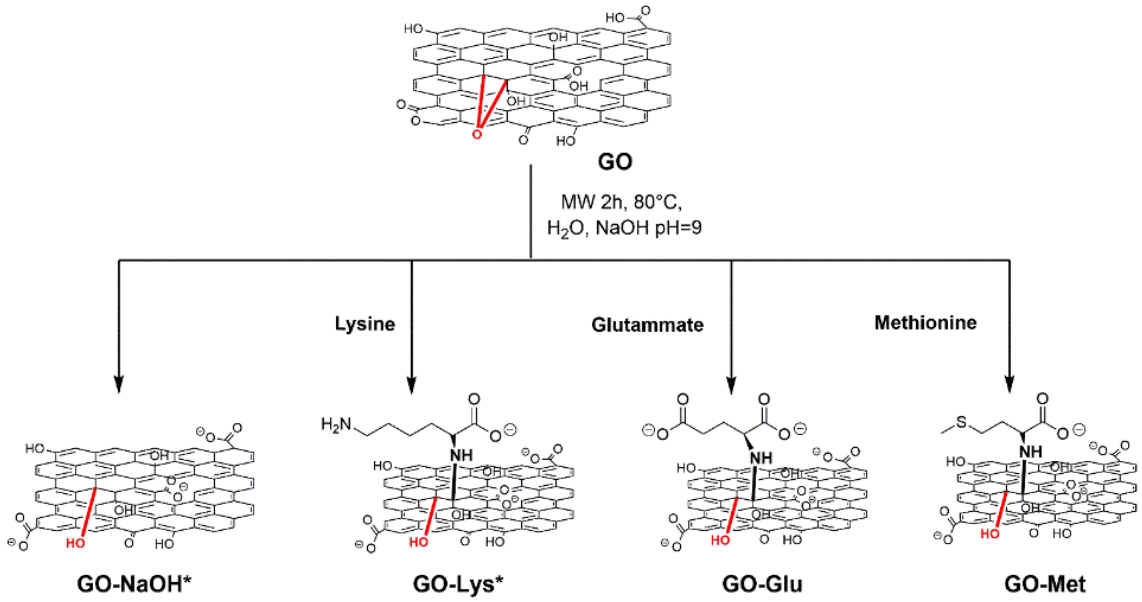

***Fig. 6.1**. Synthetic pathway to amino acid-modified GO.*

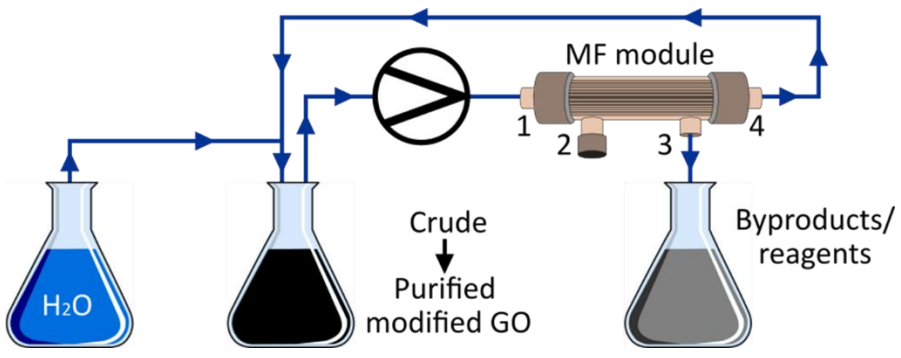

***Fig. 6.2.** Sketch of purification set-up of GO-amino acid by microfiltration*

6.2.3 Characterization

High-resolution XPS were performed with a Phoibos 100 hemispherical energy analyser (Specs GmbH, Berlin, Germany), using Mg Kα radiation (ħω = 1253.6 eV; X-Ray power = 125W) in constant analyser energy (CAE) mode, with analyser pass energies of 10 eV.

Elemental analysis was performed on modified GO powders by using Elementar Unicube Elemental analyser, method GRAPHITE.

Scanning electron microscopy (SEM) analyses were acquired with ZEISS LEO 1530 FEG. Samples were deposited on cleaned silicon wafer by dropping 100 µL of suspension at 0.1 mg/mL concentration in dimethylformamide. The energy of electrons was 5 keV and the signal was acquired by inLens detector at a working distance of 3-5 mm.

The full description of characterization method can be found at in the published version of the articles.[43, 45]

6.2.4 Adsorption selectivity and kinetic experiments

A stock solution of eight emerging contaminants (CAF, OFLOX, BP4, CBZ, BPA, RhB, DCF, BP3) (Fig. 8.1, Appendix) at 10 mg/L each was prepared in tap water. In a typical experiment, 25 mg of tested sorbent were sonicated 2 h in 5 mL of milliQ water. After that time, 5 mL of the stock solution described above were added, to reach a final concentration of 5 mg/L for each contaminant. The solutions were gently stirred in darkness for 1 h, 4 h, and 24 h and then centrifuged at 15˙000 rpm for 10 min. GO, GO-NaOH, and rGO were tested in the same conditions previously described.[43]

6.2.5 High Performance Liquid Chromatography (HPLC-UV VIS)

Analyses of the treated water samples were performed by HPLC on a Dyonex Ultimate 3˙000 system equipped with a diode array detector. 0.5 mL samples were used as sources for the automated injection. The chromatographic separation was performed on a reverse phase analytical column (Agilent Eclipse XDB-C8 4.6 x 150 mm, 5 µm) at a flow rate of 1.0 mL/min, linear gradient TFA 0.05% aqueous solution/acetonitrile from 80:20 to 0:100, detection at λmax of each analyte. In case of the absorption experiments on the selected emerging contaminants in mixture, the percentage removal of the analytes was determined by comparison

with that of the initial untreated solution. The results are expressed as the mean of two independent experiments ± SD.

6.2.6 Adsorption isotherm experiments

The adsorption isotherms of GO-Lys, GO-Glu and GO-Met on BP4, BPA, CBZ were performed varying both the concentration of contaminant and the amount of sorbent. Stock solutions of each contaminant was prepared in milliQ water, according to the maximum solubility of each molecule: BP4 1.0 mg/mL, BPA 0.3 mg/mL, and CBZ 0.1 mg/mL. For each sorbent, two suspensions were prepared, 2 mg/mL and 3 mg/mL in milliQ water and used after 2 h of sonication. A different amount of graphene suspension was added to a solution of contaminant (BP4, BPA, or CBZ) at different initial concentrations. The solutions (total volume 5 mL) were gently stirred in darkness for 4 h and then centrifuged at 15˙000 rpm for 10 min. The solutions were analysed by HPLC. Same procedure was performed for each pair of sorbent-sorbate, varying the ratio due to the different adsorption capacity. Each run was repeated twice on different batches of materials. Isotherms on rGO, GO and GO-NaOH were performed as well.

Langmuir and Brunauer–Emmett–Teller (BET) models were used to fit the adsorption data obtained. All equations and parameters are provided in Appendix, Table 8.1

6.2.7 Molecular dynamics (MD)

GO-Lys, GO-Glu and GO-Met were modelled on a 40 Å x 40 Å graphene sheet created with visual molecular dynamics (MD). The epoxy, hydroxyl, carbonyl, and carboxylic acid groups were randomly positioned on the GO sheet to reproduce the experimental XPS data. Also, the correct grafting density of the amino acids was selected to reproduce the XPS data. The gaff force field [46] was used to describe GO-amino acids. The atomic charges were obtained by AM1 calculations. The gaff force field was used to parameterize BP4, CBZ and BPA. Atomic charges were obtained by QM calculations at the HF/6-31G(d) level of theory, followed by RESP fitting. All the complexes were inserted into a box of TIP3P water molecules and counterions were added to neutralise the total charge of the system. MD simulations were carried out using AMBER 16.[47] The systems were minimised using a two-step procedure. In the first step, harmonic constraints

(500 kcal mol^{-1} $Å^{-2}$) were imposed to the molecule/graphene complexes, relaxing only the water molecules and ions. During the second step, all the atoms were free to move. Then, the resulting minimised systems were used as starting points for MD simulations. An equilibration step of 10 ns was carried out gradually heating the system from 0 to 298 K, using an Andersen thermostat and periodic boundary conditions (PBC). Then, 100 ns long MD simulations were produced. Molecular Mechanics–Generalised Born Surface Area (MM-GBSA) method,[48] was applied to compute the binding affinity of BP4, CBZ, and BPA to GO-Lys, GO-Glu and GO-Met, extracting the snapshots from the MD trajectories.

6.3 Results and Discussion

6.3.1 Synthesis and characterizations

The targeted GO-amino acids were synthesised by microwaves-assisted epoxide ring opening reaction (Fig. 6.1) and purified through microfiltration (Fig. 6.2). The control sample GO-NaOH was also prepared to study possible effects of the experimental conditions of the reaction on GO structure and their influence on the adsorption properties. Loading was estimated by N 1s signal for of each amino acid in GO-Glu, GO-Met and GO-Lys (6%, 5%, 15% respectively).

The chemical structure and the amino acid loading ratio for the new modified GO was estimated by X-ray photoelectron spectroscopy (XPS). The survey spectra of amino acid modified GO are reported in Fig. 6.3 and their atomic composition is reported in Table 6.1.

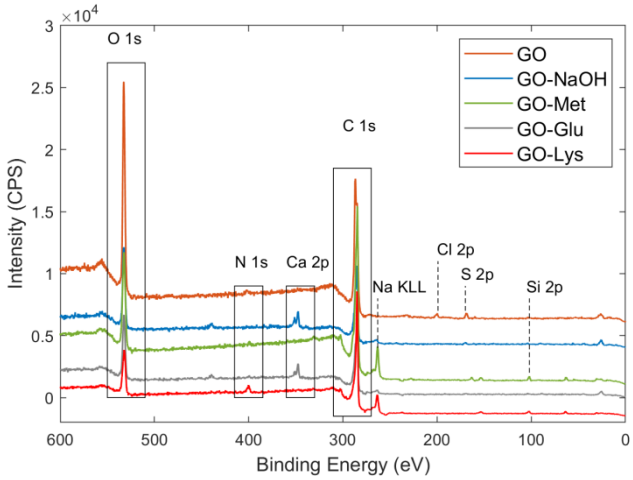

Fig. 6.3. *XPS survey spectra of GO (orange), GO-NaOH (blue), GO-Met (green), GO-Glu (grey), and GO-Lys (red).*

Table 6.1. *Atomic composition of amino acid modified graphene oxide. Errors on C and O were about ±0.9%, errors on N, Na, Cl, S and Ca about ±0.1%. Si was present in quantities < 1% in GO-Lys and GO-Met.*

Material	Atomic composition (%)							Loading %
	C	O	N	Na	Cl	S	Ca	
GO	70.4	27	0.7	-	0.8	1.0	-	
GO-NaOH	70.4	25.6	0.2	0.2	0.3	-	3.3	
GO-Lys	81.5	13.9	3.1	1.2	0.2	-	-	15
GO-Met	81.2	15.6	0.9	0.7	-	0.8	-	5
GO-Glu	77.1	19.7	0.7	0.2	-	-	2.3	6
rGO	86.1	13.7	-	-	0.2	-	-	

Elemental analysis (EA) on pristine amino acid and on modified GOs was performed to analyse the bulk composition. The atomic composition (H, C, O, S) of each material was in good accordance with that estimated by XPS (Table 6.2).

Table 6.2. *Atomic ratios of modified GO materials obtained by XPS and EA.*

Material	N/C		S/C		O/C	
	XPS	EA	XPS	EA	XPS	EA
GO	0.01	0.002	0.014	0.010	0.38	0.77
GO-NaOH	0.003	0.001	-	0.003	0.36	0.92
GO-Met	0.011	0.020	0.010	0.012	0.19	0.49
GO-Glu	0.009	0.008	-	-	0.26	0.67
GO-Lys	0.04	0.06	-	-	0.14	0.62

The observed difference can be ascribed to the different environmental conditions during the measurements of EA and XPS. The full description of characterization can be found at in the published version of the articles.[43, 45]

The morphology of the modified graphene was investigated by scanning electron microscopy (SEM) showing the typical GO nanosheets morphology for GO-amino acid, with a few micrometres lateral size, but more aggregated and multilayer nanosheets (Fig. 6.4).

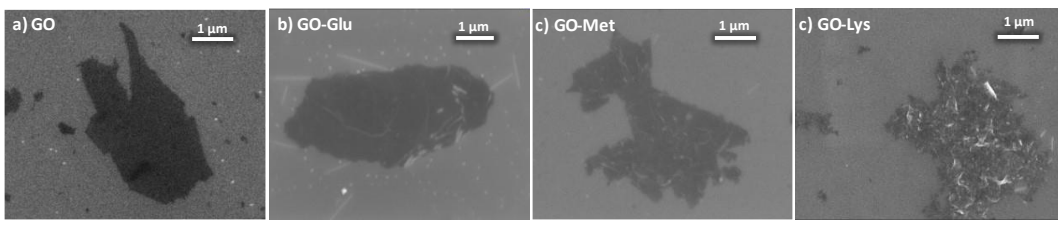

Fig. 6.4. *SEM FEG images of a) GO, b) GO-Glu, c) GO-Met and d) GO-Lys*

6.3.2 Adsorption kinetic and selectivity

Adsorption selectivity and kinetic studies were carried out on GO, GO-NaOH, GO-Lys, GO-Met, and GO-Glu by measuring the removal of each contaminant from the mixture in tap water matrix (Fig. 6.5.a), at different contact time (1 h, 4 h, and 24 h). GO and modified GO were sonicated for 2 h to exfoliate the bulk material into monolayer nanosheets.[49] Different contact times and modified GO have been tested but not reported since most of the adsorption occurred during the first hours of treatment since no significant differences in removal efficiency were observed between 4 h and 24 h. The reader can find full reported results in the published version.[45]

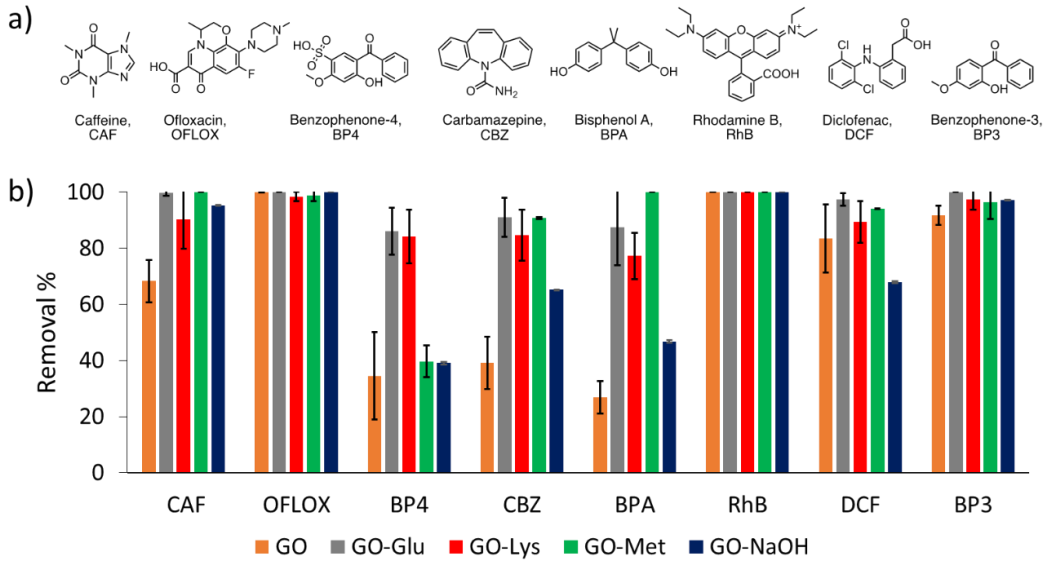

Fig. 6.5. *a) Molecular structure of selected emerging contaminants. b) Removal of each contaminant from the mixture in tap water (contact time= 4 h, total volume= 10 mL, sorbent amount= 25 mg, C_{IN}=5 mg/L of each contaminant) by GO (orange), GO-Glu (grey), GO-Lys (red) GO-Met (green) and GO-NaOH (dark blue).*

Fig. 6.5 shows the histogram of the adsorption of the different modified GO, after 4 h of contact time, for each contaminant. In the selected conditions, GO showed lower performance for caffeine (CAF), benzophenone-4 (BP4), carbamazepine (CBZ), bisphenol A (BPA), and diclofenac (DCF). The amino acid functionalization changes the surface chemistry of the nanosheets and increases the adsorption selectivity toward the selected contaminants. In fact, modified GO showed better performance than pristine GO and GO-NaOH in the removal of the contaminants (i.e. CAF, BP4, CBZ, BPA and DCF).

6.3.3 Adsorption isotherms

Adsorption isotherms were performed on modified GO for BP4, BPA, and CBZ to investigate the adsorption mechanisms and to estimate the maximum adsorption capacities. Results were compared to that of GO, GO-NaOH, and rGO, and the adsorption isotherms are reported in Fig. 6.6.

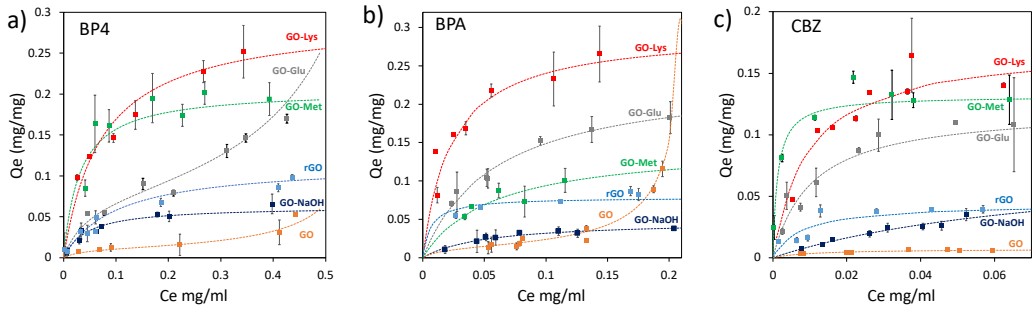

Fig. 6.6. *Adsorption isotherm of a) BP4, b) BPA and c) CBZ tested on GO-Lys (red), GO-Glu (grey), GO-Met (green), rGO (light blue), GO-NaOH (dark blue), GO (orange).*

Two models were used to fit the isotherms: i) the BET model, which considers a multilayer adsorption, where the molecule-molecule interaction is comparable to molecule substrate one, while ii) the Langmuir model, which considers a single monolayer and a much stronger molecule-substrate interaction (Equations and parameters reported in Table 8.1, Appendix). The adsorption capacity of pristine GO toward the selected molecules was low and it could be described by BET as well as by Langmuir model. As a matter of a fact, the goodness of fit was found to be similar. The treatment with NaOH led to higher adsorption capacity and to a Langmuir model describing adsorption mechanism. This can be likely ascribed to the different pH and minor structural modification of GO after NaOH treatment.

Table 6.3*. Maximum adsorption capacity (mg/g) of synthesised materials toward selected contaminants. Best fitting model Langmuir model (L) and BET (B) model marked in the cells.*

Material	Qm (mg/g)					
	BP4		BPA		CBZ	
GO	11 ± 5	(B)	14 ± 5	(B)	7 ± 2	(L)
rGO	115 ± 18	(L)	78 ± 11	(L)	43± 13	(L)
GO-NaOH	62 ± 12	(L)	48 ± 15	(L)	80 ± 15	(L)
GO-Lys	292 ± 30	(L)	295 ± 50	(L)	172 ± 20	(L)
GO-Met	205 ± 20	(L)	147 ± 30	(L)	128 ± 15	(L)
GO-Glu	77.5 ± 20	(B)	237 ± 40	(L)	121 ± 20	(L)

A remarkable improvement of adsorption capacity was observed for amino acid-functionalized GO. This is not related to a difference in pH, because while the pH of the pristine GO is acidic (pH= 3.2), each amino acid-modified GO has the same pH of the reference sample GO-NaOH (pH= 9.0). Similarly, the effect of the partial

reduction of GO during the reaction with amino acids was studied through the comparison with reduced GO (rGO): being the monolayer adsorption capacity (Qm) of rGO generally lower than those of amino acids-modified GO (with exception of BP4 values, Table 6.3), we can conclude that the reduction contributes to the increase of the number of active adsorption sites, but the main contribution is still from the adsorption sites created by the amino acids.

The Qm of GO-amino acids were significantly higher than those of GO and GO-NaOH, with values always under 80 mg/g for each contaminant. A different behaviour was observed for the adsorption of BP4. Indeed, the Qm of GO-Glu for BP4 (77 mg/g), was comparable to that of GO-NaOH (62 mg/g). In addition, BP4-GO-Glu adsorption was the only one described better by BET rather than by Langmuir model, suggesting that BP4-BP4 affinity was greater than that of BP4-GO-Glu. Similarly, the adsorption of CBZ was always better described by Langmuir model, with comparable Qm values for all modified GO materials (GO-Met 128 mg/g and GO-Glu 121 mg/g), with the maximum reached with GO-Lys (172 mg/g).

As reported in Fig.6.7, the adsorption of CBZ exhibited an almost linear increase in Qm with the percentage loading of amino acids, suggesting that the number of active sites for CBZ adsorption increases as a function of amino acid molecules on the surface. This trend is observed with only marginal influence from the specific amino acid structure. On the other hand, BP4 (and partially BPA) showed a step-like increase of the Qm vs loading, suggesting that the availability of active adsorption site mainly depend on the chemical environment created by the specific amino acid. Despite limited to three case studies (i.e. three loading amount) these results clearly show that the amino acid structure may influence the adsorption extent. However, the contaminant molecular structure also plays a key role in the overall adsorption process.

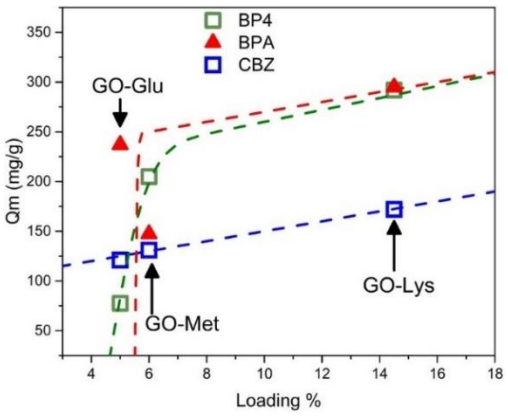

***Fig. 6.7**. Plot of the maximum adsorption capacity (Qm) calculated through isotherms as a function of the amino acid loading (calculated on N/C).*

6.3.4 Molecular dynamics simulations

Molecular dynamics (MD) simulations were carried out to investigate the interactions between BP4, CBZ, and BPA molecules and the amino acid-modified GO at an atomistic level, and to explain their adsorption performances with respect to unmodified GO. Indeed, the MD analysis of the contaminants-nanosheets interaction[50] allows to identify the favourite adsorption sites on GO sheets, thus ultimately providing general rules to identify the thermodynamic forces [51] driving the binding of the contaminants (Table 6.4 and Fig. 6.8).Calculations showed that the molecules of contaminants interact preferentially with the amino acid sidechains, grafted on the basal plane of GO (Fig. 6.8).

***Table 6.4**. Computed total binding affinity (E_{TOT})and its contributes i.e.Van der Waals (vdW), Electrostatic (E_{El}) and non polar solvation ($E_{non\text{-}polar\ solvation}$) for BP4, CBZ and BPA towards GO, GO-Glu, GO-Met and GO-Lys. All energies are reported in kcal/mol.*

Contaminant	Material	E_{TOT}	vdW	E_{El}	$E_{non\text{-}polar\ solvation}$
BP4	GO	-11,9	-20.9	10,1	-1,1
	GO-Glu	-21,1	-30.5	12,2	-2,8
	GO-Met	-22,0	-31.2	12,1	-2,9
	GO-Lys	-21.7	-32.7	11.5	-1.3
CBZ	GO	-18,4	-20.9	4,1	-0,7
	GO-Glu	-20,8	-30.5	3,6	-2,4
	GO-Met	-21,5	-31.2	3,9	-2,5
	GO-Lys	-23.1	-29.1	6.7	-0.8
BPA	GO	-15,7	-19.2	4,4	-0,8
	GO-Glu	-17,1	-19.6	4,5	-2,0
	GO-Met	-18,9	-22.1	5,7	-2,5
	GO-Lys	-20.1	-26.1	7.7	-1.7

This binding mode increases the binding affinity between BP4, CBZ, and BPA, and amino acid-modified GO, when compared to GO, in agreement with the experimental results. The energy values involved in the adsorption are reported in Table 6.4. The total energy of interaction is the sum of three contributes, i.e. electrostatic and van der Waals interactions and surface energy (E_{surf}). The electrostatic terms are little sensitive to the adsorption process, since the process happens in water (and simulations are carried out in explicit water molecules), which strongly quenches the coulombic terms, due to its high dielectric constant. Consequently, the adsorption extent on oppositely charged (Glu and Lys), or neutral (Met) amino acids were similar. The higher removal observed for amino acid-modified GO can be ascribed to the enhanced van der Waals contacts between the surface of the chemically modified nanosheets and BP4, CBZ, BPA, and to the highest stabilizing $E_{non\text{-}polar\ solvation}$ term. The higher removal observed for amino-acid modified GO can be ascribed to the enhanced van der Waals contacts between chemically modified nanosheets surface with BP4, CBZ, BPA, and to the highest stabilizing $E_{non\text{-}polar\ solvation}$ term. This term takes into account the non-polar solvation energy, which is more stabilizing in the case of modified GO, as a result of the interaction of the hydrophobic core of the contaminants with the hydrophobic portion of the amino acid side chains, i.e. their aliphatic chain. In GO, the stabilizing $E_{non\text{-}polar\ solvation}$ term is small and thus the adsorption of the contaminants on the surface of unmodified GO is less favorable than on the surface of amino acid-modified GOs. The adsorption process between carbon nanomaterials and molecules is mainly driven by shape complementarity.[52-54]

Hydrophobic interactions, which govern the binding between contaminant and adsorption site, are directly proportional to the van der Waals interactions and $E_{non\text{-}polar\ solvation}$. Both these terms depend directly on the contact area between the adsorption site and the contaminant, i.e. their shape complementarity (Fig. 6.8). As a hydrophobic contaminant occupies one adsorption site: i) new van der Waals interactions are established, ii) cavitation energy is reduced; iii) associated water molecules are shed (hydrophobic effect). Shape complementarity can be quantitatively measured calculating the variation of the solvent accessible surface area (DSASA, Fig. 6.8) upon binding.

Consequently, the observed improvement in adsorption capacity can be ascribed to the increased shape complementarity between BP4, CBZ, BPA, and

the amino acid modified GO nanosheets (Fig. 8.25 and Table 8.9, Appendix) through 3D recognition sites formed on the nanosheets surface after chemical modification. This effect is more evident with non-planar/bent molecules such as BP4, CBZ, and BPA, which benefit most from the formation of a “local corrugation” on the 2D basal plane of GO.

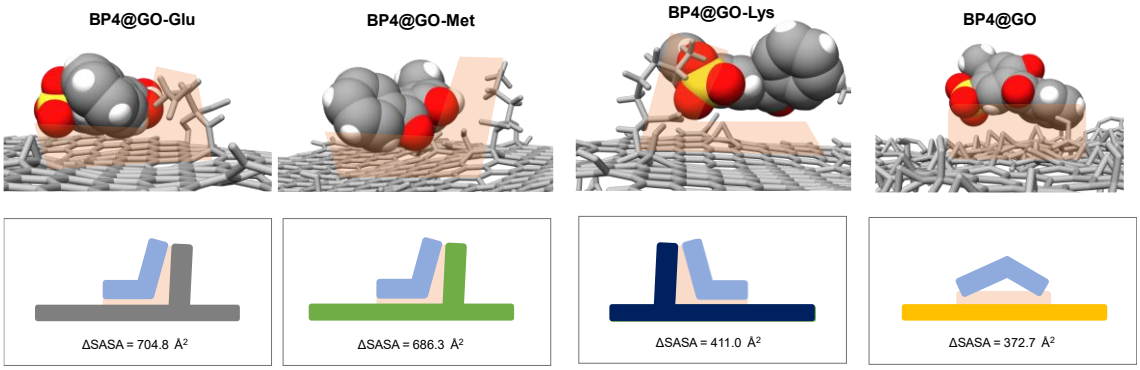

***Fig. 6.8**. Contact area in the interaction between BP4 and GO-Glu, GO-Met, GO-Lys and GO) sheets. Measure of DSASA quantifies the contact area between the contaminant and the different sorbents (shape complementarity) and it is proportional to their binding energies and removal efficiency.*

This effect is more evident with non-planar/bent molecules, such as BP4, CBZ, and BPA, which benefit most from the formation of a “local corrugation” on the 2D basal plane of GO.

6.4 Conclusions

Graphene oxide (GO) was functionalized with L-glutamic acid and L-methionine by a fast and efficient microwave-assisted protocol and worked up with a standardized purification protocol based on microfiltration on commercial modules. The synthetic approach allowed high purity of the reaction products, with a high batch to batch reproducibility, thanks to the standard microfiltration modules features. Structure analysis revealed amino acid loadings in the range 5-15%, with partial reduction of GO (from 27% down to 14-20% of oxygen). Adsorption of a mixture of eight contaminants in tap water was studied for amino acid-modified GOs and compared to unmodified GO and rGO. As a further control sample, we considered also GO subjected to the reaction conditions but treated in absence of any amino acid, called GO-NaOH. This systematic study allowed us to unambiguously unravel the role of the amino acid binding in the adsorption properties of GO. The removal of most of the targeted contaminants occurred in the first hour of treatment, with a significant improvement of the removal of BPA,

CBZ, and BP4 observed for the modified materials. Adsorption isotherms show that the Langmuir model describes the adsorption mechanism better than the BET model, except for the pairs BP4-GO-Glu, BP4-GO, and BPA-GO. In addition, maximum adsorption capacities (Qm) for amino acid-modified GOs were found to be in the range 77-292 mg/g for BP4, 147-295 mg/g for BPA, and 121-172 mg/g for CBZ, with GO-Lys expressing the best performance in each case. Qm was found to be strictly dependent on the amino acid loading, which suggests an active role in the removal of contaminants molecules by the grafting procedure. Accordingly, molecular dynamic simulations revealed higher interaction energies for amino acid modified GOs rather than unmodified GO, which may be ascribed to the higher van der Waals and hydrophobic interactions between the amino acid hydrophobic chain and the contaminant molecules. The grafting of amino acids forms 3D recognition sites on the surface of the GO nanosheets, which improve the removal capacity of the modified materials.

In conclusion, our results will promote the design of new graphenic sorbents for water treatment, with tuneable and predictable adsorption capacity on selected contaminants. Future work on these new sorbents will be dedicated to their exploitation for the purification of different water matrixes and to the development of microfiltration-based regeneration of the exhausted nanomaterials.

6.5 References

1. EEA Report No 09/2021, https://www.eea.europa.eu/publications/drivers-of-and-pressures-arising
2. S. Sharma and A. Bhattacharya, *Appl. Water Sci.*, 2017, **7**, 1043-1067.
3. S. González-Rubio, A. Ballesteros-Gómez, A. G. Asimakopoulos and V. L. B. Jaspers, *Sci. Total Environ.*, 2021, **760**, 143337.
4. J. Fick, H. Söderström, R. H. Lindberg, C. Phan, M. Tysklind and D. G. J. Larsson, *Environ. Toxicol. Chem.*, 2009, **28**, 2522-2527.
5. E. C. A. (ECHA), Candidate List ofsubstances of very high concern for authorisation, https://echa.europa.eu/it/candidate-list-table
6. S. Sorlini, M. Collivignarelli and M. Carnevale Miino, *Environ. Eng. Manag. J.*, 2019, **18**, 2203-2216.
7. R. Kumar, M. Qureshi, D. K. Vishwakarma, N. Al-Ansari, A. Kuriqi, A. Elbeltagi and A. Saraswat, *Case Stud. Chem. Environ. Eng.*, 2022, **6**, 100219.
8. N. Caporale, M. Leemans, L. Birgersson, P.-L. Germain, C. Cheroni, G. Borbély, E. Engdahl, C. Lindh, R. B. Bressan, F. Cavallo, N. E. Chorev, G. A. D'Agostino, S. M. Pollard, M. T. Rigoli, E. Tenderini, A. L. Tobon, S. Trattaro, F. Troglio, M. Zanella, Å. Bergman, P. Damdimopoulou, M. Jönsson, W. Kiess, E. Kitraki, H. Kiviranta, E. Nånberg, M. Öberg, P. Rantakokko, C. Rudén, O. Söder, C.-G. Bornehag, B. Demeneix, J.-B. Fini, C. Gennings, J. Rüegg, J. Sturve and G. Testa, *Science*, 2022, **375**, eabe8244.
9. V. Kayastha, J. Patel, N. Kathrani, S. Varjani, M. Bilal, P. L. Show, S.-H. Kim, E. Bontempi, S. K. Bhatia and X.-T. Bui, *Environ. Res.*, 2022, **212**, 113171.
10. C. G. Bornehag, C. Lindh, A. Reichenberg, S. Wikström, M. Unenge Hallerback, S. F. Evans, S. Sathyanarayana, E. S. Barrett, R. H. N. Nguyen, N. R. Bush and S. H. Swan, *JAMA Pediatr.*, 2018, **172**, 1169-1176.
11. Y. Ben, C. Fu, M. Hu, L. Liu, M. H. Wong and C. Zheng, *Environ. Res.*, 2019, **169**, 483-493.
12. N. Cheng, B. Wang, P. Wu, X. Lee, Y. Xing, M. Chen and B. Gao, *Environ. Pollut.*, 2021, **273**, 116448.
13. N. A. Ahammad, M. A. Ahmad, B. H. Hameed and A. T. Mohd Din, *Environ. Sci. Pollut. Res.*, 2022, DOI: 10.1007/s11356-022-19829-0.
14. M. Varsha, P. Senthil Kumar and B. Senthil Rathi, *Chemosphere*, 2022, **287**, 132270.
15. F. Perreault, A. Fonseca de Faria and M. Elimelech, *Chem. Soc. Rev.*, 2015, **44**, 5861-5896.
16. P. L. Yap, M. J. Nine, K. Hassan, T. T. Tung, D. N. H. Tran and D. Losic, *Adv. Funct. Mater.*, 2021, **31**, 2007356.
17. S. Khaliha, T. D. Marforio, A. Kovtun, S. Mantovani, A. Bianchi, M. L. Navacchia, M. Zambianchi, L. Bocchi, N. Boulanger, A. Iakunkov, M. Calvaresi, A. V. Talyzin, V. Palermo and M. Melucci, *FlatChem*, 2021, **29**, 100283.
18. S. Khaliha, A. Bianchi, A. Kovtun, F. Tunioli, A. Boschi, M. Zambianchi, D. Paci, L. Bocchi, S. Valsecchi, S. Polesello, A. Liscio, M. Bergamini, M. Brunetti, M. L. Navacchia, V. Palermo and M. Melucci, *Sep. Purif. Technol.*, 2022, **300**, 121826.
19. S. Mantovani, S. Khaliha, L. Favaretto, C. Bettini, A. Bianchi, A. Kovtun, M. Zambianchi, M. Gazzano, B. Casentini, V. Palermo and M. Melucci, *Chem. Commun.*, 2021, **57**, 3765-3768.

20. M. Zambianchi, M. Durso, A. Liscio, E. Treossi, C. Bettini, M. L. Capobianco, A. Aluigi, A. Kovtun, G. Ruani, F. Corticelli, M. Brucale, V. Palermo, M. L. Navacchia and M. Melucci, *Chem. Eng. J.*, 2017, **326**, 130-140.
21. M. Zambianchi, S. Khaliha, A. Bianchi, F. Tunioli, A. Kovtun, M. L. Navacchia, A. Salatino, Z. Xia, E. Briñas, E. Vázquez, D. Paci, V. Palermo, L. Bocchi, B. Casentini and M. Melucci, *J. Membr. Sci.*, 2022, **658**, 120707.
22. A. Kovtun, A. Bianchi, M. Zambianchi, C. Bettini, F. Corticelli, G. Ruani, L. Bocchi, F. Stante, M. Gazzano, T. D. Marforio, M. Calvaresi, M. Minelli, M. L. Navacchia, V. Palermo and M. Melucci, *Faraday Discuss.*, 2021, **227**, 274-290.
23. L. Y. Ng, H. S. Chua and C. Y. Ng, *J. Environ. Chem. Eng*, 2021, **9**, 105994.
24. X. Wang, Y. Zhao, E. Tian, J. Li and Y. Ren, *Adv. Mater. Interfaces*, 2018, **5**, 1701427.
25. A. Kovtun, M. Zambianchi, C. Bettini, A. Liscio, M. Gazzano, F. Corticelli, E. Treossi, M. L. Navacchia, V. Palermo and M. Melucci, *Nanoscale*, 2019, **11**, 22780-22787.
26. A. Nordenström, N. Boulanger, A. Iakunkov, I. Baburin, A. Klechikov, A. Vorobiev and A. V. Talyzin, *J. Phys. Chem. C*, 2021, **125**, 6877-6885.
27. N. Boulanger, A. S. Kuzenkova, A. Iakunkov, A. Y. Romanchuk, A. L. Trigub, A. V. Egorov, S. Bauters, L. Amidani, M. Retegan, K. O. Kvashnina, S. N. Kalmykov and A. V. Talyzin, *ACS Appl. Mater. Interfaces*, 2020, **12**, 45122-45135.
28. A. Nordenström, N. Boulanger, A. Iakunkov, G. Li, R. Mysyk, G. Bracciale, P. Bondavalli and A. V. Talyzin, *Nanoscale Adv.*, 2022, DOI: 10.1039/D2NA00362G.
29. P. L. Yap, S. Kabiri, Y. L. Auyoong, D. N. H. Tran and D. Losic, *ACS Omega*, 2019, **4**, 19787-19798.
30. Y. Shen, Q. Fang and B. Chen, *Environ. Sci. Technol.*, 2015, **49**, 67-84.
31. D. Tian, D. Geng, W. Tyler Mehler, G. Goss, T. Wang, S. Yang, Y. Niu, Y. Zheng and Y. Zhang, *Sci. Total Environ.*, 2021, **783**, 147041.
32. V. W. O. Wanjeri, C. J. Sheppard, A. R. E. Prinsloo, J. C. Ngila and P. G. Ndungu, *J. Environ. Chem. Eng*, 2018, **6**, 1333-1346.
33. K. Spyrou, M. Calvaresi, E. K. Diamanti, T. Tsoufis, D. Gournis, P. Rudolf and F. Zerbetto, *Adv. Funct. Mater.*, 2015, **25**, 263-269.
34. M. Yan, Q. Liang, W. Wan, Q. Han, S. Tan and M. Ding, *RSC Advances*, 2017, **7**, 30109-30117.
35. A. O. E. Abdelhalim, V. V. Sharoyko, A. A. Meshcheriakov, M. D. Luttsev, A. A. Potanin, N. R. Iamalova, E. E. Zakharov, S. V. Ageev, A. V. Petrov, L. V. Vasina, I. L. Solovtsova, A. V. Nashchekin, I. V. Murin and K. N. Semenov, *J. Mol. Liq.*, 2020, **314**, 113605.
36. I. A. Vacchi, C. Spinato, J. Raya, A. Bianco and C. Ménard-Moyon, *Nanoscale*, 2016, **8**, 13714-13721.
37. C. Jiang, X. Wang, B. Hou, C. Hao, X. Li and J. Wu, *J. Agric. Food Chem.*, 2020, **68**, 3050-3060.
38. H. Ge and W. Zou, *J. Dispers. Sci. Technol.*, 2017, **38**, 241-247.
39. W. Li, Q. Liu, J. Liu, H. Zhang, R. Li, Z. Li, X. Jing and J. Wang, *Appl. Surf. Sci.*, 2017, **403**, 378-388.
40. J. Xiao, W. Lv, Z. Xie, Y. Song and Q. Zheng, *J. Mater. Sci.*, 2017, **52**.
41. Y.-R. Zhang, P. Su, J. Huang, Q.-R. Wang and B.-X. Zhao, *Chem. Eng. J.*, 2015, **262**, 313-318.
42. S. Yadav, A. Asthana, A. K. Singh, R. Chakraborty, S. S. Vidya, A. Singh and S. A. C. Carabineiro, *Nanomaterials*, 2021, **11**, 568.

43. S. Mantovani, S. Khaliha, T. D. Marforio, A. Kovtun, L. Favaretto, F. Tunioli, A. Bianchi, G. Petrone, A. Liscio, V. Palermo, M. Calvaresi, M. L. Navacchia and M. Melucci, *Chem. Commun.*, 2022, **58**, 9766-9769.
44. www.medica.it,
45. S. Mantovani, T. D. Marforio, S. Khaliha, A. Pintus, A. Kovtun, F. Tunioli, L. Favaretto, A. Bianchi, M. L. Navacchia, V. Palermo, M. Calvaresi and M. Melucci, *Environ. Sci. Water Res. Technol.*, 2023, **9**, 1030-1040.
46. J. Wang, R. M. Wolf, J. W. Caldwell, P. A. Kollman and D. A. Case, *J. Comput. Chem.*, 2004, **25**, 1157-1174.
47. R. M. B. D.A. Case, D.S. Cerutti, T.E. Cheatham, III, T.A. Darden, R.E. Duke, T.J. Giese, H. Gohlke, A.W. Goetz, N. Homeyer, S. Izadi, P. Janowski, J. Kaus, A. Kovalenko, T.S. Lee, S. LeGrand, P. Li, C. Lin, T. Luchko, R. Luo, B. Madej, D. Mermelstein, K.M. Merz, G. Monard, H. Nguyen, H.T. Nguyen, I. Omelyan, A. Onufriev, D.R. Roe, A. Roitberg, C. Sagui, C.L. Simmerling, W.M. Botello-Smith, J. Swails, R.C. Walker, J. Wang, R.M. Wolf, X. Wu, L. Xiao and P.A. Kollman, *AMBER*, University of California, San Francisco., 2016.
48. B. R. Miller, III, T. D. McGee, Jr., J. M. Swails, N. Homeyer, H. Gohlke and A. E. Roitberg, *J. Chem. Theory Comput.*, 2012, **8**, 3314-3321.
49. A. Liscio, K. Kouroupis-Agalou, X. D. Betriu, A. Kovtun, E. Treossi, N. M. Pugno, G. De Luca, L. Giorgini and V. Palermo, *2d Mater.*, 2017, **4**, 025017.
50. M. Calvaresi and F. Zerbetto, *J. Mater. Chem. A*, 2014, **2**, 12123-12135.
51. M. Calvaresi, A. Bottoni and F. Zerbetto, *J. Phys. Chem. C*, 2015, **119**, 28077-28082.
52. M. Di Giosia, T. D. Marforio, A. Cantelli, F. Valle, F. Zerbetto, Q. Su, H. Wang and M. Calvaresi, *J. Colloid Interface Sci.*, 2020, **571**, 174-184.
53. M. Di Giosia, F. Valle, A. Cantelli, A. Bottoni, F. Zerbetto, E. Fasoli and M. Calvaresi, *Carbon*, 2019, **147**, 70-82.
54. M. Di Giosia, F. Zerbetto and M. Calvaresi, *Acc. Mater. Res.*, 2021, **2**, 594-605.

7 Conclusions and future perspectives

Water purification represents a critical and evolving field, driving efforts toward the development of innovative materials to address this urgent issue. Nanotechnologies, particularly graphene and related materials, stand at the forefront of these developments, enabling solutions that were previously unreachable with traditional technologies.

During my phD I investigated the potential use of graphene-related materials as promising solutions for the removal of emerging contaminants from drinking water.

As demonstrated graphene oxide has the potential to become a viable sorbent for a variety of contaminants in tap water, and specific selectivity can be achieved by designing of graphene oxide surface.

To evaluate the applicability of graphene materials as sorbents, kinetic studies are crucial as minimizing contact time is imperative in real-case applications. Our research demonstrated that graphene materials exploit their adsorption capacity in a short equilibrium time (15 minute) to the hours required by standard technologies like Granular Activated Carbon (GAC).

In-depth studies were performed to explain the interactions that could occur between graphene surfaces and contaminants, revealing different mechanisms driving adsorption. For instance, planar molecules with delocalized surface charge are preferentially adsorbed by reduced graphene oxide (rGO) due to π-π interactions, while positively charged molecules are primarily captured via electrostatic interactions promoted by oxygenated groups. Exploring the relationship between defects and oxygenated groups has revealed new possibilities for the application of graphene oxide as a sorbent, offering the potential to tailor surface chemistry to specific contaminants. This tunability is crucial in selecting the appropriate graphene sorbent in relation to the contaminant considered. The information about the adsorption mechanism, as well with the adsorption isotherm, confirmed the applicability of GO as sorbent and open the road to real scale application with a more conscious approach.

However, the practical application of GO nanosheets as sorbent in water purification is strictly limited by the tedious recovery process typically involving

centrifugation, which is also not entirely efficient. Complete removal of graphene material from treated water is essential to prevent secondary contamination.

An accessible and scalable procedure was developed by combining batch adsorption and microfiltration on commercial hollow fiber modules (GO+MF). This method takes advantages of the fast adsorption kinetics of GO, and in only 30 minutes, drinking water can be purified from a wide range of molecules (i.e. antibiotics, dyes and PFAS). In this configuration GO is fully exfoliated and available for adsorption, yielding results slightly lower than those achieved with adsorption isotherms (i.e. Adsorption of OFLOX: 356 mg/g in isotherm vs 240 mg/g in GO+MF). Exhausted GO and adsorbed pollutants are fully retained by the module, which can be regenerated at the end of the process. Additionally, the use of MF module with a cut off of 100-200 nm enable the removal of bacteria and microorganism. The set-up is fully customizable, using different type of graphene materials and could be extended to the removal of metal ions as well.

The combination of hollow fiber filtration and graphene oxide (GO) adsorption was further investigated and combined in a single device. The incorporation of GO in extrusion process of polymeric hollow fibers membranes (i.e. PSU), produce an ultrafiltration adsorptive membrane (PSU-GO), suitable for Point of use (POU) applications. These modules can effectively remove fluoroquinolone antibiotics, PFOA, and heavy metals. Notably, the capacity of PSU-GO modules outperforms that of standard technologies (GAC), which is ineffective on heavy metals like lead (Pb). Furthermore, the fast kinetic adsorption of GO is preserved in the composite, as confirmed through test under real Tap water conditions (2 bar, 5 L/min). The detaching of GO from the composite was tested under high-stress conditions and no detectable release of GO nanosheets was found (LOD 0,1 ppb). The potability of water treated using PSU-GO membranes complies with EU and Italian regulations, opening new market opportunities for this technology. The fabrication of the composite was executed using an ad-hoc developed industrial pilot plant (Medica S.p.A), which currently has a production capacity of 200,000 km/year of fibers. Medica has now include the composite into their water treatment portfolio, offering a safe and enhanced solution to the global market for POU water systems.

In comparison to the MF+GO protocol, the PSU-GO system integrates both adsorption and filtration properties into a single device, resulting in reduced waste

generation. Furthermore, the porosity of the PSU membrane (5-10 nm) enables ultrafiltration of water, effectively removing viruses in addition to bacteria and microorganisms, which are also eliminated by the MF module (100-200 nm).
Both systems offer high levels of customizability, allowing for the substitution of graphene oxide (GO) with more suitable graphene-related materials. However, the GO+MF system, with its two-step configuration, presents an easier substitution process compared to modifying the extrusion process required for PSU-GO. Additionally, PSU-GO composite is designed to be used in real tap water conditions, (2 bar, 5 L/min), while GO+MF requires lower flow rate to prevent system clogging. Consequently, the contact time of contaminated water with GO differs between the two approaches. In GO+MF, the contact time is 30 minutes plus filtration time, whereas in PSU-GO, the contact time is approximately 35 seconds. Moreover, GO in PSU-GO is embedded within the composite, thereby limiting its adsorption capacity compared to GO+MF, where GO is fully exfoliated. However, achieving this exfoliation in GO+MF requires more time, necessitating careful consideration during the process, whereas the PSU-GO module is readily available for installation and use. A comparison of the two technologies is presented in Table 7.1.

Table 7.1 Comparison between standard protocol proposed for the application of graphene materials in water treatments.

	Configuration	**Filtration type**	**Contact time**	**Flow**	**Adsorption capacity (vs isotherm)**	**Application**
GO+MF	Two step set-up (Batch + MF)	Microfiltration	30 min	55 mL/min	Ofloxacin: 240mg/g vs 356 mg/g	Suitable for POU with some improvement
PSU-GO	Single module (adsorptive membrane)	Ultrafiltration	35 sec	5 L/min	Ciprofloxacin: 168 mg/g vs 250 mg/g	Already commercialized for POU

To further enhance the obtained results, both technologies could be advanced by substituting standard GO with a covalently modified GO.
The thesis has previously illustrated the relationship between surface structure and adsorption selectivity, highlighting that modification of surface chemistry can optimize the efficacy of GO in water treatment. In this regard, this thesis has demonstrated that the adsorption capacity of GO can be selectively enhanced through covalent surface modification. GO modified with Amino acids (GO-AA), such as Lysine (GO-Lys), Methionine (GO-Met), and Glutamic acid (GO-Glu),

were successfully synthetized, and the role of grafting in the adsorption properties was deeply investigated. The selected amino acids were an ideal case study due to their similar chain lengths but different properties (i.e. charges and pendant group). Selectivity tests revealed an enhanced adsorption capacity for bisphenol A (BPA), benzophenone-4 (BP4), and carbamazepine (CBZ), while preserving the same selectivity for other contaminants, compared to standard GO. This improvement derives from the 3D recognition sites that amino acids form on the surface of GO nanosheets.

Remarkably, adsorption occurs within the first hour of contact time, making them suitable for use in the MF+GO protocol or embedding them within PSU hollow fibers. Given the significant concern surrounding these contaminants, which are considered potential endocrine disruptors, the utilization of GO-AA instead of standard GO could lead to a more comprehensive system with potentially broader applications in POU systems.

In conclusion, my thesis promotes the design of new graphenic sorbents suitable for water treatment, with tuneable and predictable adsorption capacity on selected contaminants (Fig. 7.1) The broad spectrum of contaminants that can be effectively removed using the proposed technologies is of significant interest due to their toxicity, carcinogenicity, and ecological impact. Despite current concentrations of these contaminants being below regulatory limits, their widespread presence in drinking water raises significant concerns about future water quality. For instance, the urban area of Milan reports the presence of 80 Emerging Contaminants (ECs) ubiquity found in drinking water at concentrations of ng/L, and these concentrations are expected to rise. Therefore, having practical solutions that can be easily implemented in standard water treatment technologies is important in both preventing the spread of contamination and ensuring water safety.

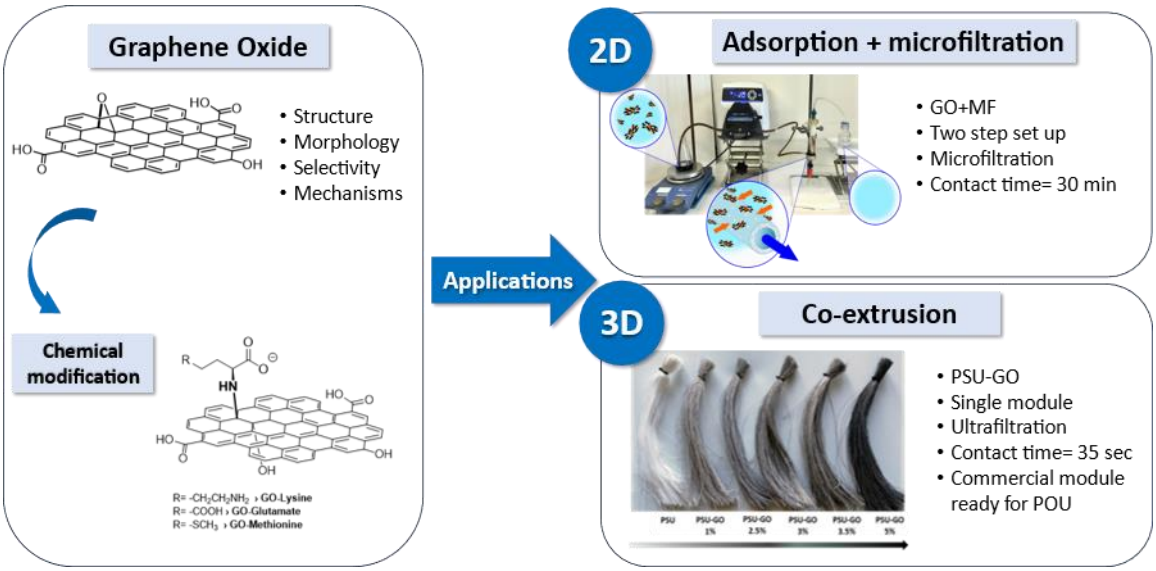

Fig 7.1 Proposed protocols to use GO and modified GO as sorbent in water treatment.

To ensure more reliable and realistic results evaluating the application of the proposed protocols, a dedicated pilot line operating under real tap water conditions has been installed. Tests focusing on Pb and PFOA removal are currently ongoing to validate the system.

Future work on these new sorbents will be dedicated to their exploitation for the purification of more complex water matrices (i.e. water from Po River), which may contain algae and microorganism.

As part of future work, priority will be placed on developing methods to regenerate exhausted materials, aiming to reduce the ecological impact of the proposed technologies. Furthermore, exploring the substitution of plastic polymers with natural alternatives will be pursued as an effective strategy for minimizing environmental impact. In line with this objective, testing the possibility of recycling scraps generated during the extrusion process, currently considered as waste, as a potential alternative sorbent is planned.

8 Appendix: Methodology and supporting information

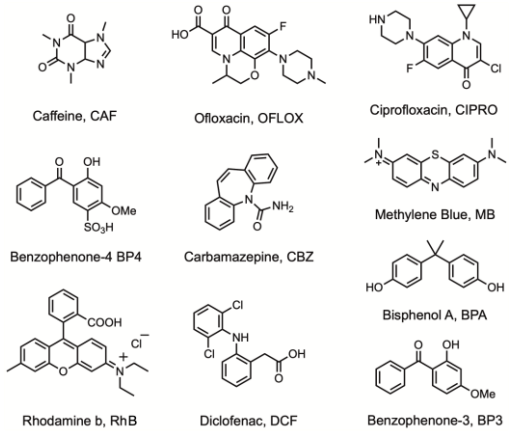

Fig. 8.1. *Chemical structure of the emerging contaminants (ECs) considered herein.*

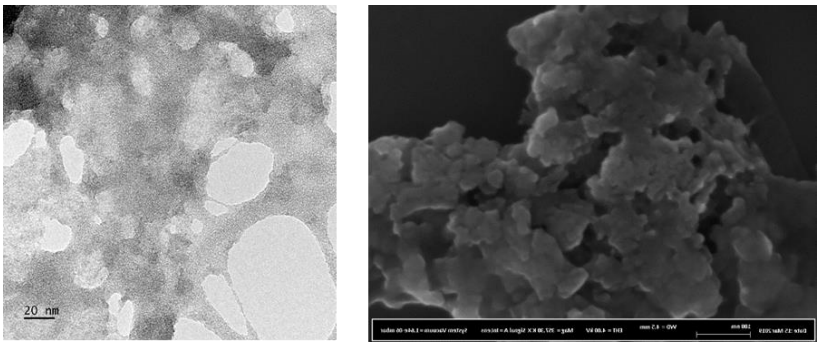

Fig. 8.2. *TEM image of dGO flake (left) and SEM image of dGO aggregates (right).*

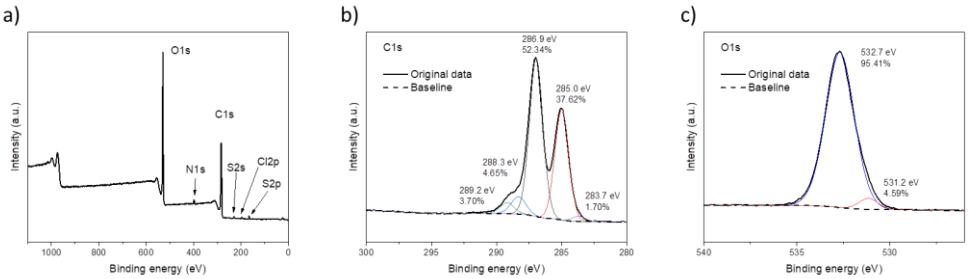

Fig. 8.3. *XPS spectra of hGO: a) survey spectrum, b) C1s and c) O1s.*

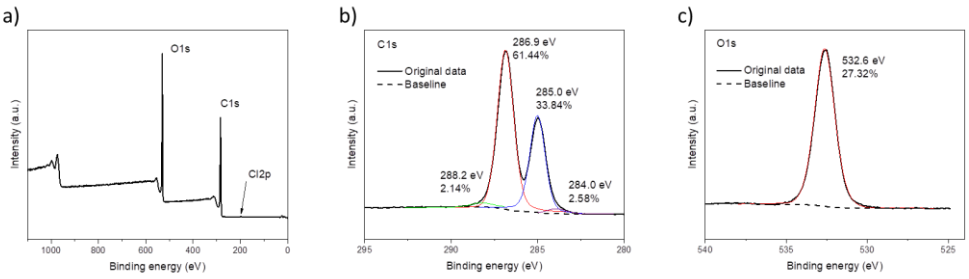

Fig. 8.4. *XPS spectra of bGO: a) survey spectrum, b) C1s and c) O1s.*

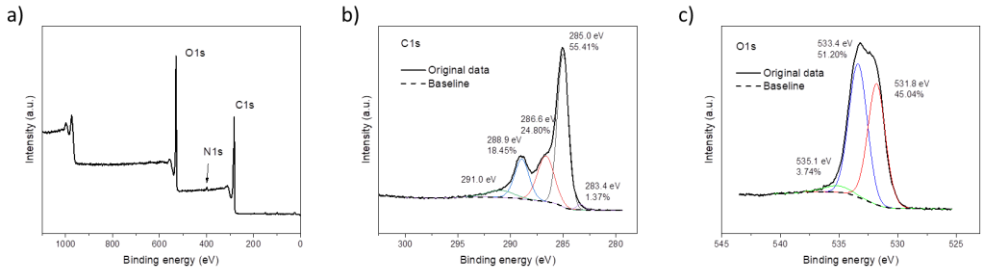

Fig. 8.5. *XPS spectra of dGO: a) survey spectrum, b) C1s and c) O1s.*

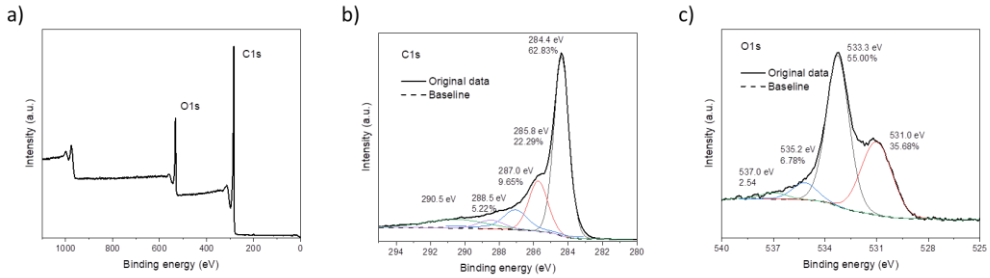

Fig. 8.6. *XPS spectra of rGO: a) survey spectrum, b) C1s and c) O1s*

Table 8.1. *Langmuir and Bruener-Emmett-Teller (BET) equations used to fit the adsorption isotherm*

Model	Equation	Parameters and constants
Langmuir	$Q_e = Q_m \cdot \frac{C_e \cdot K_L}{1 + K_L \cdot C_e}$	Q_m [mg/g]: maximum value of adsorbate adsorbed per g of sorbent K_L [mL/mg]: Langmuir constant C_e [mg/mL]: equilibrium concentration of adsorbate
Bruener-Emmett-Teller (BET)	$Q_e = \frac{Q_m \cdot C_{BET} \cdot x}{(1-x) \cdot (1 + C_{BET} \cdot x - x)}, \quad x = \frac{C_e}{C_s}$	Q_m [mg/g]: maximum value of contaminant adsorbed per g of sorbent C_{bet} [mg/mL]: BET adsorption isotherm C_s [mg/mL]: adsorbate monolayer saturation concentration C_e [mg/mL]: equilibrium concentration of adsorbate

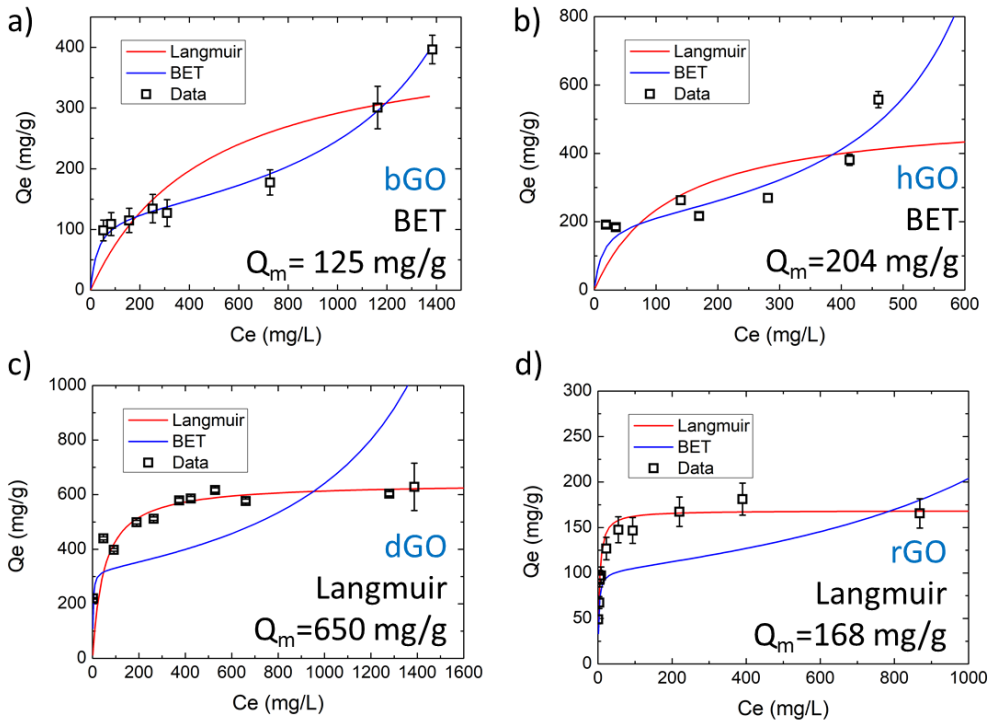

Fig. 8.7. *Adsorption isotherms of OFLOX on a) bGO, b) hGO, c) dGO and d) rGO.*

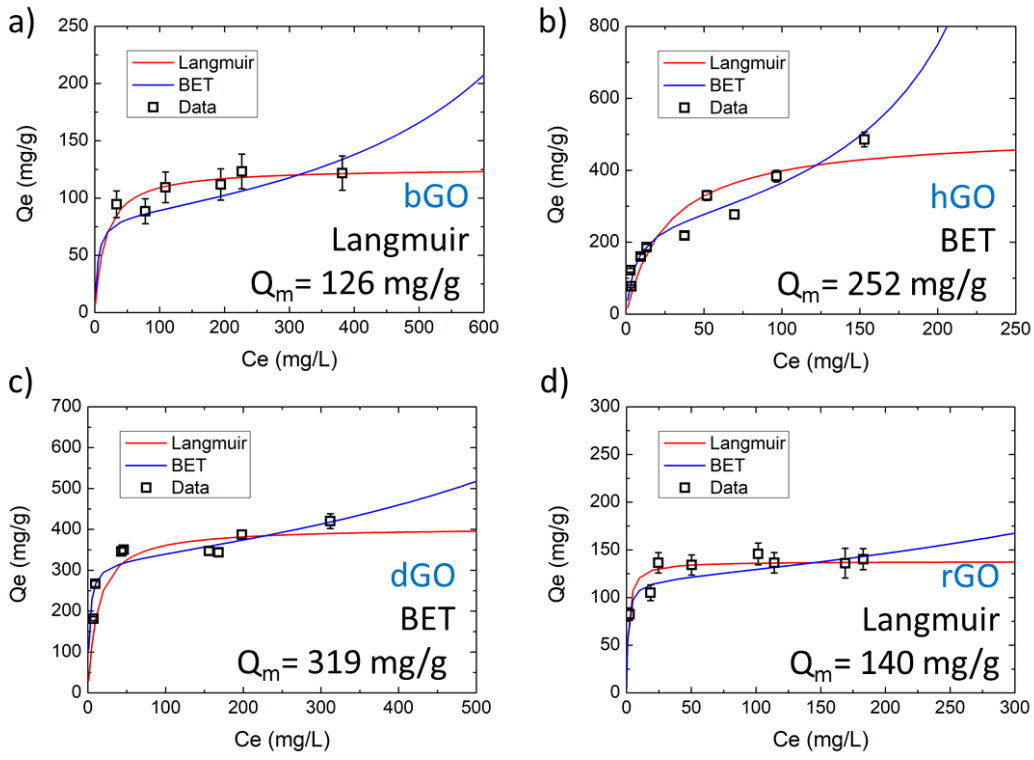

Fig. 8.8. *Adsorption isotherms of CIPRO on a) bGO, b) hGO, c) dGO and d) rGO.*

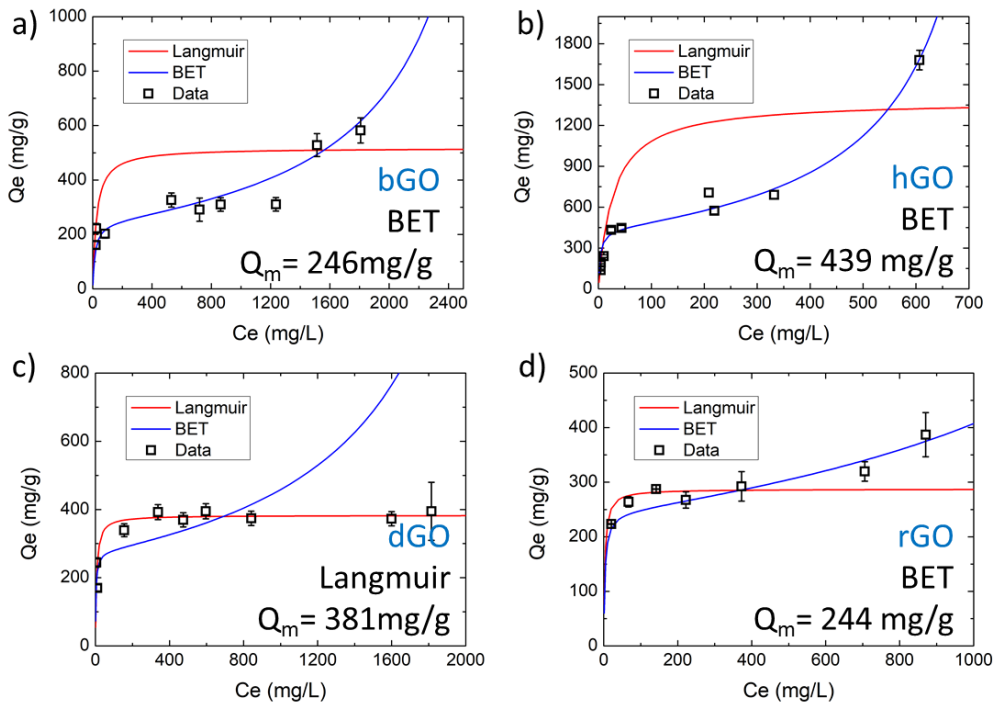

Fig. 8.9. *Adsorption isotherms of RhB on a) bGO, b) hGO, c) dGO and d) rGO.*

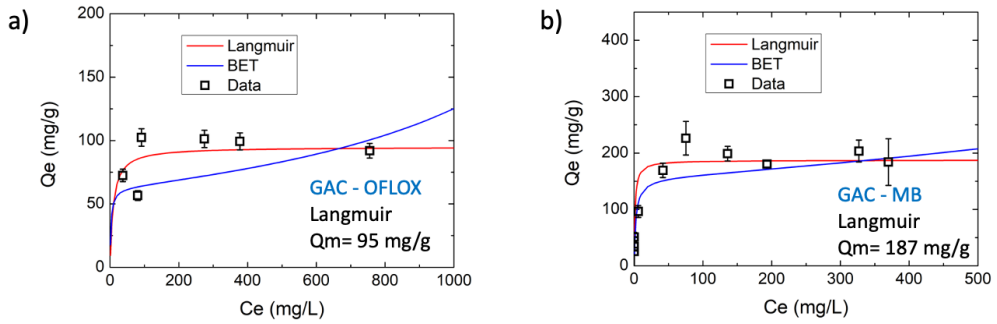

Fig. 8.10. *Adsorption isotherms of GAC for OFLOX and MB.*

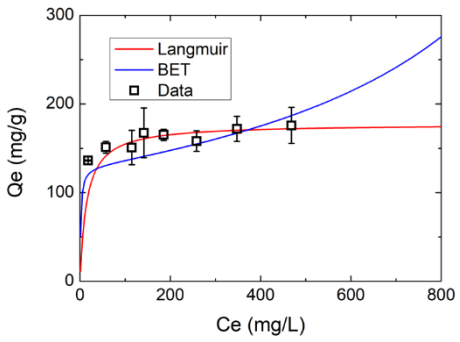

Fig. 8.11. *Adsorption isotherms of rGO for MB.*

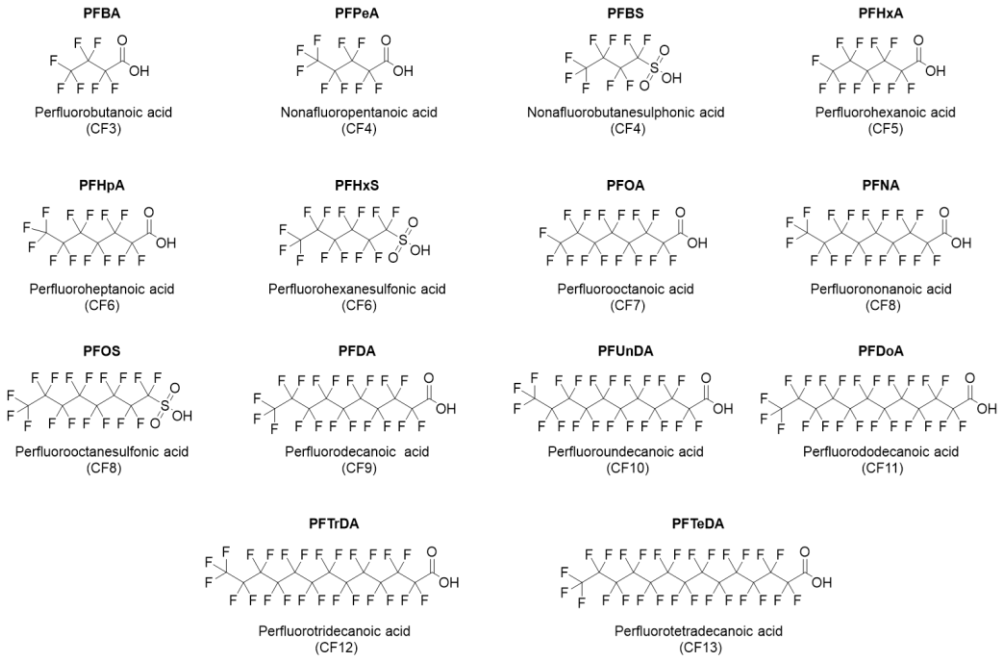

Fig. 8.12. *Molecular structure of selected PFAS.*

Table 8.2. *Technical details of GAC.*

GAC Specifications	
Iodine number *(ASTM D 4607, 2014)*	> 1000 mg/g
Methylene blue index *(MU 182:98 M35)*	> 240 mg/g
Water soluble ashes *(MU 182:98 M33)*	< 11%
Granulometry >8 US mesh *(MU 182:98 M32)*	< 5 %
Granulometry <30 US mesh *(MU 182:98 M32)*	< 5%
Moisture (as packed)	< 5%
Ball-pan hardness *(ASTM D 3802)*	> 90
Apparent density *(MU 182:98 M31)*	> 450 kg/m^3
Molasses index *(Norit Standard Test Method)*	> 230
Pores distribution	Micro: > 45%; Meso: > 30%
Total pores volume	0.9-1.1 mL/g
Surface area *(BET method)*	> 1000 m^2/g
Uniformity coefficient	> 1.9
Density backwashed and drained	> 400 kg/m^3
Bed expansion	> 8% at lineat rate 12.5 m/h at 20 °C

Table 8.3. *Elution gradients used by the analytical pump. Mobile phases: (A) MeOH: aqueous NH_4OAc 2 mM 95:5; (B) NH_4OAc 2 mM in MeOH.*

Time (min)	Analytical pump		
	Flow(mL min^{-1})	A%	B%
0	0.3	100	0
1	0.3	80	20
6	0.3	55	45
13	0.3	20	80
15	0.35	5	95
17	0.35	5	95
18	0.3	100	0
21	0.3	100	0

Table 8.4. *LC/MS/MS parameters for all PFAS target analytes using UPLC-MS/MS ACQUITY UPLC H-Class PLUS – XEVO TQS Micro MS.*

		ES(-)	Collision energy (eV)	LOQ
PFBA	Perfluorobutanoic acid	212.97→168.99	8	0.01
PFPeA	Perfluoropentanoic acid	263.09→218.93	6	0.01
PFBS	Perfluorohexanoic acid	299.03→79.84	32	0.01
PFHxA	Perfluoroheptanoic acid	312.90→269.02	6	0.01
PFHpA	Perfluorooctanoic acid	262.90→168.98	6	0.01
PFHxS	Perfluorononanoic acid	398.96→79.90	38	0.01
PFOA	Perfluorodecanoic acid	412.98→168.98	18	0.01
PFNA	Perfluoroundecanoic acid	462.96→218.97	16	0.01
PFOS	Perfluorododecanoic acid	498.90→79.90	54	0.01
PFDA	Perfluorotridecanoic acid	513.12→469.00	10	0.01
PFUnDA	Perfluorotetradecanoic acid	562.96→519.06	10	0.05
PFDODA	Perfluorobutanesulfonic acid	613.06→569.04	14	0.05
PFTrDA	Perfluorohexanesulfonic acid	622.90→168.97	28	0.05
PFTA	Perfluorooctanesulfonic acid	712.96→168.96	32	0.1

Table 8.5. *Morphological parameters characterising GO nanosheets.*

	Size (nm)	Aspect Ratio	Form Factor
Mean	351	1.51	0.40
Percentile 10%	77	1.12	0.23
Percentile 50%	170	1.37	0.42
Percentile 90%	567	1.98	0.55

The last two parameters, aspect ratio and form factor, describe respectively the shape anisotropy and the border irregularity of the object considered. The minimum value of aspect ratio (=4/π) is found for a circular object. A square object instead has an aspect ratio equal to 1. Larger aspect ratios values are expected for objects that are more elongated in one spatial direction. On the contrary, the form factor has its maximum value for a circular object (= 1).

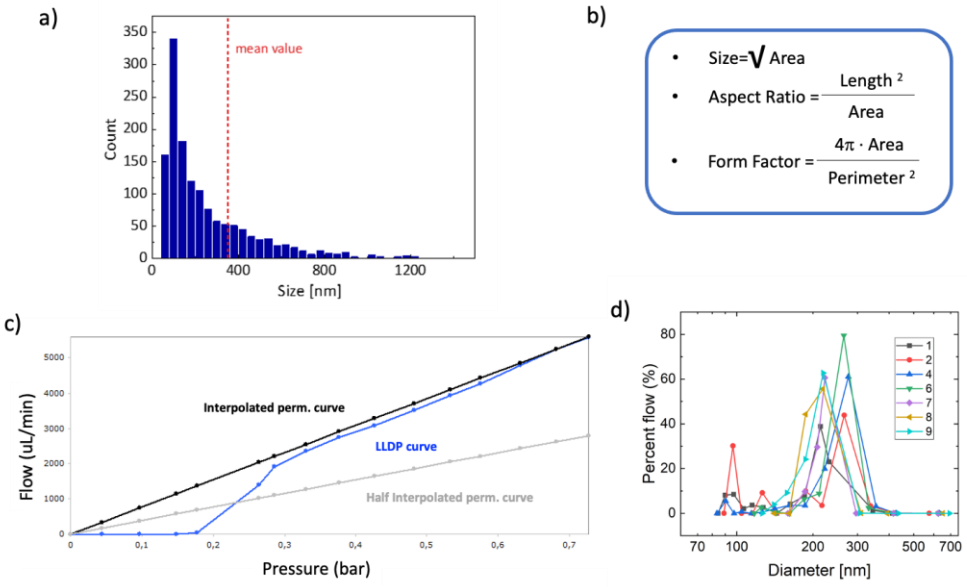

Fig. 8.13. *(a) Size distribution of analyzed GO nanosheets. (b) Size parameter for GO. (c) Permeability curve of PES: flow vs pressure plot. The number of point measurable in permeability curve is limited by pressure step selectable by instrumental configuration, of c.a. 50 mbar. (d) Pore size distributions: reproducibility of different*

samples of PES. The peak of distribution was in the range of 200-250 nm. The number of points present in each distribution is limited by the number of point measurable in permeability curve (minimum step of 50 mbar).

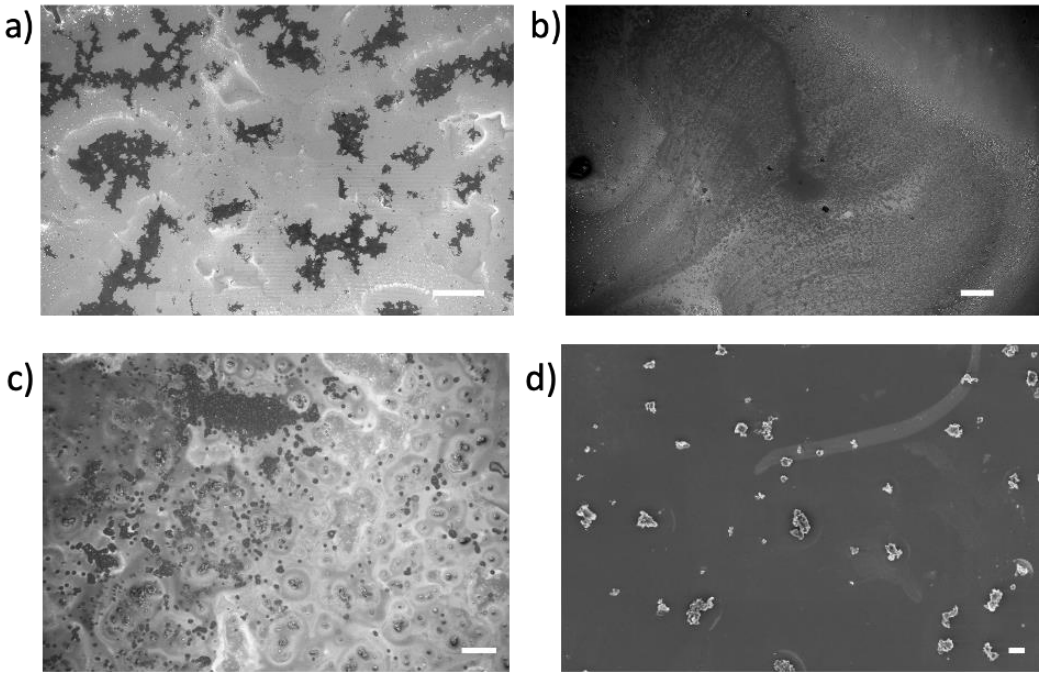

Fig. 8.14. *SEM images of (a) GO in tap water and (b) GO in Milli-Q water, (c) rGO in tap water and (d) rGO in Milli-Q water. GO and rGO were deposited on Silicon substrate 10 min after the preparation of suspensions. Bars size 200 μm.*

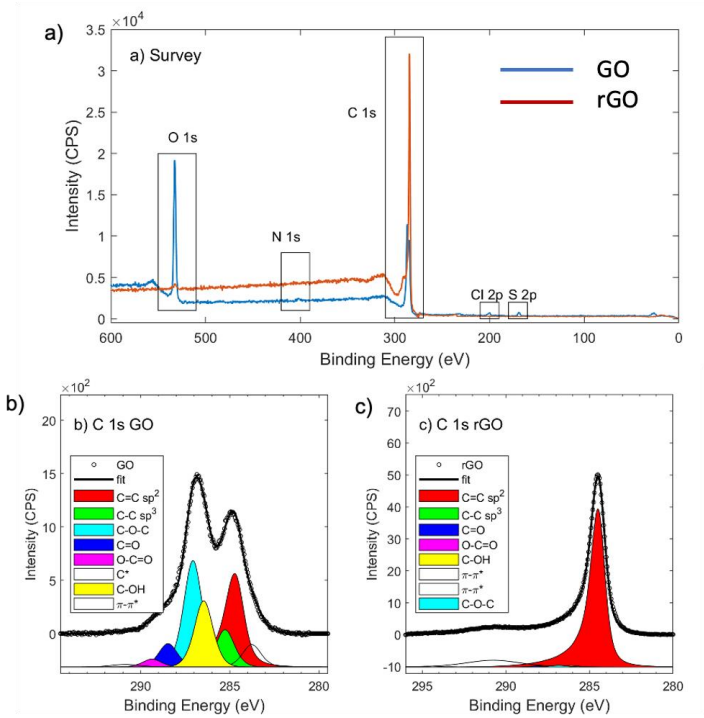

Fig. 8.15. *XPS survey spectrum of GO and rGO. (a) High resolution XPS C 1s spectra of (b) GO and (c) rGO.*

Table 8.6. *Potability tests results. From left, GO suspension in tap water (250 mg/L), GO suspension (250 mg/L) after microfiltration, and tap water. Analyses according to Italian drinking water regulation D. Lgs. 31/01.*

Parameter *Method*	**GO** 250 mg/L		**GO+ MF** 250 mg/L		**TAP**		**Limits**
Turbidity *APAT CNR IRSA 2110 Man 29 2003*	445		<0.02		<0.02		
Smell *APAT CNR IRSA 2050 Man 29 2003*	Odorless		Odorless		Odorless		
Taste *APAT CNR IRSA 2080 Man 29 2003*	Tasteless		Tasteless		Tasteless		
Color *APAT CNR IRSA 2020 A Man 29 2003*	Dark brown		Colorless		Colorless		
pH *APAT CNR IRSA 2060 Man 29 2003*	7.9	*±0.4*	8.4	*±0.4*	7.8	*±0.4*	6.5/9.5
TOC (mg/L) *UNI EN 1484:1999*	147	*±25*	3	*±1*	2	*±1*	
Conductivity (microS/cm) *APAT CNR IRSA 2030 Man 29 2003*	410	*±31*	240	*±18*	669	*±50*	<2500
Water hardness (°F) *APAT CNR IRSA 3010 B* *+ APAT CNR IRSA 3020 Man 29 2003*	26	*±5*	25	*±5*	30	*±6*	15/50
Fixed residue a 180°C (mg/L) *APAT CNR IRSA 2090 B Man 29 2003*	319.8	*±25.6*	186.4	*±14.9*	534	*±42.7*	<1500
Ammoniacal nitrogen$^{(NH4+)}$ (mg/L) *UNI 11669:2017*	<0.02		<0.02		2.4	*±0.3*	
Chloride (mg/L) *APAT CNR IRSA 4020 Man 29 2003*	27.12	*±2.71*	24.48	*±2.45*	30.14	*±3.01*	<250
Sulphate (mg/L) *APAT CNR IRSA 4020 Man 29 2003*	66.6	*±8*	60.3	*±7*	70.8	*±8*	<250
Nitrite (mg/L) *APAT CNR IRSA 4020 Man 29 2003*	<0.05		<0.05		<0.05		<0.5
Iron (ICP-MS) (ug/L) *EPA 6020B 2014*	<0.1		<0.1		0.5	*±0.04*	<200
Aluminium (ICP-MS) (ug/L) *EPA 6020B 2014*	0.6	*±0.1*	0.6	*±0.1*	0.2	*±0.1*	<200
Manganese (ICP-MS) (ug/L) *EPA 6020B 2014*	7.5	*±0.7*	9	*±0.8*	15.6	*±1*	<50
Sodium (mg/L) *APAT CNR IRSA 3010 B* *+ APAT CNR IRSA 3020 Man 29 2003*	<1.25		<1.25		21.71	±3.13	<200

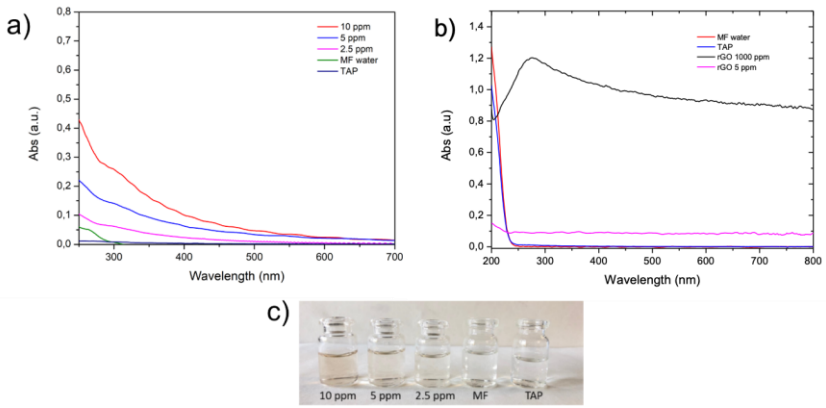

Fig. 8.16. *a) GO nanosheets (50 mL of a 2 mg/mL suspension) are introduced in tap water (total volume 100 mL) and the solution is stirred at room temperature for 30 min in darkness; the suspension is filtered through the MF module (OUT-IN transmembrane modality, flow rate 55 mL/min). Treated water was analyzed by UV-Vis. No evidence of GO was found within the intrinsic LOD of the analysis (about 2.5 ppm). b) UV-Vis spectra of rGO (1*

mg/mL) before (pink curve) and after filtration (red curve) on a MF module, compared to TAP water (blue curve) and to a suspension of 5 ppm of rGO. c) Standard GO suspensions in water at decreasing concentration (from left to right).

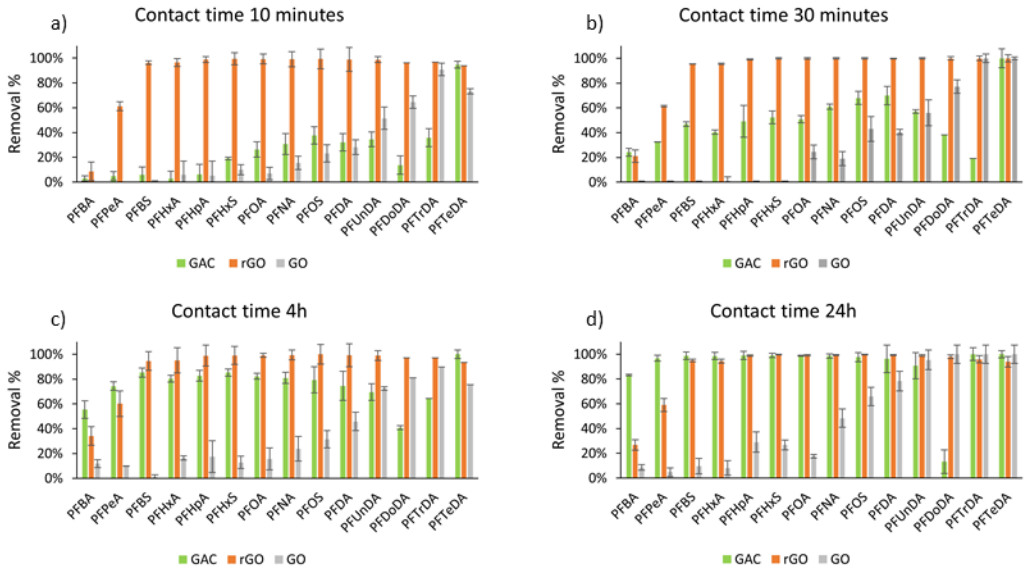

Fig. 8.17. *Kinetic experiments on a mixture of fourteen PFAS, 10 μg/L each at (a) 10 min, (b) 30 min, (c) 4 h, and (d) 24 h.*

Table 8.7. *Total μg of PFAS removed per g of sorbent at different contact times.*

Contact time	GAC	GO	rGO
	$\mu g_{total\ PFAS}/g_{\ sorbent}$	$\mu g_{total\ PFAS}/g_{\ sorbent}$	$\mu g_{total\ PFAS}/g_{\ sorbent}$
10 min	17.9	31.7	93.3
30 min	43.7	36.1	138.2
1h	80.6	35.4	140.6
24h	96.3	39.7	143.3

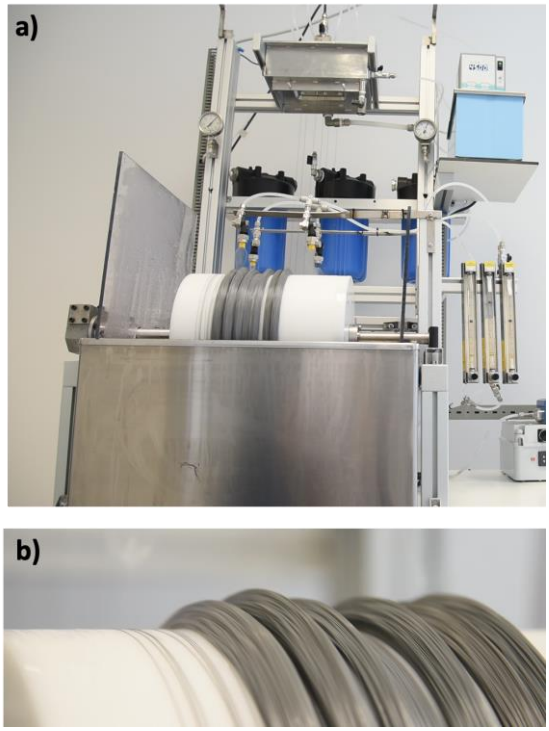

Fig. 8.18. *a) Spinning plant pilot for hollow fiber fabrication. b) Collection wheel with hollow fibers bundle.*

a)

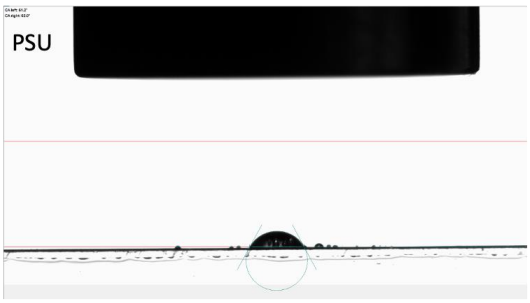

PSU	
Sample #	CA [°]
1	56
2	64
3	58,8
4	56,5
5	65,7
6	65,8
7	58,8
8	64,6
9	55,3
10	55,4
11	61,1
12	62,9
Avg.	60,4
Std. Dev.	4,104201

b)

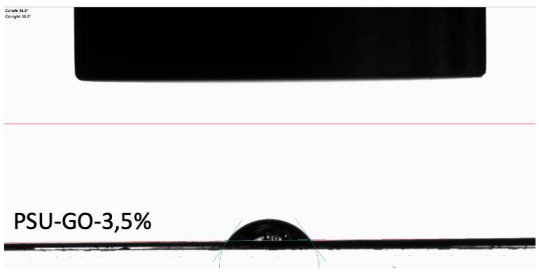

PSU-GO-3,5%	
Sample #	CA [°]
1	57,81
2	53,85
3	52,17
4	52,1
5	52,85
6	50,55
7	52,21
8	57,12
9	51,49
10	52,72
11	53,6
12	54,01
Avg.	53,4
Std. Dev.	2,154215

Fig. 8.19. *Contact angles values and images of PSU and PSU-GO 3.5% HFs. Contact angle of PSU-HF and PSU-GO 3.5% HF were measured with OCA Dataphysics instrument. Fibers were flattened before measurement to remove the outer porosity of the fiber and allow the measurement of the contact angle of the material.*

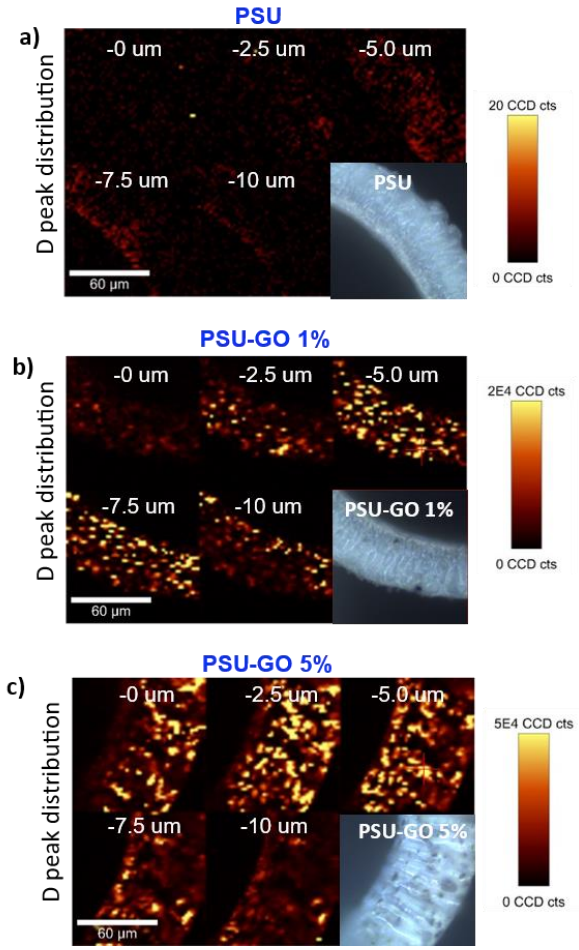

Fig. 8.20. *Z stack of Raman maps and the relative optical images of original PSU, PSU-GO 1% and PSU-GO 5%, constructed by mapping the D-band region. Raman stack mapping was performed on a confocal Raman micro-spectroscope (Alpha300R, WITec, Germany). The light source used was a 532 nm laser with the output power of around 0.7 mW cm^{-2}. The diffraction grating of 600 g/mm was employed together with a 50x microscope objective. Fibers were imaged by collecting Raman images from 5 layers of 2.5 mm increment in the z direction. A 2 mm step size was used in the x and y direction for each Raman image with 0.5 s integration time and a spectral range from 0 to 3600 cm^{-1}.*

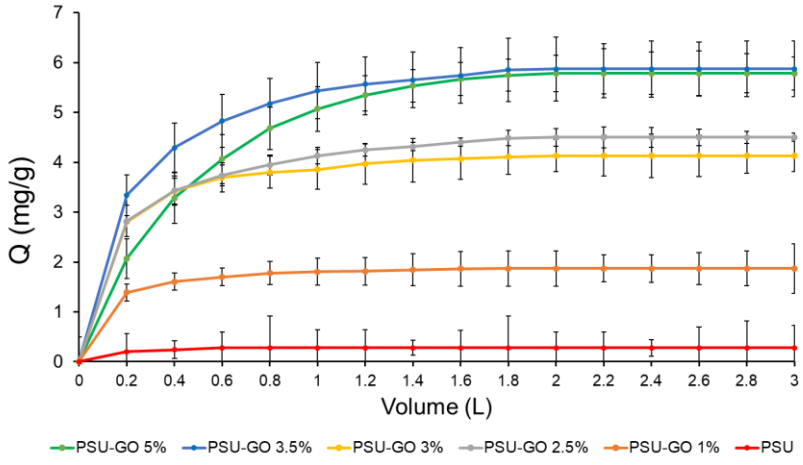

Fig. 8.21. *Comparison between the Ciprofloxacin adsorption efficiency of PSU and PSU-GO materials at five different GO (percentage mg/g composite).*

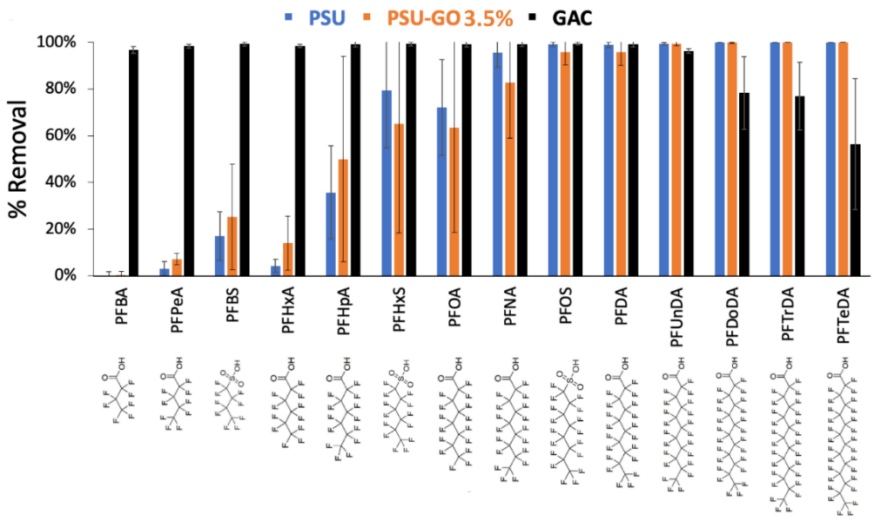

Fig. 8.22. *Removal of a mixture of fourteen PFAS in tap water, total volume=250 mL, C_{IN}= 10 µg/L, flow rate= 5 mL/min. Amount of material in the module: PSU 0.26 g, PSU-GO 3.5% 0.27 g, GAC 2.3 g.*

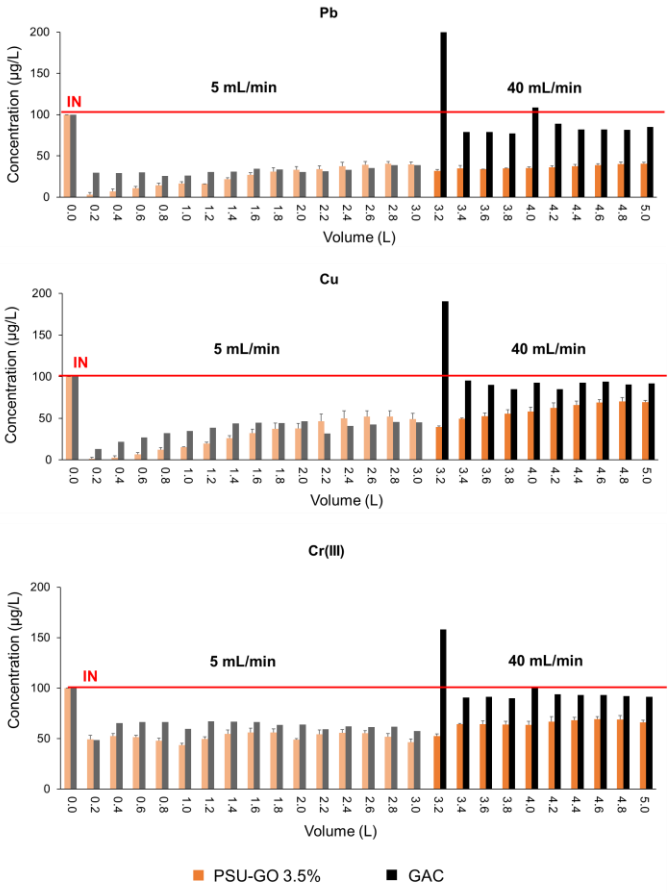

Fig. 8.23. *Treated water concentration comparison of PSU-GO 3.5% (orange) and GAC (black) performance at two different flow rate (5 and 40 mL/min). Reported trend for selected heavy metals with higher removal efficiency (Pb, Cu and Cr (III)).*

Table 8.8. *Water potability tests results.*

Risultati analitici

Parametro *Metodo*	U.M.	Risultato	Incertezza	Limiti
ATTIVITA' DI LABORATORIO				
* Torbidità APAT CNR IRSA 2110 Man 29 2003	NTU	**< 0,02**		
Odore APAT CNR IRSA 2050 Man 29 2003		**Inodore**		
Sapore APAT CNR IRSA 2080 Man 29 2003		**Insapore**		
Colore APAT CNR IRSA 2020 A Man 29 2003		**Incolore**		
pH APAT CNR IRSA 2060 Man 29 2003	upH	**8,0**	±0,4	6,5÷9,5
* Carbonio organico totale (TOC) UNI EN 1484:1999	mg/l	**< 1**		
Conducibilità APAT CNR IRSA 2030 Man 29 2003	microS/cm	**508**	±38	< 2500
Durezza totale (da calcolo) APAT CNR IRSA 3010 B + APAT CNR IRSA 3020 Man 29 2003	°F	**55**	±11	15÷50
* Residuo fisso a 180 °C APAT CNR IRSA 2090 B Man 29 2003	mg/l	**389,0**	±31,1	< 1500
Azoto ammoniacale (come NH4+) UNI 11669:2017	mg/l	**< 0,02**		
Cloruri APAT CNR IRSA 4020 Man 29 2003	mg/l	**38,50**	±3,85	< 250
Solfati APAT CNR IRSA 4020 Man 29 2003	mg/l	**117,1**	±14,1	< 250
Nitriti APAT CNR IRSA 4020 Man 29 2003	mg/l	**0,07**	±0,01	< 0,5
Ferro (ICP-MS) EPA 6020B 2014	ug/l	**9,2**	±0,8	< 200
Alluminio (ICP-MS) EPA 6020B 2014	ug/l	**7,6**	±0,7	< 200
Manganese (ICP-MS) EPA 6020B 2014	ug/l	**< 0,1**		< 50
Sodio APAT CNR IRSA 3010 B + APAT CNR IRSA 3020 Man 29 2003	mg/l	**38,81**	±5,59	< 200
Conta Escherichia coli UNI EN ISO 9308-1:2017	UFC/100 ml	**0**		< 0
Conta Enterococchi intestinali UNI EN ISO 7899-2:2003	UFC/100 ml	**0**		< 0

Bologna lì: 30/03/2021

Il presente Rapporto di Prova si riferisce esclusivamente ai campioni sottoposti a prove ed è valido per tutti i casi previsti dalla legge come da R.D. 1/3/'28 n. 842, art 16. Questo Rapporto di Prova non può essere riprodotto parzialmente salvo approvazione scritta del Laboratorio. Analisi eseguite presso la sede di Bologna

ACCREDIA

LAB N° 1051 L

Risultati analitici

Parametro *Metodo*	U.M.	Risultato	Incertezza	Limiti
Conta coliformi totali UNI EN ISO 9308-1:2017	UFC/100 ml	**0**		< 0
Microrganismi vitali a 22°C UNI EN ISO 6222:2001	UFC/ml	**0**		< 100

Limiti: » D. Lgs. 31/01 Agg. D.M. 14/06/2017
Il simbolo "<" riportato nei limiti sopra elencati va inteso come "inferiore o uguale".

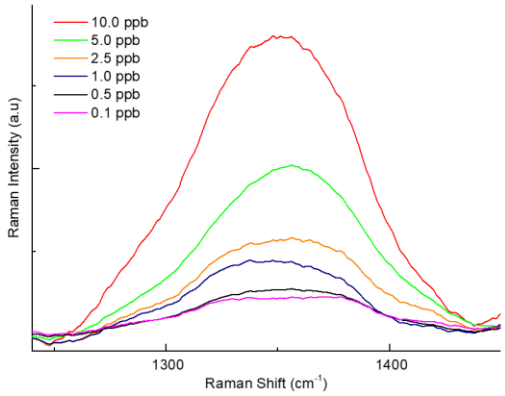

Fig. 8.24. *Average Raman spectra of different concentration of GO (0.1- 10 ppb) measured on SERS substrates (R2 = 0.995; LOD (ppb) = 0.11; P-LOQ (ppb) = 0.10).*

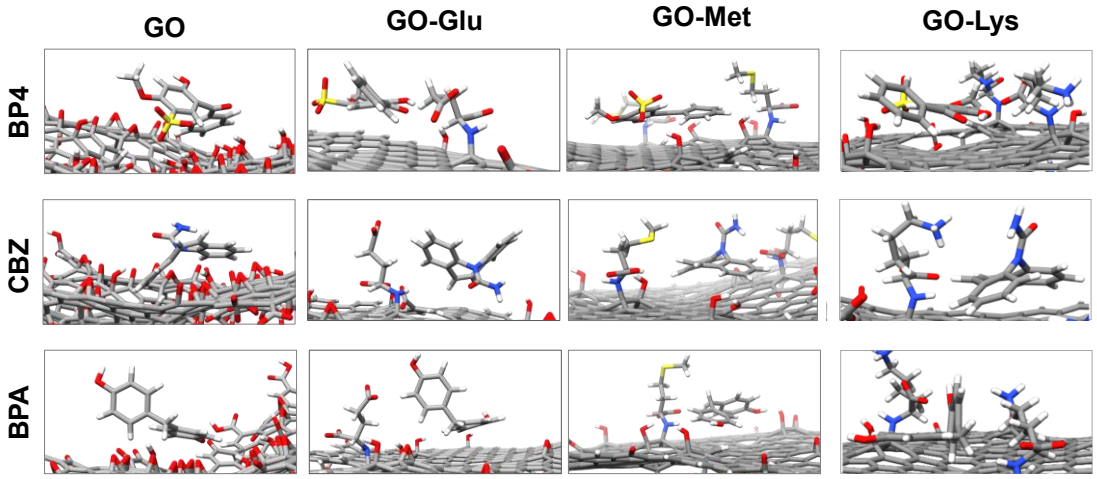

Fig. 8.25. *Representative snapshots from MD simulations of the favourite adsorption sites BP4, CBZ, and BPA on GO, GO-Glu, GO-Met and GO-Lys (from left to right).*

Table 8.9. *Variation of the solvent accessible surface area (ΔSASA) of BP4, CBZ, BPA and GO, GO-Glu, GO-Met and GO-Lys nanosheets, upon binding. ΔΔSASA is the variation of ΔSASA of amino acid modified GO nanosheets, compared to GO*

Contaminant	Material	ΔSASA [Å²]	ΔΔSASA [Å²]
BP4	GO	372.7	-
	GO-Glu	686.3	313.6
	GO-Met	704.8	332.1
	GO-Lys	411.0	38.3
CBZ	GO	298.9	-
	GO-Glu	612.5	313.6
	GO-Met	657.7	358.8
	GO-Lys	478.7	161.7
BPA	GO	317.3	-
	GO-Glu	538.7	221.4
	GO-Met	631.0	313.7
	GO-Lys	309.0	10.1